


Winter 2014

Molecular Characterization and Photochemical Transformation of Dissolved Organic Matter From Land to Ocean

Hongmei Chen
Old Dominion University

Follow this and additional works at: https://digitalcommons.odu.edu/chemistry_etds

 Part of the [Biogeochemistry Commons](#), [Chemistry Commons](#), [Geochemistry Commons](#), and the [Oceanography Commons](#)

Recommended Citation

Chen, Hongmei. "Molecular Characterization and Photochemical Transformation of Dissolved Organic Matter From Land to Ocean" (2014). Doctor of Philosophy (PhD), dissertation, Chemistry and Biochemistry, Old Dominion University, DOI: 10.25777/ptez-ew82
https://digitalcommons.odu.edu/chemistry_etds/25

This Dissertation is brought to you for free and open access by the Chemistry & Biochemistry at ODU Digital Commons. It has been accepted for inclusion in Chemistry & Biochemistry Theses & Dissertations by an authorized administrator of ODU Digital Commons. For more information, please contact digitalcommons@odu.edu.

**MOLECULAR CHARACTERIZATION AND PHOTOCHEMICAL
TRANSFORMATION OF DISSOLVED ORGANIC MATTER FROM LAND TO
OCEAN**

by

Hongmei Chen
M.S. Environmental Science, July 2007, Xiamen University, China

A Dissertation Submitted to the Faculty of
Old Dominion University in Partial Fulfillment of the
Requirements for the Degree of

DOCTOR OF PHILOSOPHY

CHEMISTRY

OLD DOMINION UNIVERSITY
December 2014

Approved by:

Patrick G. Hatcher (Director)

Kenneth Mopper (Member)

James W. Lee (Member)

Peter N. Sedwick (Member)

Aron Stubbins (Member)

ABSTRACT

MOLECULAR CHARACTERIZATION AND PHOTOCHEMICAL TRANSFORMATION OF DISSOLVED ORGANIC MATTER FROM LAND TO OCEAN

Hongmei Chen
Old Dominion University, 2014
Director: Dr. Patrick G. Hatcher

Molecular characterization and photochemical transformation of dissolved organic matter (DOM) in both rivers and the ocean is the main research focus of this dissertation. Chemical characterization of DOM is hampered by the limited application of advanced techniques to desalt, concentrate, isolate and then molecularly characterize DOM. An affordable, commercially available mini-electrodialysis (mini-ED) system has been evaluated and recommended for the efficient desalting of small volume samples of seawater prior to analysis by electrospray Fourier transform ion cyclotron resonance mass spectrometry (ESI FTICR-MS).

A high-recovery technique of DOM isolation – reverse osmosis coupled with electrodialysis (RO/ED) – was used to isolate DOM from various major oceanic water masses, prior to ESI FTICR-MS analysis. RO/ED isolated DOM samples share a significant number of common molecular formulas, accounting for 54-79% of formulas in each sample. MS peaks enriched in surface samples have higher H/C values than peaks enriched in deep samples. This enrichment pattern is likely due to the selective photo-degradation of aromatic compounds and the bio-production of aliphatic and carbohydrate-like compounds in surface waters, and the selective bio-degradation of aliphatic and carbohydrate-like compounds with increasing depth. MS peaks enriched in

the North Pacific intermediate and deep DOM have significantly higher O/C values than the North Atlantic oxygen minimum layer and deep DOM. This suggests oxidation of DOM, possibly via microbial activity during the ageing of DOM or the preferential remineralization of DOM from sinking particles at depth in the Pacific.

Our studies show that terrestrial DOM exposed to simulated sunlight is altered to produce POM with a markedly different molecular composition enriched in newly-formed aliphatic and condensed aromatic molecules. This process is closely tied to the chemistry of iron, which primarily exists as dissolved Fe(II) and Fe(III)-organic complexes in initial DOM and photochemically matures to Fe(III) oxyhydroxides before co-precipitating out with POM. The newly formed condensed aromatic compounds resemble black carbon, which until now was thought to be produced only by combustion. These new molecules contribute a novel pool of Fe-rich, aliphatic and black carbon organic matter to sediments as the terrestrial DOM is transported through rivers.

This dissertation is dedicated to all of those who helped me make it this far, especially to my family and friends for their endless support and encouragement, in particular to my husband Wenkui Peng and our daughter Grace Meiya Peng.

ACKNOWLEDGMENTS

I would like to express my sincere thanks to my advisor, Dr. Patrick G. Hatcher, for his continuous support, guidance, patience, and wisdom throughout my seven years of graduate study. He has been more than patient to inspire me in a wide variety of scientific experiences, which were not limited to my dissertation research. His generosity with the whole Hatcher group, like attending conferences, having writing retreats, hosting a baby shower for me, and numerous other events have made my time in ODU full of joy and memories.

My sincere appreciation is also expressed to my committee members, Dr. Kenneth Mopper, Dr. James W. Lee, Dr. Peter N. Sedwick, and Dr. Aron Stubbins, for their advices in my dissertation work. Dr. Mopper has dedicated his time to guide me on experiments, to discuss literature papers with me, and to help expand my knowledge on a wide variety of topics. Dr. Stubbins is the one who took me to field cruises to collect oceanic samples. He is also specially appreciated for encouragement and intellectual support throughout my graduate study.

I would like to extend special thanks to Dr. E. Michael Perdue and Nelson Green from Georgia Institute of Technology, for their assistance to collect the RO/ED isolated oceanic DOM samples and numerous other supports to me. I also thank Dr. Hussain Abdulla and Luni Sun, for their help on the photochemical experiments and sample collection in the Great Dismal Swamp. They were always available to answer my questions and lend me a hand when I need. I also specially thank Dr. Rachel Sleighter, for her continuous guidance to me on FTICR-MS. She is always selfless to share her

results and data processing tools to the entire group.

I thank all of the members of the Hatcher group and the Mopper group. They have taught me and helped me in many ways. Their friendship and the countless group activities have made my life away from my home country much easier and more enjoyable. Some of the members are away from ODU now, for example, Dr. Zhanfei Liu, Dr. Elodie Salmon, Dr. John Helms, and Dr. Thais Bittar. However, their help and advices to me will stay in my memory forever. I also want to specially thank Dr. Rajaa Mesfioui, my girlfriend in the Hatcher group, who is always there to comfort me during my emotional time.

I would also like to thank Susan Hatcher, Mahasilu Amunugama, Jared Callan, and Junyan Zhong at the COSMIC (College of Sciences Major Instrumentation Cluster) facility for their assistance with the FTICR-MS and NMR analyses. I thank the ODU Chemistry department faculty and staff, especially Alicia and Tammy, who have been very helpful to me throughout these years. I thank the scientists and crew on *R/V Oceanus* during the Cruise OC449-3 in September 2008. I especially thank the cruise chief scientist Dr. Phoebe J. Lam for her excellent organization and help. I also thank the crew on *R/V Kilo Moana* during the cruise in September 2009. I thank Keith Olson at the Natural Energy Lab Hawaii Authority (NELHA) for providing laboratory space for my experiments in September 2009.

Finally, and most importantly, I want to thank my family in China for their unconditional supports throughout my whole life. They deserve numerous thanks far beyond what any language can express. I am deeply indebted to my husband, Wenkui Peng, who has come to the states to take good care of me and keep me from losing

balance. Without his precious love, continuous support, and endurance over the last ten years, I could never have the enthusiasm to get even close to where I am. Lastly, I want to thank our precious daughter, Grace Meiya Peng, who is a true blessing to my life. She has given us unrestrained joy in the past two years. She will continuously pass energy to me to pursue my career.

This dissertation work is funded by the Frank Batten Endowment to Dr. Patrick G. Hatcher, and by the National Science Foundation (OCE-0728634).

TABLE OF CONTENTS

	Page
LIST OF TABLES.....	xi
LIST OF FIGURES	xii
 Chapter	
I. INTRODUCTION.....	1
II. A MINI-ELECTRODIALYSIS SYSTEM FOR DESALTING SMALL VOLUME SALINE SAMPLES FOR FOURIER TRANSFORM ION CYCLOTRON RESONANCE MASS SPECTROMETRY	9
INTRODUCTION	9
MATERIALS AND PROCEDURES	11
RESULTS AND DISCUSSION	17
COMMENTS AND RECOMMENDATIONS.....	31
III. ULTRAHIGH RESOLUTION MASS SPECTROMETRIC DIFFERENTIATION OF DISSOLVED ORGANIC MATTER ISOLATED BY COUPLED REVERSE OSMOSIS-ELECTRODIALYSIS FROM VARIOUS MAJOR OCEANIC WATER MASSES.....	33
INTRODUCTION	33
EXPERIMENTAL METHODS.....	36
RESULTS AND DISCUSSION	43
SUMMARY AND CONCLUSIONS	78
IV. PRODUCTION OF BLACK CARBON-LIKE AND ALIPHATIC MOLECULES FROM TERRESTRIAL DISSOLVED ORGANIC MATTER IN THE PRESENCE OF SUNLIGHT AND IRON	83
INTRODUCTION	83
MATERIALS AND METHODS.....	85
RESULTS AND DISCUSSION	91
V. SUMMARY AND CONCLUSIONS	111
CONCLUSIONS.....	111
FUTURE DIRECTIONS	116
REFERENCES	119
 APPENDICES	
A. COPYRIGHT PERMISSIONS.....	139
B. ABBREVIATIONS AND ACRONYMS USED	147

C. LIST OF EXACT MASSES, ELEMENTAL FORMULAS, AND AVERAGE PEAK INTENSITIES FOR THE 540 CHO FORMULAS AND 293 CHON FORMULAS (SHOWN IN FIGURE 7) SHARED IN MARINE RO/ED ISOLATED DOM SAMPLES IN THIS STUDY	150
VITA	172

LIST OF TABLES

Table	Page
1. The number of peaks in the Congo River and estuary water DOM (S/N above 4)	23
2. The percentage of peaks assigned a molecular formula, the total number of formulas, the number averaged percentage (% a) and magnitude-weighted percentage (% b) of each type of molecular formula present in each sample, excluding the instrumental blank peaks and peaks due to ¹³ C isotope	28
3. The number averaged percentage (% a) and magnitude-weighted percentage (% b) of each type of CHON formulas identified in each sample	28
4. The number averaged percentage (% a) and magnitude-weighted percentage (% b) of each type of CHO-only formulas identified in each sample.....	30
5. Location and seawater properties at each sampling site	37
6. Mass balance analysis of the RO/ED isolated DOM samples	45
7. Comparison of assigned molecular formulas between RO/ED DOM and C ₁₈ SPE DOM	47
8. General information of mass peaks in samples.....	53
9. Percentage of three different types of molecular formulas in all samples	55
10. Results of total carbohydrate concentrations in RO/ED isolated DOM and the carbohydrate-like peak percentages in FTICR-MS	60
11. Sum of relative magnitudes of each area according to Figure 11b and 12 for each sample's CHO formulas.....	66
12. Sum of relative magnitudes of each area according to Figure 13b and 14 for each sample's CHON formulas.....	72
13. The elemental H/C ratios from bulk analysis of organic matter in the samples	95
14. The elemental C/N ratios from bulk analysis of organic matter in the samples	95
15. Molecular composition for each sample as revealed by ultrahigh resolution mass spectra	97

LIST OF FIGURES

Figure	Page
1. Left: The mini-ED system from Harvard Apparatus; Right: A diagram showing the various components of the system	12
2. Negative ESI FT-ICR mass spectra of DOM from the Congo River and estuary	22
3. van Krevelen diagrams for the DOM, obtained from the assigned formulas (CHO-only) in each sample	24
4. Negative ESI FT-ICR mass spectra of fresh Dismal Swamp (DS) DOM and mini-ED processed Dismal Swamp samples from different salinity level	26
5. Comparison of RO/ED and C ₁₈ extracted DOM in van Krevelen diagram using CHO (left) and CHON (right) formulas from the North Atlantic Senegal-Mauritanian upwelling edge region 5 m sample	47
6. Representative negative ESI FTICR mass spectra of the samples	50
7. van Krevelen diagram using the 833 common formulas shared in marine RO/ED isolated DOM samples in this study.....	52
8. van Krevelen diagram using CHO formulas from the North Atlantic Senegal-Mauritanian upwelling core region surface sample	57
9. Fraction of different compound classes of CHO molecular formulas in all samples ...	59
10. Dendrogram from the cluster analysis using the relative magnitudes of the total 2880 formulas in each sample.....	61
11. Statistical plots using the relative magnitudes of the selected 750 CHO formulas	65
12. van Krevelen diagram of the selected areas and colored according to the biplot of the loadings shown in Figure 11b for the CHO formulas.....	68
13. Principal component plots using the relative magnitudes of the selected 496 CHON formulas.....	71
14. van Krevelen diagrams [(a) H/C vs. O/C, and (b) N/C vs. O/C] of the selected areas and colored according to the biplot of the loadings shown in Figure 13b for the CHON formulas.....	74

Figure	Page
15. Distribution of the three photochemical pools of molecular formulas defined by Stubbins et al. (2010) at each site	78
16. Changes in total organic carbon (TOC) and particulate organic carbon (POC) concentrations during photoirradiation.....	92
17. C K-Edge XANES of DOM (a) and POM (b) samples	93
18. N K-Edge XANES of DOM (a) and POM (b) samples.....	94
19. Changes in molecular composition of molecules identified by ultrahigh resolution mass spectrometry	98
20. Changes in molecular composition of molecules identified by ESI FTICR-MS.....	100
21. Kendrick mass defect plot of aromatic formulas in photo produced POM and natural POM samples calculated by use of COO KMD analysis	102
22. The van Krevelen diagram of molecules identified by ESI FTICR-MS, showing distinct regions for aliphatic formulas photoproducted in POM and DOM, respectively.....	103
23. Changes in DOM and POM Fe speciation with time	106
24. The van Krevelen diagram showing the newly formed POM (a) and DOM (b) molecular formulas from photoflocculation together with the numbers of formulas for both regions observed in ultrahigh resolution mass spectra of various respective samples (base extracts) of peat and DOM from riverine, coastal, and open ocean waters (Sleighter and Hatcher, 2008; Chen et al., 2014)...	110

CHAPTER I

INTRODUCTION

Natural dissolved organic matter (DOM) represents a dynamic pool of carbon on Earth (Hedges, 1992) and plays a key role in global biogeochemical processes. It is operationally defined as that component which passes through a filter/membrane pore size (normally 0.1-1 μm). In this dissertation, DOM refers to the fraction that passes through a 0.1 μm nominal pore size filter. DOM molecules are typically characterized by the elements that contain primarily carbon, hydrogen, and oxygen, but also incorporate other elements that are covalently bound to carbon (e.g., nitrogen, sulfur, and phosphorus). They also include metal-organic complexes where the metals are usually covalently bound to oxygen-and nitrogen-containing functionalized structures.

DOM molecules can be derived from soil, primary production, and organisms in the water. They can also be chemically and biologically altered biomolecules. Based on the source, DOM can be classified as terrestrial DOM which originates from land plants or associated soils, and marine DOM which originates from oceanic autochthonous biomolecules. Rivers worldwide transport approximately 0.4×10^{15} g of C year⁻¹ of terrestrial dissolved organic carbon (DOC) to the ocean (Schlesinger and Melack, 1981), an amount sufficient to support more than half of the annual turnover of marine dissolved organic carbon (DOC) (Williams and Druffel, 1987). However, the physical and chemical changes that terrestrial DOM undergoes during its transport from river to ocean are yet to be fully understood.

This dissertation has been formatted according to the journal *Marine Chemistry*.

With increasing concerns relating to climate change, a great deal of research has explored the role of marine DOC in the global carbon cycle. The marine DOC pool (662 ± 32 Pg; Hansell et al., 2012) is one of the Earth's largest C pools, comparable in size to the C in atmospheric CO₂ (750 Pg C; Hedges, 1992) or living terrestrial biomass (610 Pg C; Hedges, 1992). Marine DOM is an exchangeable pool of organic carbon, coupling between the rapidly interchanging atmospheric CO₂ pool and the slowly exchanging sedimentary organic carbon pool which cycles on geological timescales (millennia to millions of years). The linking of the atmospheric carbon pool and sedimentary carbon pool through marine DOC mainly occurs in the surface oceans, where CO₂ rapidly exchanges between the atmosphere and marine DOC, but also between the water and suspended particles or water and sediment interfaces. Because of its great size, even a minor change in marine DOC dynamics can impact the global carbon cycle significantly with unknown climate feedback mechanisms. For example, oxidation of only 1% of the marine DOC pool could produce an amount of CO₂ that exceeds the annual anthropogenic derived CO₂ (Hedges, 2002).

Hedges (2002) pointed to the importance of determining molecular information about DOM by stating that "the future of oceanographic research belongs in large part to those who can learn to read these molecular messages". The detailed composition and structure of DOM provide important information associated with its source, reactivity, and fate, as well as its alterations during transport (Hedges, 1992). DOM molecules carry the source signatures that can be used as tracers. Despite its importance, DOM cycling and chemical compositions are poorly constrained. Chemical characterization of DOM is

hampered by the limited application of advanced techniques to desalt, concentrate, isolate and then molecularly characterize marine DOM.

Numerous studies have employed bulk elemental ratios, isotope ratios and compound-specific determinations (e.g., analyses of carbohydrates or individual sugars, amino acids, lipids, lignin phenols as surrogates for lignin, etc.) to infer the distribution and cycling of DOM. Due to DOM's molecular complexity, about 80% of DOM components are uncharacterized. During the last two decades, some major advances have been made to chemically characterize DOM, delivering a greater understanding of its origin, structure, and function in the global carbon cycle (see review by Mopper et al., 2007). One technique that has perhaps made the greatest impact in the molecular analysis of DOM is electrospray ionization (ESI) Fourier transform ion cyclotron resonance mass spectrometry (FTICR-MS), which has been applied to offer new insights into the nature and reactivity of DOM (Bhatia et al., 2010; D'Andrilli et al., 2010; Dittmar et al., 2007; Grannas et al., 2006; Hertkorn et al., 2006; Kim et al., 2003; Koch et al., 2005, 2008; Kujawinski et al., 2004, 2009; Reemtsma et al., 2008; Sleighter and Hatcher, 2008; Stenson et al., 2003; Stubbins et al., 2010). Since the advent of FTICR-MS (reviewed by Marshall et al., 1998), there has emerged a significant increase in the make-up of DOM compounds, at least their molecular formulas.

The ultrahigh mass resolution (average 400,000 at m/z 400) and mass accuracy (< 1 ppm) of ESI FTICR-MS often allows for the resolution of 10-20 peaks at each nominal mass (Marshall and Rodgers, 2008) and the assignment of elemental formulas to each measured peak mass. Thus, ESI FTICR-MS is able to recognize the mass of specific compounds within DOM, assign unique elemental formulas, and subsequently infer

compositional differences among pools of DOM based on these elemental formulas (Sleighter and Hatcher, 2007). Recently, FTICR-MS has become even more powerful, because multivariate statistical analysis approaches have been introduced and applied to explore the large data sets acquired from mass spectra of DOM (Abdulla et al., 2013; Kujawinski et al., 2009; Sleighter et al., 2010).

Unfortunately, ESI FTICR-MS is a technique that is not tolerant of inorganic salts and direct analysis of marine DOM is not possible, requiring desalting prior to analysis, ideally without altering or fractionating the DOM. This has commonly been accomplished by solid phase extraction (SPE) using C₁₈, XAD, and PPL resins to isolate, recover, and concentrate the DOM without concentrating the salts (Aiken et al., 1979; Dittmar et al., 2001; Kim et al., 2003; Lara and Thomas, 1994a, 1994b; see Mopper et al., 2007 and Dittmar et al., 2008 for reviews). SPE techniques are readily implemented for inexpensive and rapid ship-board isolation of DOM. They typically require acidification of the sample to pH 2 prior to loading onto the resin and generally recover less than 50 % of the DOM from open ocean waters (Dittmar et al., 2008), excluding substances that are either ionic at pH 2 or are so hydrophilic that they escape sorption (Sleighter and Hatcher, 2008). Another salt-removal approach is ultrafiltration, which isolates DOM on the basis of size and typically recovers 10-40 % of DOM from open ocean samples (Benner and Opsahl, 2001; Buesseler et al., 1996; Guo and Santschi, 1996; Hernes and Benner, 2006; Santschi et al., 1995; Simjouw et al., 2005). The most promising non-discriminating technique for DOM isolation from saline waters is reverse osmosis coupled with electrodialysis (RO/ED), which can isolate up to 95 % of marine DOM (Koprivnjak et al., 2009; Vetter et al., 2007). However, because the dead volumes for previously

employed RO/ED systems are about 3 L, they demand large sample volumes typically exceeding 5 L. Obtaining requisite water sample volumes for these RO/ED systems places some constraints on sampling, and, in some cases, obtaining large volume samples is not feasible. Also, the equipment is rather expensive and requires trained operators for implementation. In order to overcome these limitations a novel method for desalting small volumes of seawater samples for subsequent analysis by ESI FTICR-MS was developed, evaluated, and is reported in Chapter II.

One of the overarching goals of this Thesis is to apply the most representative DOM isolation technique together with the state-of-the-art ultrahigh resolution mass spectrometry to differentiate marine DOM from various water masses, and subsequently infer the origin, nature and transformation of DOM. The RO/ED technique, featuring a high-recovery of DOM, was used to isolate DOM from the North Atlantic Senegal-Mauritanian upwelling area surface water (5 m), North Atlantic oxygen minimum water (415 m) and deep water (3000 m), North Pacific subtropical gyre surface water (5 m), and North Pacific intermediate water (674 m) and deep water (3500 m). However, a higher recovery does not necessarily guarantee more diversity of compounds. To ascertain whether RO/ED can extract DOM with greater molecular diversity than other techniques, it is necessary to make molecular-level comparison of DOM extracted by different techniques. In the current study we compared the molecular quality of DOM isolated by RO/ED and C₁₈ solid phase extraction (SPE) methods. Samples were characterized by ultrahigh resolution ESI FTICR-MS in negative mode, which typically requires samples to be run in an alkaline matrix. The RO/ED isolated DOM samples have pH ~ 8, which allows them to be analyzed directly without additions of organic solvent

(e.g., methanol) and alkali (e.g., NH_4OH). Mass spectra obtained with and without organic solvent in the same sample were compared. Due to high similarities of DOM between samples, the differentiation of marine DOM from the North Atlantic Ocean and the North Pacific Ocean was accomplished by hierarchical cluster analysis (HCA) and principal component analysis (PCA). Such statistical analysis reduces multidimensional data into fewer dimensions that can facilitate the comparison amongst large set of similar samples. The results are included in Chapter III.

During its transport from land to the ocean, terrestrial DOM experiences efficient removal from ocean margin environments including rivers, estuaries, and coastal area, although the physical, chemical, and biological processes causing this removal are poorly understood (Del Vecchio and Subramaniam, 2004; Hedges et al., 1997; Spencer et al., 2009). Photochemical processing of DOM is cited as an important removal mechanism for terrestrial DOM (Del Castillo et al., 1999; Helms et al., 2013a; Huguet et al., 2009; Stedmon and Markager, 2005; White et al., 2010). The photochemical mineralization process consumes DOM to produce inorganic compounds and small organic molecules (Miller 1994; Wetzel et al., 1995; Zafiriou et al., 1984; Zepp and Schlotzhauer, 1981). The photobleaching reduces the ultraviolet and visible absorption of DOM (Del Vecchio and Blough, 2002). The photochemical alteration of DOM in freshwaters changes the characteristics of both the dissolved and particulate pools (Mopper et al., 1991; Stubbins et al., 2010), and leads to aggregation of organic matter, commonly referred to as photoflocculation (Helms et al., 2013a; von Wachenfeldt et al., 2008). The potential relationship between photochemical transformation of DOM and flocculation of DOM has been recognized recently but yet to be understood (Gao and Zepp, 1998; Helms et al.,

2013a; Thorn et al., 2010; von Wachenfeldt et al., 2008). Overall, photochemical processing of DOM in natural waters can alter its composition and structure, supply particulate organic matter (POM) to sediments, and deliver modified terrestrial DOM to the ocean.

Both Fe(II) and Fe(III) form complexes with organic matter in natural waters and soils, often in combination with Fe(III) hydroxides (Laglara and Van Den Berg, 2009; Powell and Wilson-Finelli, 2003; Sundman et al., 2014). Photoirradiation of DOM has been suggested to be a process where humic materials become decarboxylated, less aromatic, more hydrophic, and less soluble (Thorn et al., 2010). Prior studies found that the presence or absence of carboxyl groups affects the solubility of DOM (vanloon and Duffy, 2010) and its ability to form stable complexes with iron (Barbeau, 2006). Consequently, both the solubility of DOM and iron are affected by photochemical processes.

In Chapter IV, phototransformation of DOM in fluvial ecosystems (the Great Dismal Swamp) was evaluated abiotically without salt effects or interference from pre-existing particles. The sterile-filtered (0.1 μm) water from an important headwater to the North Atlantic, the Great Dismal Swamp (in the state of Virginia; Sleighter and Hatcher, 2008), was subjected to abiotic photodegradation in a solar simulator for 60 days in a manner analogous to that described by Helms et al. (2013a). The previous studies using spectroscopic and NMR analyses described the bulk chemistry of both dissolved and flocculated material produced from the DOM but molecular-level characterization was unavailable. The molecular composition of the phototransformed organic matter, determined by, ESI FTICR-MS became the focus of the current study, and the results are

presented in Chapter IV. The bulk chemical characteristics of both particulate and dissolved fractions were determined using C, N, and Fe X-ray absorption spectroscopy, recognizing that this process could be closely tied to the chemistry of iron, which primarily exists as dissolved Fe(II) and Fe(III)-organic complexes in initial DOM.

In summary and as outlined above, this dissertation mainly focuses on the application of ultrahigh resolution ESI FTICR-MS to characterize natural DOM, reveal molecular level differences amongst DOM from various oceanic water masses, and infer molecular-level changes in the course of photochemical transformation and photoflocculation. These studies are all geared towards obtaining a more complete understanding of oceanic DOM from samples that are minimally affected by processing (e.g., sorption onto SPE systems or ultrafiltration). I have developed and evaluated a method for desalting small volumes of seawater samples for subsequent analysis by ESI FTICR-MS. I have applied a high-recovery of DOM isolation technique -- the RO/ED technique, together with ESI FTICR-MS to differentiate marine DOM from various water masses, and subsequently infer the origin, nature and transformation of DOM. As an added goal linked to understanding the source of DOM to oceanic systems, I have sought to examine the influence that photochemical processing of terrestrial material has on DOM and particulate organic matter.

CHAPTER II

**A MINI-ELECTRODIALYSIS SYSTEM FOR DESALTING SMALL VOLUME
SALINE SAMPLES FOR FOURIER TRANSFORM ION CYCLOTRON
RESONANCE MASS SPECTROMETRY**

PREFACE

The content of this Chapter was published in 2011 in *Limnology and Oceanography: Methods*, and below is the full citation. See Appendix A for the copyright permission.

Chen, H., Stubbins, A., Hatcher, P.G., 2011. A mini-electrodialysis system for desalting small volume saline samples for Fourier transform ion cyclotron resonance mass spectrometry. *Limnology and Oceanography: Methods*, 9: 582-592.

1. Introduction

Dissolved organic matter (DOM) in the ocean is one of the largest pools of dynamic carbon on earth (Hedges, 1992). Major advances are being made in the chemical characterization of DOM, delivering greater understanding of its origin, structure, and function in the global carbon cycle (Mopper et al., 2007). One of the most powerful techniques currently in use for the analysis of DOM is electrospray ionization (ESI) Fourier transform ion cyclotron resonance mass spectrometry (FTICR-MS), which has been applied to offer new insight into the nature and reactivity of DOM (Bhatia et al., 2010; D'Andrilli et al., 2010; Dittmar et al., 2007; Grannas et al., 2006; Hertkorn et al., 2006; Kim et al., 2003; Koch et al., 2005, 2008; Kujawinski et al., 2004, 2009; Reemtsma et al., 2008; Sleighter and Hatcher, 2008; Stenson et al., 2003; Stubbins et al., 2010).

However, salty samples are not conducive to ESI and need to be desalted prior to analysis, ideally without altering or fractionating the DOM. This has commonly been accomplished by solid-phase extraction (SPE) using C₁₈, XAD, and PPL resins to isolate, recover, and concentrate the DOM without concentrating the salts (Aiken et al., 1979; Dittmar et al., 2001; Kim et al., 2003; Lara and Thomas, 1994a, 1994b; see Mopper et al., 2007 and Dittmar et al., 2008 for reviews). SPE techniques are readily implemented for inexpensive and rapid ship-board isolation of DOM. They typically require acidification of the sample to pH 2 prior to loading onto the resin and generally recover less than 50 % of the DOM from open ocean waters (Dittmar et al., 2008), excluding substances that are either ionic at pH 2 or are so hydrophilic that they escape sorption (Sleighter and Hatcher, 2008). Another salt-removal approach is ultrafiltration, which isolates DOM on the basis of size and typically recovers 10-40 % of DOM from open ocean samples (Benner and Opsahl, 2001; Buesseler et al., 1996; Guo and Santschi, 1996; Hernes and Benner, 2006; Santschi et al., 1995; Simjouw et al., 2005).

The most promising non-discriminating technique for DOM isolation from saline waters is reverse osmosis coupled with electrodialysis (RO/ED), which can isolate up to 95 % of marine DOM (Koprivnjak et al., 2009; Vetter et al., 2007). However, because the dead volumes for previously employed RO/ED systems are about 3 L, they demand large sample volumes typically exceeding 5 L. Obtaining requisite water sample volumes for these RO/ED systems places some constraints on sampling, and, in some cases, obtaining large volume samples is not feasible. Also, the equipment is rather expensive and requires trained operators for implementation. In order to overcome these limitations a novel method for desalting small volumes of seawater samples for subsequent analysis by

ESI FTICR-MS was developed, evaluated, and is reported herein. This method couples small scale electrodialysis (mini-ED) with rotary evaporation. Naturally saline samples and freshwater samples amended with salt were desalted and subsequently analyzed using ESI FTICR-MS to determine the level of molecular information retrievable. Blanks were evaluated to determine if contamination was a problem. The most pressing concern was to evaluate whether the mini-ED was able to recover all ESI FTICR-MS peaks in a freshwater DOM sample from the Great Dismal Swamp, VA, USA, to which artificial sea-salts were added. The mini-ED isolates of two samples collected from locations in the Congo River and estuary were compared, one is freshwater and the other having a measurable salt content.

2. Materials and procedures

Sampling—Samples used to test the mini-ED system were taken from the Great Dismal Swamp (Suffolk, Virginia, USA), and the Congo River and estuary (near Kinshasa, Democratic Republic of Congo; Spencer et al., 2009). All samples were filtered through a 0.2 μm filter (Whatman, Polycap TC) to remove particulates and bacteria.

Sample amendment—Artificial seawater was made with combusted (450 °C, 5 h) NaCl and MgSO₄ (Fisher Sci., certified ACS grade) mixed with ultra-quality MilliQ water (Millipore). The salts were added to MilliQ water with a mass ratio of 64 : 7 for NaCl : MgSO₄. Freshwater samples amended with different amounts of artificial seawater were used to test the mini-ED system. The salinity of each sample prior to desalting was measured by a calibrated conductivity meter.

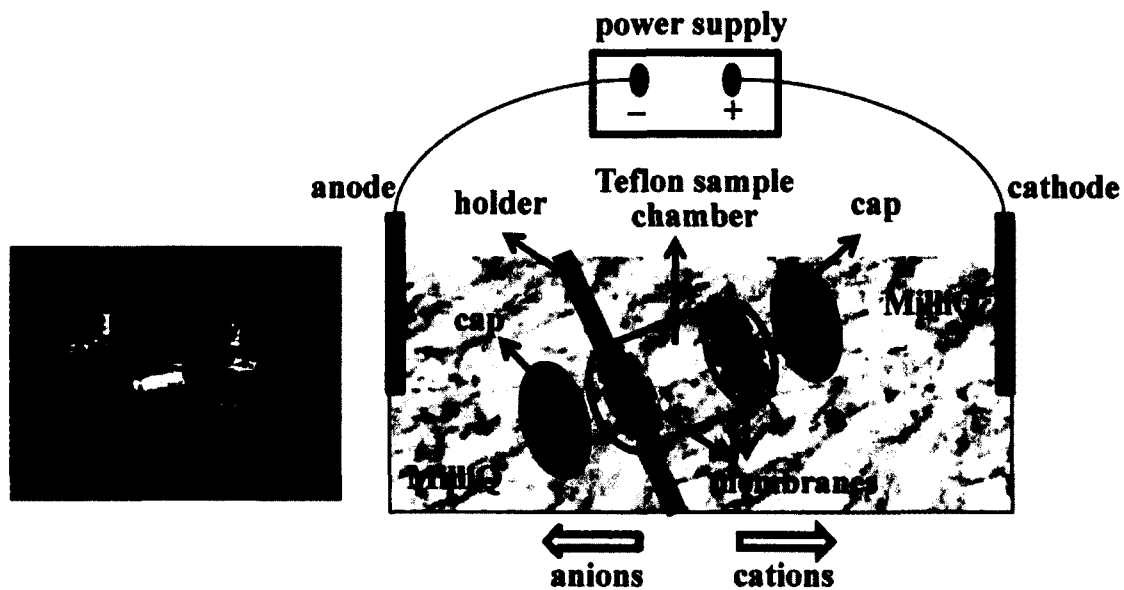


Figure 1. Left: The mini-ED system from Harvard Apparatus; Right: A diagram showing the various components of the system.

Mini-electrodialysis system—The mini-ED system (Harvard Apparatus; Figure 1) used here was designed for the rapid purification of proteins, nucleic acids, carbohydrates, and other biomolecules (see www.harvardapparatus.com for further details). The system comes along with a small power supply (maximum 200Vdc, 100mA). The sample chamber is made of Teflon, a completely inert material suited for high sample recovery and low sample contamination, which is important when dealing with low dissolved organic carbon (DOC) seawater samples. The membranes of the mini-ED system are commercially available at molecular weight cut-offs (MWCO) ranging from 100 Da to 300,000 Da and constructed of three materials— polycarbonate, regenerated cellulose, and cellulose acetate (see www.harvardapparatus.com for further details). However, only cellulose acetate membranes are available for molecular weight

cutoffs below 1000 Da. Cellulose acetate 100 and 500 Da membranes were chosen for the current study as they allow passage of the major inorganic ions present in seawater, while still retaining more DOM molecules than conventional ultrafiltration systems (1000 Da). Membranes from Harvard Apparatus arrived pre-cut and stored in a 0.05% sodium azide solution. Prior to use, membranes were soaked in MilliQ water. The mini-ED system was stored and operated at room temperature (~ 25 °C) in a dedicated chemical fume hood to maintain a relatively clean environment.

DOM isolation by mini-ED—A pre-rinsed dialysis membrane was placed over one end of the Teflon sample chamber and the Teflon end cap was installed to hold it in place. The chamber was then inverted and 1.5 mL of sample was added using a pre-combusted glass Pasteur pipette. Once filled, a second membrane was placed on the top and secured in place using the second end cap, making sure that no bubbles were trapped in the chamber. The chamber was then placed in the holder at the center of the mini-ED bath (Figure 1). The chamber holder supports the chamber and orientates it in the plane of the electrodes. The holder also provides a physical barrier between the anode and cathode ends of the bath forcing any current applied to flow through the sample chamber. MilliQ water was placed in the bath surrounding the chamber and the power supply was connected to the electrodes. In order to begin desalting a voltage of 200 V was applied to the system. In theory, mobile charged ions (e.g. Na^+ , Cl^- , SO_4^{2-}) move from the sample chamber to the bath driven by the applied electrical field, whereas neutral and less mobile molecules are preferentially retained in the chamber. These conditions promote the loss of inorganic salts and the retention of DOM. However, dissolved organic molecules may

be lost if they are charged and have a dynamic radius that is smaller than the membrane cutoff.

At the beginning of desalting, the low conductivity of MilliQ in the mini-ED bath external to the sample chamber prohibited a high current through the system and desalting occurred slowly. Over time, salts moved from the sample chamber into the surrounding MilliQ water, increasing the conductivity and the electrical current. After few hours, the exact timing depending upon initial sample salinity, the electrical current began to decrease along with the electrolyte concentration differential between the sample in the chamber and the surrounding water. At this point the movement of ions from the chamber to the bath slowed. When the conductivity in the surrounding water stabilized, the voltage was turned off and the surrounding water was partly replaced with new MilliQ water. Thus, renewing the salt gradient between the sample and the surrounding water, while retaining some salts in the surrounding water in order to facilitate an electrical current. Desalting was recommenced at 200 V and the conductivity of the surrounding water was monitored until it leveled off again. At this point the bath water was re-diluted with MilliQ. By repeating these procedures several times, the samples were desalted until their salinity was below 0.2 practical salinity units (PSU), which was low enough to run FTICR-MS. For the estuarine Congo DOM sample (salinity 0.2 PSU; DOC 10 mgC L⁻¹) desalting to an even lower salinity (< 0.01 PSU) was accomplished and completed within 24 h. Because of its reasonably high DOC concentration, this sample did not require further treatment prior to ESI FTICR-MS analysis.

For typical seawater (salinity ~35 PSU and DOC < 1 mgC L⁻¹), approximately 5 h was required to accomplish the first step of the process, during which the samples were desalted to a salinity of ~5 PSU. For these low DOC seawater samples both concentrating and desalting was required to obtain appropriate samples for ESI FTICR-MS analysis. Therefore, numerous (10 to 15) subsamples were desalted as described above and then combined and concentrated to ~2 mL by rotary evaporation. The exact number of subsamples required for this process depended upon the concentration factor required to bring the final DOC concentration to > 6 mgC L⁻¹ which is sufficient to obtain high quality ESI FTICR-MS spectra (personal observation). As evaporation concentrated both the DOM and salts in the sample, the concentrated sample was returned to the mini-ED and the desalting process was repeated. The entire process, including the original desalting of multiple subsamples, required 3~7 d. To minimize the adsorption of DOM onto the membranes, the chamber was shaken for few minutes before the desalted sample was transferred out of the chamber.

Solid phase extraction of DOM using C₁₈—DOM was also isolated with C₁₈ solid phase extraction disks (3M, Empore) using previously established protocols (Kim et al., 2003) to compare with the results obtained from the mini-ED method.

Dissolved organic carbon measurement—DOC concentrations for filtered samples were determined as non-purgeable organic carbon (NPOC) by high temperature combustion (720 °C) on a Shimadzu TOC-5000V analyzer equipped with a high sensitivity platinum catalyst (Shimadzu Scientific Instruments). Reference materials for low carbon water and deep seawater obtained from the Consensus Reference Materials

Project, Hansell Laboratory, University of Miami, were used to correct and monitor the performance of the instrument (Doval and Hansell, 2000).

ESI FTICR-MS data acquisition—Immediately prior to ESI FTICR-MS analysis, samples were diluted 50:50 (v/v) with LC-MS grade methanol (contains 0.1%, v/v, NH₄OH) to improve DOM ionization efficiency. This dilution was conducted less than half an hour before analyzing the samples to minimize potential esterification of the DOM by methanol (Bateman et al., 2008; Flerus et al., 2011). Samples were analyzed under negative ion mode without further treatment using a Bruker Daltonics 12 Tesla Apex Qe ESI FTICR-MS housed in the College of Sciences Major Instrumentation Cluster (COSMIC) at Old Dominion University (Virginia, USA). Instrument blanks were analyzed with 50:50 (v/v) H₂O: MeOH (contains 0.1%, v/v, NH₄OH) before and after running the samples. Blanks and samples were infused into the ESI ion source using a syringe pump with an infusion rate of 120 $\mu\text{L h}^{-1}$. Ions were accumulated in the hexapole for 2.0 s before being transferred to the ICR cell. Exactly 300 transients were co-added for each sample and digitized with a 4M Word data acquisition size. Fourier transformation and magnitude calculation of the free induction decay signal (FID) was accomplished by the Bruker Daltonics Data Analysis software.

ESI FTICR-MS data analysis—Mass spectra were internally calibrated using naturally present fatty acids (Sleighter et al., 2008). Data lists of m/z values and peak height were copied out with a signal-to-noise ratio (S/N) above 4 and m/z range from 200 to 700. Each sample's m/z list was aligned with the instrumental blanks' m/z lists in MATLAB allowing the maximum m/z difference to be the m/z divided by 400,000, which is the average resolving power at m/z 400 (where resolving power is defined as

$m/\Delta m_{50\%}$ where $\Delta m_{50\%}$ is the peak width at half-height of peak m). Following alignment, all peaks found in instrumental blanks were removed from the sample's peak list. These blank-corrected peak lists were imported to a molecular formula calculator (Molecular Formula Calc v.1.0 ©NHMFL, 1998) to obtain molecular formulas using ^{12}C (number range: 1 to 50), ^{13}C (0 to 1), ^1H (1 to 100), ^{14}N (0 to 6), ^{16}O (0 to 30), ^{34}S (0 to 2), ^{31}P (0 to 2) and ^{35}Cl (0 to 1). We allow the difference between the exact mass of calculated formula and the measured m/z to be less than 1 ppm. We only retain those formulas that possibly occur within natural DOM by the following criteria of the atomic ratio in each formula: (i) $2 \leq \text{H} \leq (2\text{C} + 2)$, $0 \leq \text{O} \leq (\text{C}+2)$, $\text{O}/\text{C} < 1.2$, $0.3 < \text{H}/\text{C} < 2.25$, $\text{N}/\text{C} < 0.5$, $\text{S}/\text{C} < 0.2$, $\text{P}/\text{C} < 0.1$, $(\text{S}+\text{P})/\text{C} < 0.2$ (Stubbins et al., 2010); (ii) Formulas containing an odd number of N have odd nominal mass, while those containing even numbers of N have even nominal mass (McClafferty and Turecek, 1993); (iii) Double bond equivalents (DBE) ≥ 0 , and must be a whole number (McClafferty and Turecek, 1993), where $\text{DBE} = 1 + \frac{1}{2}(2\text{C} - \text{H} + \text{N} + \text{P} + \text{Cl})$. For some of the peaks, they were removed as salt peaks from the final dataset because they can only be calculated as formulas containing Cl. The ^{13}C isotopic peaks were identified as those meeting both the following criteria: (i) if there are matched ^{12}C formula and ^{13}C formula; (ii) if the ^{13}C formula peak height is lower than the ^{12}C formula peak height. Once identified, these ^{13}C isotope peaks were removed from the dataset.

3. Results and discussion

Initial results comparing the 100 and 500 MWCO Da membranes indicate that the 100 Da membranes were not able to desalt samples efficiently, most likely due to their retention of anions with large ionic radii (e.g. SO_4^{2-}). In contrast, the 500 Da MWCO

membranes resulted in efficient and fairly rapid desalting of samples. Based upon these findings, the performance of the 500 Da membranes was further explored. Compared with the commonly-used isolation method of ultrafiltration, which generally employs a 1000 Da membrane, mini-ED is expected to retain lower molecular weight DOM and achieve higher total recoveries. In addition, ultrafiltration relies upon the passive diffusion of salts across the membrane. Under these conditions if DOM is small enough to cross the membrane at higher concentration in the sample then it will be lost to the waste. In ED, an electrical current causes the active transport of charged ions across the membrane. Under these conditions, DOM would have to be both small (<500 Da) and charged to be actively removed to waste with similar efficiency as the salts. Thus, the mini-ED should retain DOM in the range from 500 to 1000 Da as well as DOM <500 Da that is neutral or poorly charged and therefore not actively transported across the membrane. Compared with solid phase extraction techniques (SPE), the mini-ED does not require the samples to be acidified to pH 2 which can potentially affect the molecular characteristics of DOM. Further, it does not rely on chemical affinities between the SPE substrate and the DOM. Thus, the mini-ED is expected to recover a large, minimally fractionated proportion of the DOM, ensuring that the recovered DOM is as representative of the original sample as is possible at present for small volume samples.

Blank test—Collecting, processing, and analyzing low DOC water requires extreme care to avoid contamination. Thus, to assess potential contamination from the mini-ED, a system blank was determined. First, MilliQ water was used to fill the mini-ED bath, as per normal operating procedure (Section '*DOM isolated by mini-ED*'). Approximately 31.5 PSU artificial seawater was then placed inside the sample chamber,

and the system was operated for 48 h as described for seawater samples. Artificial seawater DOC increased from an initial $\sim 0.1 \text{ mgC L}^{-1}$ to $\sim 2 \text{ mgC L}^{-1}$ in the desalted sample indicating contamination.

Although the artificial seawater DOC increased by 2 mgC L^{-1} after desalting, the ESI FTICR-MS for the blank contained mainly peaks displaying mass defects between 0.7 and 0.8 Da. These peaks were assigned as salt-derived peaks based upon their mass defects. Mass defect is the distance a peak is displaced from the closest exact nominal mass (i.e. whole number). The displacement between the nominal mass and a peak is determined by the atoms contained in the analyte molecule and is the basis of formula assignment using FTICR-MS. Even before calculating the molecular formula for each peak in the FTICR mass spectra, it is possible to classify the peaks by elemental composition based upon their mass defects. The ultrahigh resolution of FTICR-MS enables mass defects to be calculated at least to the 5th decimal place. The atomic masses of isotopes ^1H , ^{12}C , and ^{16}O are 1.00783 Da, 12.00000 Da, and 15.99491 Da, respectively. Normally DOM molecules are observed with mass defect range from 0.0 to 0.4, although some long-chain fatty acids appear at mass defects of 0.4 to 0.6 (Sleighter et al., 2008). When DOM-chloride adducts are present they have mass defects of 0.7 to 0.8, because the atomic mass of the isotope ^{35}Cl is 33.96787 Da.

In the ESI FTICR-MS for the blank, we also observed few peaks where normal DOM molecules are generally observed (mass defects 0.0 to 0.4) but they were consistent with peaks found commonly in the instrument blank run on the FTICR-MS at ODU. This instrument blank was obtained from a mixture of 50:50 (v/v) MilliQ water and LC-MS grade methanol (containing 0.1%, v/v, NH_4OH). These results indicate that DOC

contamination from the mini-ED did not affect the mass spectral data. Apparently, the contaminating organic molecules were not charged during negative ESI or were smaller or greater in mass than the limits of mass spectral window detected by ESI FTICR-MS as configured in the experiments conducted. Given that the ED membranes used were cellulose acetate, it is likely that the DOC blank from the mini-ED was also cellulosic and, as such, would be expected to have very low ionization efficiencies in negative ion mode ESI (Shen and Perreault, 1998). The salt-derived peaks in the blank were clearly separated in each nominal mass window from those of the analyte DOM, and as such were readily discarded and eliminated from consideration in the dataset. Besides removing the blank peaks by the way we mentioned earlier in the data analysis section, we also discarded all peaks with a mass defect ≥ 0.7 in all samples.

Molecular information retrieved by the mini-ED system for low salinity samples—To evaluate the effectiveness of the mini-ED system for recovery of DOM molecular information, mass spectra were compared for samples before and after desalting. This was accomplished by analyzing samples that contained no salt, and samples with low enough levels of salts that they could be analyzed directly by FTICR-MS. Here we used two closely-spaced samples from the lower Congo River system: Congo River site (salinity 0 PSU) and Congo estuary site (salinity 0.2 PSU). The first of these has been well characterized and is representative of DOM from major tropical rivers (Spencer et al., 2009; Stubbins et al., 2010). Both samples were amenable to direct analysis on the FTICR-MS, yielding well-resolved mass spectra (Figure 2a and 2c). The mass spectrum of the river sample shows typical characteristics for DOM derived from terrestrial biomass (e.g. clusters of peaks between 0.0 and 0.4 Da at each nominal mass

extending m/z range from 200 to 600 Da; Sleighter and Hatcher, 2008). Molecular formula information obtained from the FTICR-MS data covered all the typical compound classes in the van Krevelen diagram (Figure 3a). In the expanded mass spectral region of the estuary sample (Figures 2d, f, and h), most peaks were common to the river water sample (Figure 2b). However, the estuary sample contained additional peaks with mass defects approximately from 0.7 to 0.8 displayed over the whole m/z range from 200 to 600 (Figure 2d; Table 1) which were likely due to the presence of salts in the estuarine sample. The number of peaks with low mass defects, i.e. between 0.00 and 0.06, was significantly lower for the estuary sample than the river sample (compare Figures 2b and 2d, this pattern was common at nominal masses throughout the spectrum, also see Table 1). These low-mass-defect peaks should have been present in both samples, due to their proximity in the Congo River. The absence of these peaks in the spectrum of the estuary sample is probably because non-volatile salts such as NaCl interfere with spray formation and suppress ionization by forming salt-solvent adducts (Brown and Rice, 2000). The presumption that the presence of salt suppressed the ionization of DOM causing the absence of low-mass-defect peaks was made with the expectation that the two water samples were identical except in salinity. This may not be the case and the observation of diminished signals in the low-mass-defect region may have arisen from inherent differences in the DOM at the two sites.

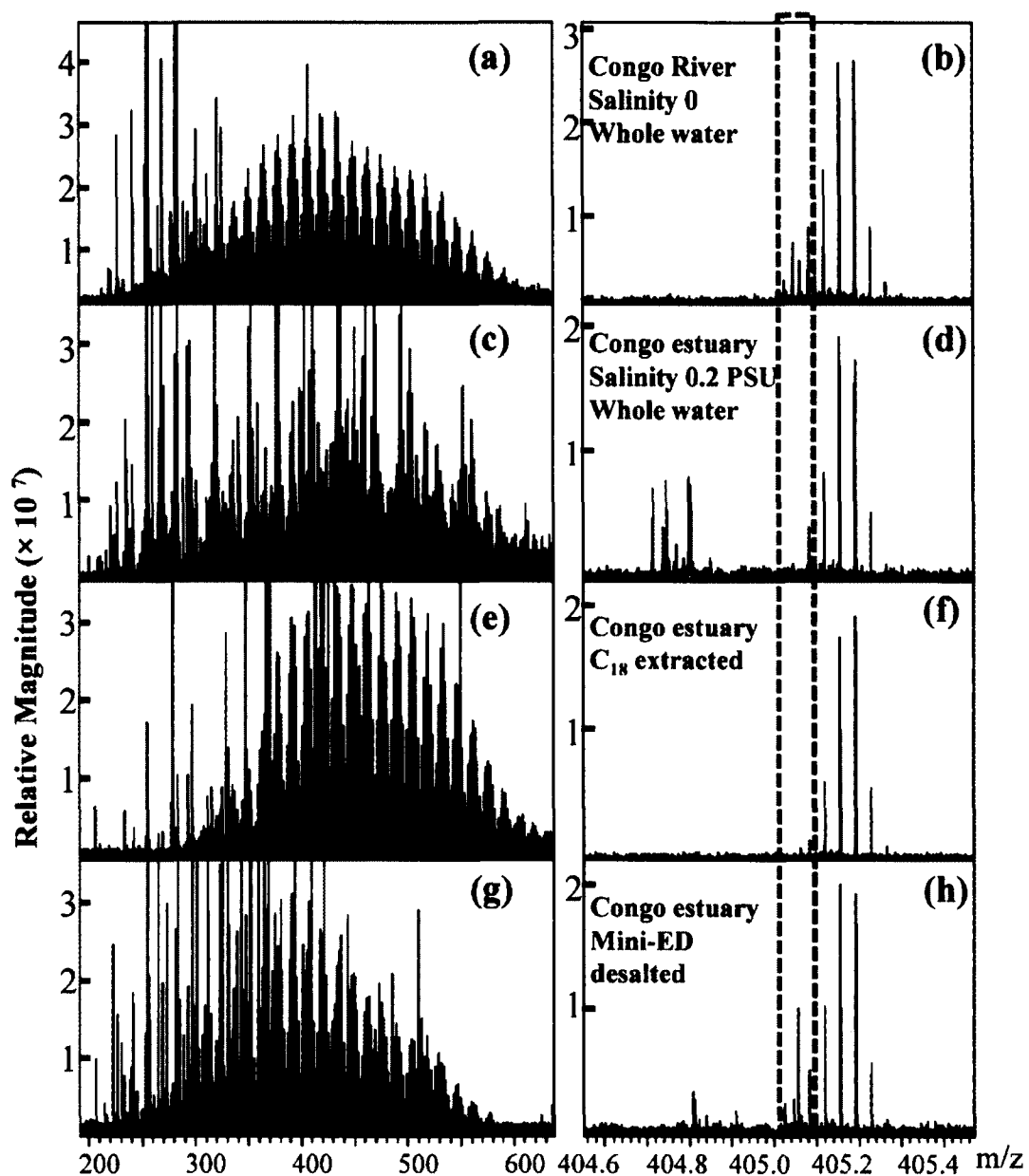


Figure 2. Negative ESI FTICR mass spectra of DOM from the Congo River and estuary. The spectra of untreated water (a, b, c, and d), C_{18} -extracted water (e and f), and water desalted by the mini-ED (g and h) are shown. On the left, full spectra are displayed while on the right each expanded region m/z between 404.50 and 405.50 is shown. The boxed-in area represents peaks with mass defects between 0.00 and 0.06.

Table 1

The number of peaks in the Congo River and estuary water DOM (S/N above 4).

Sample	Total	mass defect ≥ 0.7	mass defect 0.00 to 0.06
Congo River, Whole water	3215	62	421
Congo estuary, Whole water	2808	986	41
Congo estuary, C ₁₈ extracted	2232	139	19
Congo estuary, mini-ED desalted	2021	505	173

Desalting the estuarine sample by both C₁₈ extraction and mini-ED allowed these two methods of salt removal to be evaluated and the molecular information they retain to be compared to whole water spectra where salt removal was not employed. The mass spectra obtained for these two sample-processing methods are shown in Figure 2e and Figure 2g. Salt peaks were significantly removed by both desalting methods (Figures 2f and 2h; Table 1). A number of peaks with mass defects between 0.00 and 0.06 appeared in the FTICR-MS spectra of the estuary sample following mini-ED desalting (boxed-in Area, in Figure 2; Table 1). These peaks also occurred in the Congo river sample as mentioned above, but they were not observed following C₁₈ extraction, suggesting that the SPE method discriminates against these molecules. We can exclude the possibility that these low-mass-defect peaks were from the mini-ED blank because we did not observe them in the blank test. These peaks represent compounds either with low H/C ratios or with high O/C ratios such as tannin-like compounds (Figure 3). A similar discrimination was observed with DOM isolation by C₁₈ (Sleighter and Hatcher, 2008) and was attributed to the fact that these molecules are hydrophilic and not readily extracted by the resin.

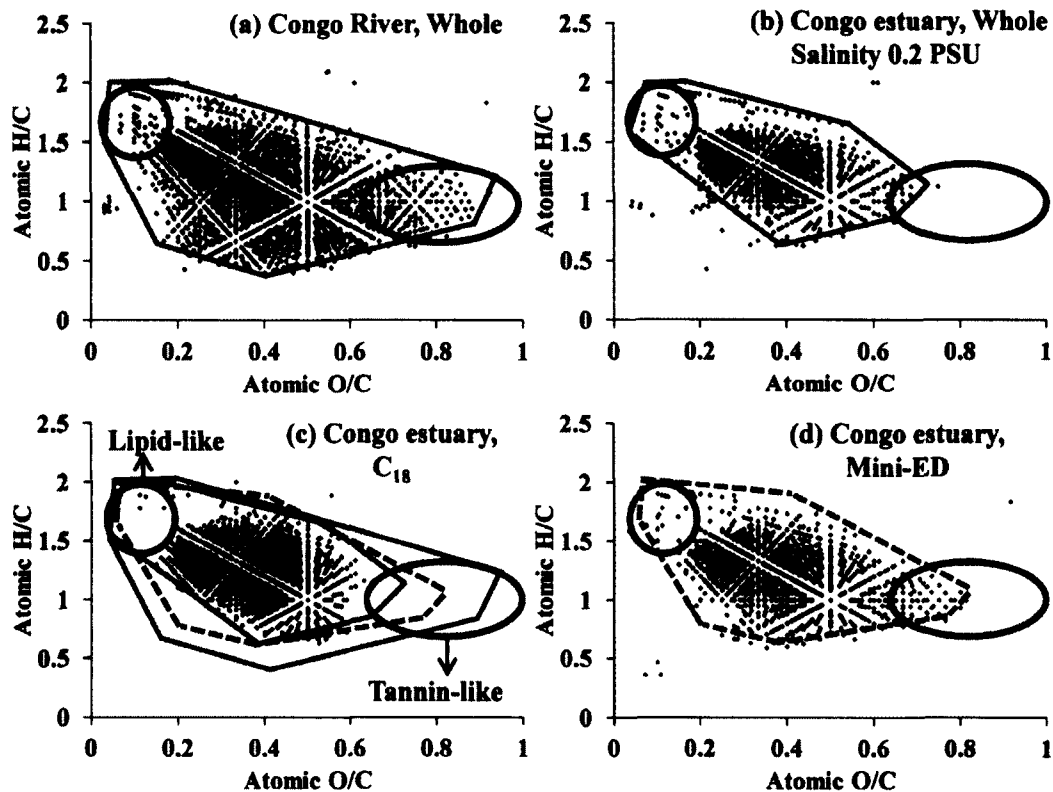


Figure 3. van Krevelen diagrams for the DOM, obtained from the assigned formulas (CHO-only) in each sample. Angular colored boxes represent the regions of main data coverage for each sample. Regions defined in diagrams (a), (b), and (d) are also plotted in diagram (c) to show the relative coverage compared to the sample extracted by C₁₈. Circled areas represent regions in which tannin-like and lipid-like compounds are normally observed.

Molecular information retrieved by the mini-ED system for higher salinity samples—The salinity for seawater is normally above 35 PSU. So it was important to evaluate the mini-ED system using samples with salinities greater than those for the

Congo estuary sample. However, FTICR mass spectra for high salinity samples are not attainable without salt removal. This makes the comparison of FTICR-MS data before and after mini-ED impossible for seawater. Instead artificial salts were added to the Dismal Swamp freshwater DOM (DOC ~ 40 mgC L⁻¹). Prior to salts addition, the mass spectrum of diluted Dismal Swamp sample (DOC ~ 10 mgC L⁻¹) was obtained. The Dismal Swamp sample was then mixed with high salinity MilliQ water to yield samples with a DOC of 10 mgC L⁻¹ and salinities of 15 PSU and 35 PSU. The resultant samples were then desalted using the mini-ED system. A further aliquot of diluted Dismal Swamp water (DOC ~ 10 mgC L⁻¹) without addition of any salts was also processed using the mini-ED system. The resultant samples were analyzed by FTICR-MS. The addition of salts resulted in residual salt peaks with mass defects of 0.7 to 0.8 that could not be completely removed. However, other than peaks assigned to salts, the peak distribution within each nominal mass window was well preserved (Figure 4). Other differences between the treatments' mass spectra were minor. The mass spectra for the two desalted samples were near-identical, indicating the combined mini-ED / FTICR-MS technique delivered reproducible results as found for replicate analyses of untreated Dismal Swamp samples (Sleighter et al., 2010).

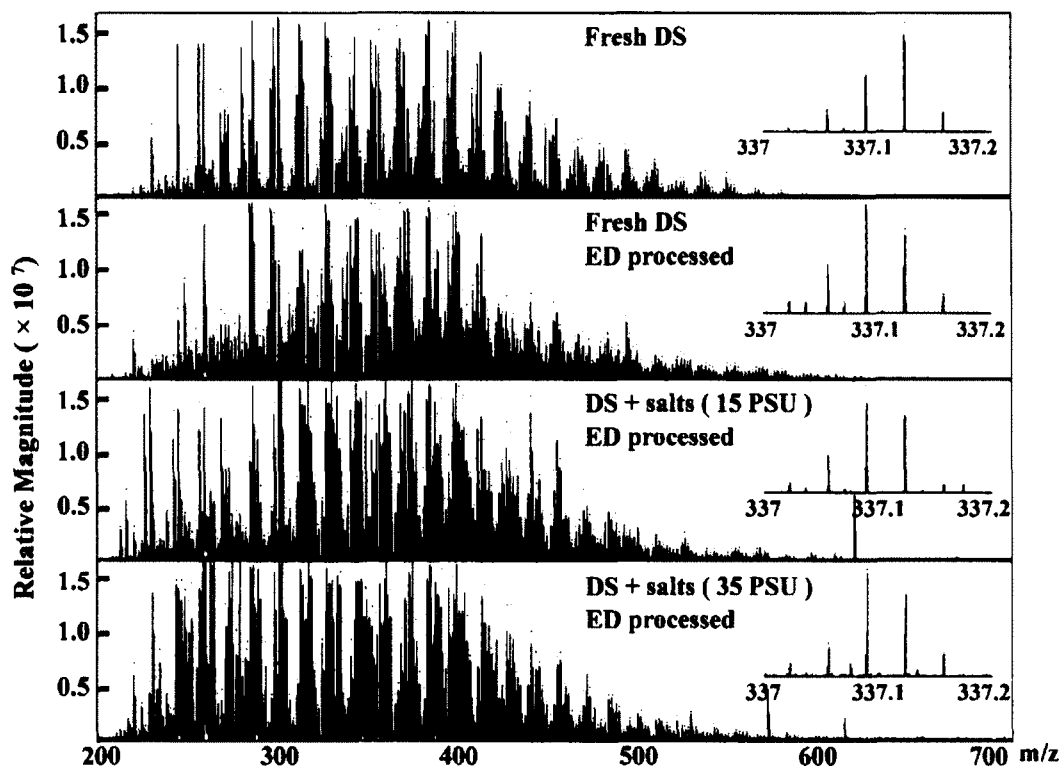


Figure 4. Negative ESI FTICR mass spectra of fresh Dismal Swamp (DS) DOM and mini-ED processed Dismal Swamp samples from different salinity level. The inset shows the region m/z between 337.0 and 337.2 as an example of the similarity among spectra.

To further examine the molecular signatures retrieved using mini-ED, molecular formulas for peaks in the desalted and original Dismal Swamp samples were compared. Above 80% of peaks in each treatment were successfully assigned formulas, which is promising for comparison. Table 2 summarizes the information of peaks and assigned molecular formulas retrieved in each treatment. The number averaged percentage (% a in Table 2) and magnitude-weighted percentage (% b in Table 2) were calculated with the same equation formulated by Sleighter et al. (2009).

Number averaged % = (Number of each formula type / Total number of formulas)
× 100

Magnitude-weighted % = (Sum of peak magnitudes of each formula type /
Summed total peak magnitude) × 100

After mini-ED the percentage of peaks assigned a molecular formula decreased from above 95% in the fresh Dismal Swamp DOM to below 90% in the mini-ED desalted DOM. This was attributed to the samples after mini-ED containing more heteratomic molecular formulas, which are more difficult to assign molecular formula than are CHO-only formulas. The total number of formulas in each of the four Dismal Swamp treatments are close to each other and the percentages are in the same order as the CHO-only formulas dominate in each treatment, indicating that the DOM after mini-ED is similar to the fresh Dismal Swamp DOM. The desalted samples provide similar mass spectral data, suggesting the mini-ED method isolates a reproducible fraction of the DOM. The major difference is that in the desalted Dismal Swamp (35 PSU) DOM, there is a higher percentage of CHON formulas and more formulas with atomic N/C ratios above 0.1 (Table 3). N/C ratios of 0.0 to 0.1 suggest long-chain alkyl amines, while N/C ratios of 0.1 to 0.4 suggest peptides and proteins (Sleighter and Hatcher, 2007). The occurrence of more peptides or proteins in the desalted 35 PSU Dismal Swamp DOM than in the 15 PSU treatment is not readily explained and further work is required to address this potential mini-ED fractionation effect.

Table 2

The percentage of peaks assigned a molecular formula, the total number of formulas, the number averaged percentage (% a) and magnitude-weighted percentage (% b) of each type of molecular formula present in each sample, excluding the instrumental blank peaks and peaks due to ^{13}C isotope. CHONSP includes CHOS, CHOP, CHONS, CHONP, CHOSP, and CHONSP formulas.

Sample	% of Peaks assigned formulas	# Formulas	CHO		CHON		CHONSP	
			% a	% b	% a	% b	% a	% b
DS	96.4	1488	94.4	97.9	3.7	1.4	1.9	0.8
DS, ED processed	81.2	1572	86.2	92.9	7.1	2.9	6.7	4.2
DS + salts (15 PSU), ED processed	84.7	1379	81.2	87.1	8.8	4.1	10.0	8.8
DS + salts (35 PSU), ED processed	88.9	1387	72.6	79.9	18.2	12.1	9.2	8.0

Table 3

The number averaged percentage (% a) and magnitude-weighted percentage (% b) of each type of CHON formulas identified in each sample.

Sample	N/C < 0.1		0.1 < N/C < 0.4	
	% a	% b	% a	% b
DS	96.4	96.4	3.6	3.6
DS, ED processed	92.0	91.4	8.0	8.6
DS + salts (15 PSU), ED processed	92.6	89.7	7.4	10.3
DS + salts (35 PSU), ED processed	79.1	81.7	20.9	18.3

In each treatment the majority of peaks were assigned as CHO-only formulas. Van Krevelen diagrams for the CHO-only formulas show the four treatments to have

considerable overlap (figure not shown). There is no specific area in the diagrams showing any unique formulas from one treatment to the other. As no systematic differences were apparent from visual inspection of the van Krevelen diagrams of the CHO-only formulas that were assigned to various compound classes following Stubbins et al. (2010). Carboxylic-rich alicyclic molecules (CRAM) are a class of molecules hypothesized to dominate the refractory DOM pool of the oceans and are defined as having $\text{DBE/C} = 0.30$ to 0.68 ; $\text{DBE/H} = 0.20$ to 0.95 ; $\text{DBE/O} = 0.77$ to 1.75 (Hertkorn et al., 2006). Aliphatics are defined as having $\text{DBE/C} < 0.3$ and H/C 1.0 to 3.0 (Perdue, 1984). Aromatics are defined by having high aromaticity index (AI; Koch and Dittmar, 2006). AI is calculated from molecular formula as: $\text{AI} = (1 + \text{C} - \text{O} - 0.5\text{H}) / (\text{C} - \text{O})$. When $\text{AI} > 0.5$, the corresponding molecular formulas are determined to be aromatic. Tannin-like formulas are defined as those having atomic O/C ratios between 0.60 and 0.95 and atomic H/C ratios between 0.55 and 1.40 . This is inferred from Sleighter and Hatcher (2007). The percentages of each compound class in each sample are similar (Table 4), suggesting that the mini-ED method recovers DOM representative of the whole initial DOM. The major difference here is that in the mini-ED desalted samples, the percentage of CRAM-like formulas decreased but the percentage of tannin-like formulas increased. This suggests that the mini-ED retains tannins-like compounds preferentially to CRAM-like compounds. In oceanic DOM samples, which do not contain much tannin-like material, this problem may be avoided.

Table 4

The number averaged percentage (% a) and magnitude-weighted percentage (% b) of each type of CHO-only formulas identified in each sample.

Sample	CRAM-like		Aliphatics		Aromatics		Tannin-like		Others	
	% a	% b	% a	% b	% a	% b	% a	% b	% a	% b
DS	59.1	71.6	4.5	3.9	8.2	4.4	19.6	15.8	8.6	4.3
DS, ED processed	49.8	60.4	2.1	1.8	13.8	9.0	24.7	26.9	9.5	1.9
DS + salts (15 PSU), ED processed	51.5	56.7	4.8	3.6	7.1	4.1	30.3	33.2	6.3	2.4
DS + salts (35 PSU), ED processed	47.0	47.6	8.5	9.1	4.8	2.9	33.1	33.5	6.7	7.0

DOC recovery—DOC recovery experiments were initially planned to be conducted together with each sample desalting process prior to FTICR-MS analysis. However, the desalted sample volume (1.5 mL) was not enough to fulfill both FTICR-MS analysis and DOC measurement. Therefore, DOC recovery was determined in a separate set of test. Freshwater from the Dismal Swamp, which had an original DOC of 40 mgC L⁻¹, was 1:3 (v:v) diluted with artificial seawater to a DOC concentration of 10 mgC L⁻¹. Two different salinity levels of artificial seawaters were used and the salinity was adjusted accordingly to ~15 PSU and ~35 PSU. The saline samples were then desalted using mini-ED as all the real samples were treated. The test with an adjusted salinity of ~15 PSU gave a DOC recovery of ~57%. The test with an adjusted salinity of ~35 PSU gave a DOC recovery of ~55%. Note that the DOC recovery calculation here was corrected by excluding the contamination DOC (~2 mgC L⁻¹) mentioned above (Section '*Blank test*'). These recoveries are somewhat similar to recoveries of terrestrial

DOM obtained using the C₁₈ extraction methodology (Kim et al., 2003; Mopper et al., 2007; Simjouw et al., 2005) or ultrafiltration (Benner and Opsahl, 2001; Buesseler et al., 1996; Guo and Santschi, 1996; Hernes and Benner, 2006). However, when compared with the large-scale RO/ED methodology that typically shows recoveries of better than 75% (Koprivnjak et al., 2009; Vetter et al., 2007), the mini-ED system is not as effective at retaining DOM. This may be due to the use of a 500 Da mini-ED membrane rather than the 300 Da membrane that is commonly used in the larger RO/ED system (Vetter et al., 2007; membrane cutoff information obtained from personal communication with Dr. Mike Perdue at Georgia Institute of Technology). Much of the lost DOC (~45% of the initial DOC), may end up in the surrounding MilliQ water in the mini-ED system. Future work should determine carbon mass balances for the system and the molecular classes of compounds lost to the surrounding MilliQ bath water. While recoveries are lower than the large-scale RO/ED system, the mini-ED does not show fractionation as observed in C₁₈ extraction approaches. The FTICR-MS spectra are representative of the whole DOM offering a method for the isolation of DOM from saline waters without the loss of DOM molecular information.

4. Comments and Recommendations

Mini-ED is an efficient method for desalting small volume (0.5 to 10 mL) samples prior to analysis by ESI FTICR-MS. More representative molecular information can be expected from this method when compared with C₁₈ extraction. Contamination from the mini-ED system does not significantly affect ESI FTICR mass spectra. If mini-ED is applied to desalt samples prior to other analyses, e.g. HPLC or NMR, analysis-specific blanks and recoveries should be assessed. In this regard, future study should

attempt to find a source of other membrane and bath materials to reduce contamination, thereby enabling coupling of mini-ED to other analytical techniques. Significantly, the desalting approach described here can be done quite easily on small amounts of sample either aboard ship or in the laboratory. The small sample size requirement makes this technique amenable to studies of pore waters and other environmental samples and experimental designs where large water volumes are not feasible. There are still a lot of tests to be completed to optimize this method, such as looking for bigger chambers to minimize the processing time. An important consideration when coupling to other analytical techniques will be the DOC mass balance. It is also unknown how the DOC recovery will change under different initial DOC concentrations and qualities. Testing the system with real oceanic DOM samples, which are both much lower in DOC concentration and chemically distinct from those samples studied herein, is a major priority. Finally, as part of this oceanic sample isolation, the mini-ED performance should be systematically compared with currently available DOM isolation techniques such as PPL extraction, ultrafiltration, and the larger volume RO/ED.

CHAPTER III

**ULTRAHIGH RESOLUTION MASS SPECTROMETRIC DIFFERENTIATION
OF DISSOLVED ORGANIC MATTER ISOLATED BY COUPLED REVERSE
OSMOSIS-ELECTRODIALYSIS FROM VARIOUS MAJOR OCEANIC WATER
MASSES**

PREFACE

The content of this Chapter was published in 2014 in *Marine Chemistry*, and below is the full citation. The formatting here has been altered to incorporate the supporting information and additional results of C₁₈ isolated DOM into the body of the manuscript.

See Appendix A for the copyright permission.

Chen, H., Stubbins, A., Perdue, E. M., Green, N. W., Helms, J. R., Mopper, K., and Hatcher, P.G., 2014. Ultrahigh resolution mass spectrometric differentiation of dissolved organic matter isolated by coupled reverse osmosis-electrodialysis from various major oceanic water masses. *Marine Chemistry*, 164: 48-59.

1. Introduction

Marine dissolved organic matter (DOM) is important to numerous key oceanic biogeochemical processes because it is one of the largest pools of dynamic carbon on the earth (Hedges, 1992). The marine DOM pool is composed of a tremendous number of molecules of varying complexity derived from biota present in the water, molecules from organisms that have previously inhabited the water, and chemically and biologically altered autochthonous and allochthonous biomolecules (Carlson, 2002). The detailed

composition and structure of marine DOM is a potential treasure-trove of information relating to its source, reactivity and fate, as well as its alterations during transport (Hedges, 1992).

A complete detailing of the chemical composition of DOM, and its origin, structure and function in the global carbon cycle is hampered by the limited application of advanced techniques to desalt, concentrate, isolate and then molecularly characterize marine DOM. The commonly used techniques to concentrate and isolate marine DOM are tangential-flow ultrafiltration (e.g. Benner et al., 1992; Buesseler et al., 1996) and solid phase extraction (SPE) with XAD resins (e.g. Lara and Thomas, 1994a, 1994b; Meyers-Schulte and Hedges, 1986; Stuermer and Harvey, 1977), C₁₈ material (e.g. Kim et al., 2003; Sleighter and Hatcher, 2008) or PPL (e.g. Dittmar et al., 2008), which all fractionate the total marine DOM pool to varying degrees (Mopper et al., 2007). Here we have applied a recent technique using reverse osmosis coupled with electrodialysis (RO/ED), which can isolate an average of 75% of marine DOM (Green et al., 2014; Koprivnjak et al., 2009), to collect DOM samples from various major oceanic water masses. Spectroscopic evidence suggests that the DOM extracted by this technique is less fractionated (i.e. more representative) than DOM extracted by other techniques (Helms et al., 2013b; Koprivnjak et al., 2009). The molar C/N ratios of RO/ED isolated DOM were more consistent with the original seawater DOM (Green et al., 2014; Koprivnjak et al., 2009). However, a higher recovery does not guarantee more diversity of compounds. To ascertain whether RO/ED can extract DOM with greater molecular diversity than other techniques, it is necessary to make molecular-level comparison of DOM extracted by different techniques. In the current study we compared the molecular quality of DOM

isolated by RO/ED and C₁₈ SPE, while, at the same time, attempting to find important molecular-level identifiers in well-known marine water masses from the world's major oceans.

Electrospray ionization combined with ultrahigh resolution Fourier transform ion cyclotron resonance mass spectrometry (ESI FTICR-MS) provided a molecular fingerprint for the DOM isolates (Sleighter and Hatcher, 2007; and references therein). ESI FTICR-MS has shown great promise in characterizing DOM at the molecular level (D'Andrilli et al., 2010; Flerus et al., 2012; Hertkorn et al., 2006; Kujawinski et al., 2004; Reemtsma et al., 2008; Sleighter and Hatcher, 2008; Stubbins et al., 2010). The ultrahigh mass resolution (average 400,000 at m/z 400) and accuracy (< 1 ppm) of ESI FTICR-MS allows the resolution of 10-20 peaks at each nominal mass (Marshall and Rodgers, 2008) and the assignment of elemental formulas to each measured peak mass. Thus, ESI FTICR-MS is able to identify specific compounds within DOM, assign unique elemental formulas, and subsequently infer compositional differences among pools of DOM based on these elemental formulas. Recently, FTICR-MS has become even more powerful as multivariate statistical analysis approaches have been introduced and applied to explore the large data sets encountered from mass spectra of DOM (Abdulla et al., 2013; Kujawinski et al., 2009; Sleighter et al., 2010).

In this study, seven sites were selected in an attempt to capture globally relevant and biogeochemically distinct pools of marine DOM, including two distant points along the global deep ocean conveyor belt, one in the Atlantic and one in the Pacific. Two DOM samples from the surface waters (5m, both core and edge area) of the productivity maximum of Senegal-Mauritanian upwelling in the North Atlantic were collected and

were expected to represent biolabile DOM on top of background refractory DOM. Another DOM sample from the surface water (5 m) of the North Pacific subtropical gyre at the ALOHA-series site was expected to be enriched in semi-biolabile DOM and highly photo-bleached DOM on top of background refractory DOM. The remaining four DOM samples were collected from deep waters from the North Atlantic (415 m and 3000 m, respectively) and the North Pacific (674 m and 3500 m, respectively) and were expected to be enriched in background refractory DOM. This focused sampling approach differs from the recent work of Flerus et al. (2012), which utilized low volume, high throughput PPL SPE extraction to examine a larger set of water samples from the Atlantic Ocean. The focused approach we employed was necessitated by the cost and time required for processing of RO/ED-collected DOM (10-12 hours per ~200 L sample).

2. Experimental methods

2.1. Sample collection

Four sites in the eastern North Atlantic Ocean were sampled aboard the R/V *Oceanus* during Cruise OC449-3 in September 2008. Water was collected from Niskin bottles on a CTD rosette. The samples include North Atlantic deep water (3000 m), oxygen minimum layer water (415 m) and two samples of high productivity surface seawater (5 m) from the Senegal-Mauritanian upwelling zone: one on the edge and one in the core region. The water from the core area had a lower temperature but higher chlorophyll fluorescence than the edge sample (Table 5). Water from the North Pacific Ocean was collected aboard the R/V *Kilo Moana* at the ALOHA Hawai'i Ocean Time series site (<http://hahana.soest.hawaii.edu/hot/>) in September 2009 from near surface (5 m) in the subtropical gyre and from North Pacific Deep Water (NPDW; 3500 m).

Intermediate water (674 m) from the North Pacific Ocean was collected at the Natural Energy Laboratory of Hawaii Authority (NELHA). At NELHA, seawater was pumped through a 1915 m long, 1 m diameter high-density polyethylene pipeline into the laboratory where it was filtered and processed by RO/ED. Multiple 674 m water samples were processed by RO/ED, using approximately 200 L of initial seawater per day, in order to examine sampling variability of the RO/ED technique (see Green et al., 2014 for more information on the site and the collection of these samples). Table 5 lists relevant oceanographic parameters for each sample. These samples were also characterized by nuclear magnetic resonance (NMR) spectroscopy by Helms (2012) except the North Atlantic Senegal-Mauritanian upwelling edge region sample. The North Pacific samples were named as ALOHA samples in Helms (2012). The absorbance, fluorescence and photoreactivity of a NELHA deep water sample are presented in Helms et al. (2013b).

Table 5

Location and seawater properties at each sampling site.

Sample	Longitude (°W)	Latitude (°N)	Temperature (°C)	Salinity	Chlorophyll (mg m ⁻³)
N. Atlantic Upwelling Edge_5 m	17.508	19.921	25.1	36.1	508
N. Atlantic Upwelling Core_5 m	17.406	20.161	23.1	36.0	873
N. Atlantic_415 m	21.487	18.995	12.5	35.5	0
N. Atlantic_3000 m	23.397	18.485	2.7	35.0	0
N. Pacific_5 m	158.00	22.450	25.0	35.2	n.d.
N. Pacific_674 m	156.05	19.715	6.0	34.3	0
N. Pacific_3500 m	158.00	22.450	< 4.0	34.6	0

n.d. – not determined.

2.2. *The isolation of DOM*

Samples were filtered through a 0.1 μm pore-size polyethersulfone capsule filter (Whatman PolycapTM TC). The RO/ED procedure has been described thoroughly in previous papers (Koprivnjak et al., 2009; Vetter et al., 2007). Briefly, the RO/ED system, tanks and lines were first rinsed in a once-through mode with 50 L of filtered seawater that was to be processed, after which up to 220 L of a seawater sample were transferred to the RO/ED system tank. An initial ED phase removed most (~75%) of the sea salts, subsequently a coupled RO/ED phase removed water and sea salts at the same rate (maintaining constant conductivity) until the volume of the sample had been minimized. At this point, additional seawater sample, if any, was added to the RO/ED system tank and the first two phases were repeated. A final ED phase was used to remove remaining sea salts from the concentrated sample. Conductivity of the samples decreased significantly from above 50 mS cm^{-1} to lower than 0.050 mS cm^{-1} (equivalent to 0.0004 mol L^{-1} of NaCl). Aliquots of 142 to 473 L of filtered seawater from each site were processed by the RO/ED system. Samples were desalted and concentrated down to about 5 L, labeled as Final sample, and stored at -20 $^{\circ}\text{C}$ prior to further analysis. After each sample, the adsorbed DOM in the RO/ED system was rinsed with a 5 L 0.01 M NaOH (Fisher Sci., certified ACS grade) solution. The rinse solutions were collected separately, labeled as Rinse sample, and frozen immediately, although they were not analyzed in the present study. The RO/ED system blank was tested by processing 200 L of artificial seawater, which was made with combusted (450 $^{\circ}\text{C}$, 5 h) NaCl and anhydrous MgSO_4 (Fisher Sci., certified ACS grade) mixed with ultrapure water (Millipore, MilliQ, resistivity $\sim 18.2 \text{ M}\Omega\text{cm}^{-1}$ at 25 $^{\circ}\text{C}$). The salts were added to ultrapure water to approach

salinity 35, with a mass ratio of 64 : 7 for NaCl : MgSO₄. Replicates (n = 3) of 200 L of artificial seawater were processed by the RO/ED system in the same manner as samples were processed. Artificial seawater DOC increased by < 2.5 μMC in all of the three replicates. This increase of DOC represents < 6% of the initial DOC (normally > 40 μMC) in oceanic water.

For comparison, DOM was isolated using commercially available C₁₈ SPE cartridges. The cartridges were cleaned with 10% methanol in water and rinsed with methanol followed by acidified Milli-Q water before use. Filtered water samples (20 L) were acidified with hydrochloric acid (p.a. grade, Merck) to pH 2 and pumped through a 60 mL solid phase extraction cartridge containing 10 g of C₁₈ (Varian Mega Bond Elut) at a flow rate of <50 mL min⁻¹. After loading, the cartridges were rinsed with 100 mL acidified (pH 2) Milli-Q water to remove residual salts. The cartridges were stored at - 20 °C. The DOM was eluted with 50 mL methanol at a flow rate <10 mL min⁻¹ prior to analysis. Methanol in the eluates was rotary evaporated, and the DOM was redissolved in water and stored at - 20 °C until FTICR-MS analysis.

2.3. DOC/TDN measurements

Dissolved organic carbon (DOC) and total dissolved nitrogen (TDN) concentrations for filtered samples and RO/ED processed final samples were determined as non-purgeable organic carbon (NPOC) by high temperature combustion (720 °C) on a Shimadzu TOC-V_{CPH} (Shimadzu Scientific Instruments). Standard calibration curves were made with potassium hydrogen phthalate (KHP) and potassium nitrate (KNO₃) to quantify the DOC and TDN concentrations, respectively. Blanks and reference standards were inserted between samples. Reference standards for low carbon water and deep

seawater obtained from the Consensus Reference Materials Project, Hansell Laboratory, University of Miami, were used to monitor the performance of the instrument (Doval and Hansell, 2000). Routine minimum detection limits in the investigators' laboratory using the above configuration are $2.8 \pm 0.3 \mu\text{MC}$ and standard errors are typically $1.7 \pm 0.5 \%$ of the DOC concentration (Stubbins and Dittmar, 2012).

2.4. Total dissolved carbohydrate measurement

Total dissolved carbohydrate (TCHO) was determined using the MBTH (3-methyl-2-benzothiazolinone hydrazone hydrochloride) colorimetric method (Burney and Sieburth, 1977; Johnson et al., 1981). Samples were hydrolyzed in acid (0.09 N HCl final concentration) for 20 h at $105 \text{ }^\circ\text{C}$. A standard of soluble starch was used to test the recovery, and the yield of monosaccharides from the hydrolysis of starch was $90 \pm 2\%$ (triplicate hydrolysis tests). TCHO concentrations were measured as total monosaccharide concentrations after hydrolysis, which include the free monosaccharide in the sample before hydrolysis and the monosaccharide from the hydrolysis of polysaccharides, and were quantified using a calibration curve made from D-glucose (Sigma).

2.5. ESI FTICR-MS Instrumentation

DOM samples were analyzed on a Bruker Daltonics 12 Tesla Apex Qe FTICR-MS at the College of Sciences Major Instrumentation Cluster (COSMIC) at Old Dominion University with electrospray source in the negative ionization mode. In the COSMIC laboratory, prior to negative ESI FTICR-MS, DOM samples are routinely mixed with methanol and, for acidic samples, ammonium hydroxide (NH_4OH) is added immediately prior to ESI to bring the pH up to 8 to increase ionization efficiency. The

RO/ED samples had ~neutral pH, so they were run: 1) without additions, and 2) with dilution 50:50(v/v) with LC-MS grade methanol containing 0.1% NH₄OH. The C₁₈ extracted DOM samples, which had been rotary evaporated and redissolved in H₂O, had a lower pH. Therefore, all C₁₈ samples were diluted (50:50) with LC-MS grade methanol containing 0.1% NH₄OH prior to analysis. Results for the C₁₈ samples were compared with the results from the RO/ED samples that were also diluted with LC-MS grade methanol containing 0.1% NH₄OH. All samples were analyzed at the same DOC concentration (833 μMC, i.e., 10 mgC L⁻¹), without counting methanol, if it was used, in the DOC concentration. Additions of ultrapure water were used for these adjustments. Samples were prepared immediately before FTICR-MS. All samples were infused into the ESI ion source using a syringe pump with an infusion rate of 2 μL min⁻¹. The spray current of ESI was monitored for all samples running, and was observed to be stable at 18-20. Ions were accumulated in the hexapole for 3.0 s before being transferred to the ICR cell. Three hundred transients were co-added for each sample and digitized with a 4 MWord data acquisition size. Both blank of water only and blank of 1:1 (v:v) methanol:water with 0.1% NH₄OH were analyzed respectively for contamination checks. Fourier transformation and magnitude calculation of the free induction decay signal was accomplished by the Bruker Daltonics Data Analysis software.

2.6. Mass spectra data processing

All samples were externally calibrated with an arginine cluster standard. Empirical molecular formula assignments for each sample's raw mass list, using peaks above a signal-to-noise ratio of 4 and a mass-to-charge (m/z) range of 200 to 700, were performed with the molecular formula calculator developed at the National High

Magnetic Field Laboratory (Molecular Formula Calc v.1.0 ©NHMFL, 1998). Formulas were assigned within a 0.5 ppm error range of the detected raw m/z but only include C, H, O, and N in the calculation. A list of molecular formulas with C, H, O and/or N commonly present in each sample was obtained for internal linear calibration, ensuring that at least 1 calibrant peak existed every 14 m/z units (i.e., every CH_2) across the mass spectra.

Mass lists for all samples after internal calibration were then exported for further data analysis. Peaks detected in corresponding solvent blanks and in sample spectra (difference within 0.5 mDa) were removed from the mass lists and from further consideration. Molecular formula calculation was performed on the internally calibrated mass list using the same calculator as above by adding sulfur and phosphorus into consideration. The allowed number ranges of each element in the formulas were set as: carbon (2-50), hydrogen (2-120), oxygen (0-30), nitrogen (0 to 6), sulfur (0-2), and phosphorus (0-2). Formulas, after the correction of hydrogen values considering ionization (i.e., adding one hydrogen to the formulas in negative ion mode), with an error value of <0.5 ppm were screened to eliminate those that are highly unlikely or impossible to occur in DOM, leaving only formulas that met the following criteria (Chen et al., 2011; Stubbins et al., 2010): 1) $2 \leq H \leq (2C+2)$; 2) $O \leq (C+2)$; 3) $O/C < 1.2$; 4) $0.333 \leq H/C \leq 2.25$; 5) $N/C < 0.5$; 6) $S/C < 0.2$; 7) $P/C < 0.1$; 8) $(S+P)/C < 0.2$; 9) $P < O/3$.

The remaining formulas were sorted to obtain unique formulas (i.e., m/z value with only one possible formula) and peaks with multiple possible formulas. Then a Kendrick Mass Defect (KMD) analysis was performed using those unique formulas to find the multiple formulas which can be included as part of KMD series, as KMD

analysis identifies homologous series (e.g. formulas progressively differ by CH₂, OCH₂, COO, H₂, H₂O, O, etc.) of compounds within a sample (Sleighter and Hatcher, 2007). Consequently, if there are multiple formulas for one m/z value, the one that falls within a homologous series is retained as the more likely one. And if there were more than one homologous series assigned to the same series of detected masses, the series that was the longest, i.e., containing the most formulas, was chosen as the result.

3. Results and discussion

3.1. Recovery of DOM

RO/ED DOC yields are presented in Table 6. Only the Final samples were characterized by FTICR-MS. In more recent application of the RO/ED method, the Final and Rinse solutions are both desalted and combined to yield a single sample (Zhang et al., 2013). Previous studies of marine DOM by the RO/ED method have reported the average yields of DOC, showing greater variability in recovery when samples are collected over a wide geographical area than when all samples are isolated at the same sampling location. For example, the overall average DOC yields from 16 seawater samples across a coastal transect at different depths were reported as $75 \pm 12\%$ (including the Rinse solutions, Koprivnjak et al., 2009), although the average DOC yields from NELHA deep (674 m) seawater were reported as $82 \pm 3\%$ (including the Rinse solutions; 9 samples in total; Green et al., 2014) and the DOC yields from NELHA surface (21 m) seawater were reported as $75 \pm 5\%$ (including the Rinse solutions; 5 samples in total; Green et al., 2014). So the variability in yields of DOC is related to geographical variability, and compositional variability in DOC may be the connecting link. Recoveries in the present study were generally consistent with previously reported yields (Green et

al., 2014; Koprivnjak et al., 2009) except for the North Atlantic 415 m oxygen minimum layer water (46%, excluding the Rinse sample) and the North Atlantic 3000 m deep water (40%, excluding the Rinse sample) (Table 6). These two samples were the first two samples processed on our new RO/ED system, which, for lack of time, was not conditioned adequately prior to use. Even though recoveries were low relative to the subsequent samples, the ultraviolet-visible absorbance properties and the nuclear magnetic resonance spectra were similar to the other, higher DOC recovery samples (Helms, 2012). Thus, we think it is likely that the loss of DOM during the RO/ED process was non-selective. Consequently, we have included the data of these two samples – the North Atlantic 415 m and the North Atlantic 3000 m – in this study, although we understand that caution needs to be taken in the discussion.

DOC of the samples subjected to C_{18} extraction was not successfully measured because methanol was not removed completely. Thus, we cannot specify an exact recovery of DOC. But, based on previous studies with C_{18} extraction, the DOC recovery was likely in the range of 20~30% for oceanic water (Louchouart et al., 2000).

Table 6

Mass balance analysis of the RO/ED isolated DOM samples.

Sample	Volume (L)			DOC (μ MC)			Yield (%)		
	Initial	Final	Rinse	Initial	Final	Rinse	Final	Rinse	Total
N. Atlantic Upwelling Edge_5 m	401	6.8	4.2	85	3884	936	77	12	89
N. Atlantic Upwelling Core_5 m	473	6.6	4.3	88	4298	1104	68	11	79
N. Atlantic_415 m	365	5.9	4.6	54	1523	421	46	10	56
N. Atlantic_3000 m	355	5.4	4.5	41*	1076	323	40	10	50
N. Pacific_5 m	142	6.1	4.4	69	1325	435	83	19	102
N. Pacific_674 m (1)	219	6.4	5.2	44	1006	267	67	14	81
N. Pacific_674 m (2)	220	8.3	5.2	44	790	168	68	9	77
N. Pacific_674 m (3)	220	6.4	5.3	44	1006	260	67	14	81
N. Pacific_3500 m	249	6.7	5.6	39*	1254	343	86	20	106

* DOC values from previous studies (Hansell and Carlson 1998; Carlson et al. 2010). Measured DOC were higher, 62 μ MC (N. Atlantic 3000 m) and 52 μ MC (N. Pacific 3500 m), and were likely contaminated during the sub-sample collection.

3.2 Comparison of RO/ED-extracted DOM and C₁₈-extracted DOM

A comparison of molecular formulas between DOM samples that were extracted using RO/ED and C₁₈ SPE was conducted at two North Atlantic sites: the oxygen minimum layer (415 m) and the Senegal-Mauritanian upwelling edge region surface (5 m). A notable difference is that there are significantly higher percentages of CHON compounds extracted by RO/ED compared to the C₁₈ method (Table 7) confirming previous reports that C₁₈ SPE discriminates against N-containing compounds (Kim et al., 2003; Sleighter and Hatcher, 2008). Meanwhile, molar C/N ratios of the isolated DOM by RO/ED in this study are falling in the range of 17-20, which is very close to the

reported DOC/DON ratios for surface waters and deep waters (Bronk, 2002). Thus, the higher N-content in RO/ED isolated DOM is rather representative of the actual composition than over-representing the N-content. In addition, the RO/ED method extracts compounds with high O/C atomic ratio (>0.6) that are absent in the C_{18} SPE DOM. This trend is found in both CHO and CHON compounds (Figure 5) and in both the North Atlantic 415 m and upwelling edge 5 m samples. Similar results have been reported when comparing mini-electrodialysis extracts with those from C_{18} SPE (Chen et al., 2011). The C_{18} SPE selects for molecules having a lower O/C ratio (below 0.2) and molecules having lower H/C ratio (below 1.0), in both CHO and CHON formulas (Figure 5). These molecules are enriched in C_{18} SPE DOM probably because they are more hydrophobic. In both sites, C_{18} SPE DOM has more formula assigned peaks than RO/ED isolated DOM (Table 7). In the N. Atlantic 415 m, the percentages of FTICR-MS peaks common in both, only in RO/ED DOM, and only in C_{18} DOM are 28%, 23%, and 49%, respectively. While in the N. Atlantic upwelling edge 5 m, those percentages are 30%, 33%, and 37%, respectively. However, the higher amount of formula assigned peaks in C_{18} extracted DOM does not necessarily indicate that more types of compounds were observed in C_{18} DOM than in RO/ED DOM. From the van Krevelen diagram (Figure 5), we can see that most of the assigned formulas in C_{18} DOM are located tightly together, indicating similar atomic ratios. While the RO/ED is able to extract a higher percentage of the bulk DOC and DOM with greater ranges of O/C values than C_{18} SPE (Figure 5). Thus, RO/ED seems to obtain a more comprehensive subset of DOM molecules, providing novel insights into the character and composition of oceanic DOM as discussed below.

Table 7Comparison of assigned molecular formulas between RO/ED DOM and C₁₈ SPE DOM.

Sample	Assigned #	CHO		CHON		Others	
		%#	%w	%#	%w	%#	%w
N. Atlantic 415m_RO/ED	1631	51.3	74.1	42.2	21.4	6.5	4.4
N. Atlantic 415m_C ₁₈	2482	63.8	83.5	22.5	9.7	13.7	6.9
N. Atlantic upwelling edge 5m_RO/ED	1829	55.0	73.2	39.7	23.5	5.3	3.3
N. Atlantic upwelling edge 5m_C ₁₈	1950	62.9	74.6	22.3	9.9	14.8	15.5

%# = (Number of specific formula peaks/Total number of formula assigned peaks) × 100

%w = (Sum of peak magnitudes of specific formula peaks/Summed total peak magnitude) × 100

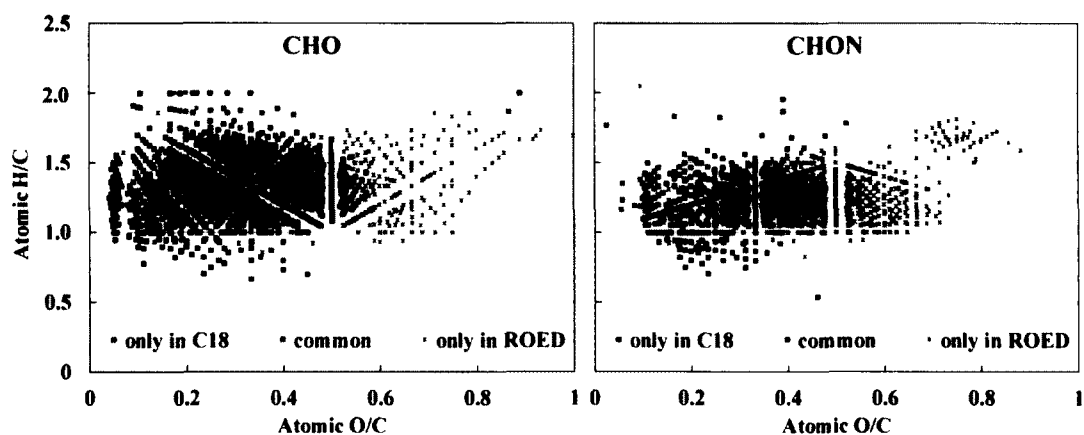


Figure 5. Comparison of RO/ED and C₁₈ extracted DOM in Van Krevelen diagram using CHO (left) and CHON (right) formulas from the North Atlantic Senegal-Mauritanian upwelling edge region 5 m sample.

3.3. General characteristics of ultrahigh resolution mass spectra

The major difference between the spectra from samples analyzed without additions of organic solvent and samples to which MeOH and NH₄OH were added is observed in the m/z range of 200-300. Peaks in this range stand out above all others in the mass spectra of samples mixed with MeOH and NH₄OH, but they are almost absent in the untreated samples (Figure 6). These peaks are identified to be fatty acids, which are often observed in high abundance due to very high ionization efficiencies compared to the rest of the DOM (Koprivnjak et al., 2009; Sleighter et al., 2008), but they are also abundant in the instrument blank. By removing these peaks from the mass spectra of samples mixed with MeOH and NH₄OH, we obtain a similar total number of peaks as the mass spectra of untreated samples, but peak intensity was significantly different because some peaks were suppressed by those high fatty acids peaks due to ion competition. Therefore, we focused the data analysis only on spectra analyzed without additions of MeOH and NH₄OH. Accordingly, this is the first report of ESI FTICR-MS obtained by directly injecting DOM-concentrated water samples without addition of other solvents such as MeOH.

Typical mass resolution (defined as $m/\Delta m_{50\%}$ where $\Delta m_{50\%}$ is the width at half-height of peak m ; average > 450,000 in present study results) and DOM mass spacing patterns were observed. The spectra are highly complex with numerous peaks per nominal mass unit as is typically observed for marine DOM (Hertkorn et al., 2006). The majority of peaks appear at odd m/z values, which indicates a predominance of zero or an even number of nitrogen atoms in the molecules. Across the entire mass range, peaks at even m/z values are mainly at 1.003355 m/z units (the mass of a neutron) higher than the

parent peak at odd m/z values and thus attributed to isomers containing one ^{13}C atom in place of a ^{12}C atom. This result indicates that most peaks are singly charged, consistent with other studies of DOM (Kim et al., 2003; Sleighter and Hatcher, 2008; Stenson et al., 2002). There are repeating patterns every 14.01566 mass units, indicating the incremental addition of a CH_2 group, which has been previously observed in mass spectra of DOM (Kim et al., 2003; Sleighter and Hatcher, 2008). Within each nominal mass, different series of peaks differing by 0.03641 m/z units are observed, which indicates the replacement of one oxygen atom with a CH_4 (Stenson et al., 2003). Even though the ROED technique removes most of the salt, there are still some peaks assigned to salts. These account for a relatively small proportion of the total of all peak magnitudes (less than about 16%; Table 8). More than 80% of total peaks (excluding ^{13}C isotopic peaks) in each sample were assigned unique formulas, which facilitates further comparison of the results among samples.

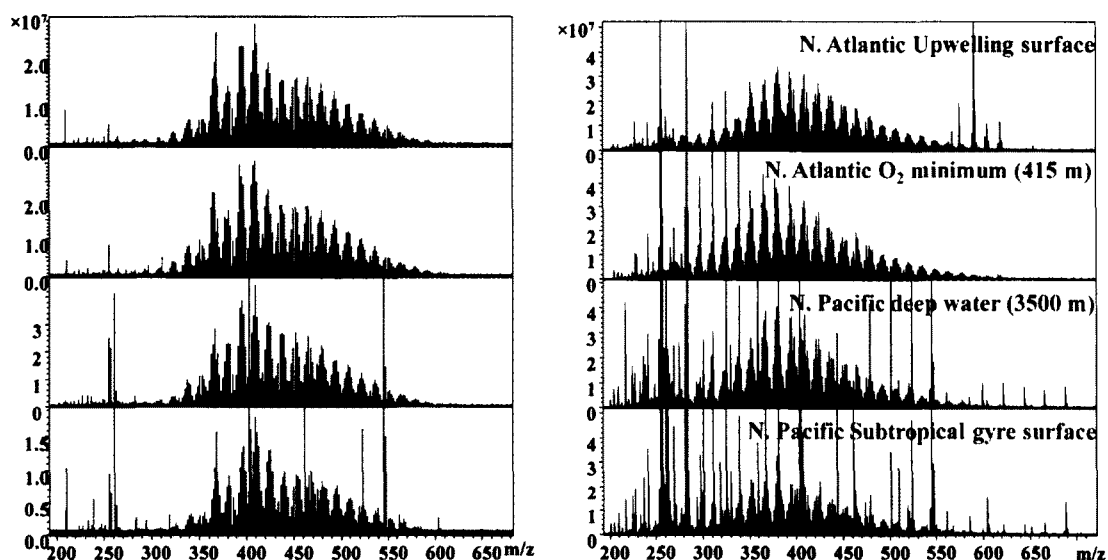


Figure 6. Representative negative ESI FTICR mass spectra of the samples. Left: analysis without organic solvent addition; Right: sample mixed with MeOH and NH_4OH .

The North Atlantic 415 m and 3000 m, and the North Pacific 5 m and 3500 m samples were analyzed in duplicate by FTICR-MS. The duplicate spectra are denoted A and B. For the North Pacific 674 m site, samples were collected over multiple days at NELHA (Green et al., 2014). North Pacific 674 m sample (1) represents RO/ED DOM isolated on day 1; 674 m (2A) and 674 m (2B) are duplicate FTICR-MS for RO/ED DOM isolated on day 2; and 674 m (3) represents RO/ED DOM isolated on day 3. The upwelling core surface sample has the highest number of peaks likely due to inputs of fresh and minimally degraded biomolecules in this area of high primary production. In contrast, the North Pacific subtropical gyre surface sample has a much lower number of peaks than the other samples. All the samples were analyzed at the same DOC concentration level so the difference for this North Pacific surface sample is probably because 1) it contains specific molecular structures not well ionized by ESI, or 2) the

sample exhibits less structural diversity and most of the peaks are of few structural types. Abiotic processes such as DOM photo-degradation are known to reduce the FTICR mass spectral complexity of DOM (Stubbins et al., 2010). Therefore the low stoichiometric diversity of DOM isolated from the subtropical North Pacific gyre may also have resulted from photo-bleaching in these intensely stratified, sunbathed waters. A significant number of “common formulas” are found in all the samples. These common peaks have higher average intensities than peaks that are not found in all samples (Table 8). The total 833 common formulas shared in most of the samples consist of 540 CHO formulas and 293 CHON formulas, with O/C 0.2-0.7 and H/C 1.0-1.6 (Figure 7; Appendix C). It is worth to mention that because N. Pacific 5 m (A) and (B) have dramatically fewer total peaks than the other samples, they were excluded from the counting of common formulas. The 833 common formulas shared in the other samples were searched in the N. Pacific 5 m (A) and (B) samples, which resulted in 627 and 603 matching formulas, respectively (Table 8). When comparing samples analyzed by FTICR-MS, it is important to account for analytical variation and the fact that many DOM molecules are present in all samples. The analytical error for the mass spectrometer and methods applied here dictate that the mass spectra of two samples must differ by more than 33% of each sample’s total peak number in order for there to be a statistically significant difference based on the presence / absence of peaks between the samples (Sleighter et al., 2012). Due primarily to the similarities of DOM between samples, this 33% threshold is not met. Thus, differences between samples were addressed based upon relative peak magnitudes, which offers greater discriminatory power (see below, section 3.5).

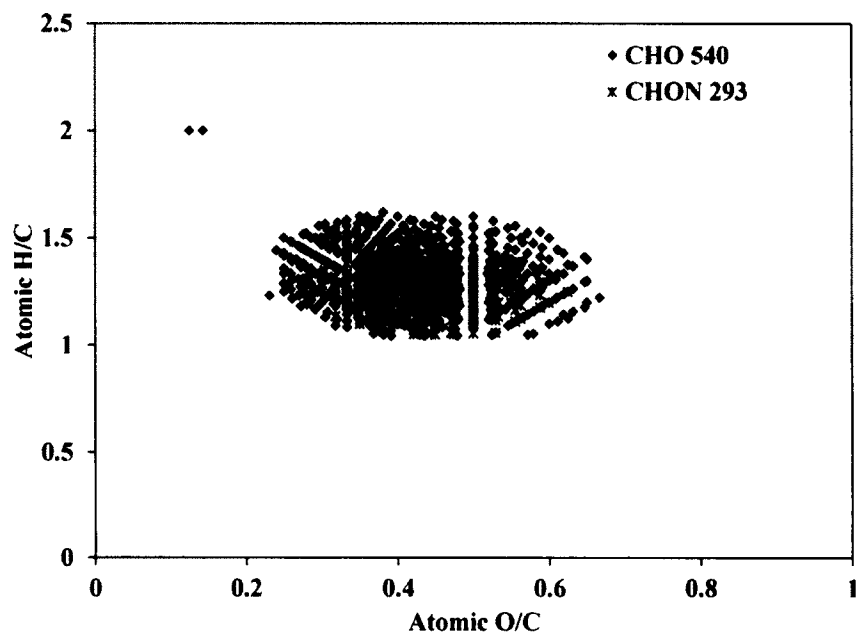


Figure 7. van Krevelen diagram using the 833 common formulas shared in marine RO/ED isolated DOM samples in this study. They consist of 540 CHO formulas and 293 CHON formulas.

Table 8

General information of mass peaks in samples.

Sample	Total Peaks S/N \geq 4 m/z 200-700	¹³ C Isotopic Peaks	Salt Peaks (mass defect > 0.6)			Formula Assigned Peaks		Common Formulas		
			#	%# ₁	%w ₁	#	%	#	%# ₂	%w ₂
N. Atlantic Upwelling Edge 5 m	1967	269	12	0.6	0.3	1451	85	833	57.4	80.8
N. Atlantic Upwelling Core 5 m	3113	443	18	0.6	0.3	2304	86	833	36.2	70.2
N. Atlantic 415 m (A)	2103	322	5	0.2	0.2	1510	85	833	55.2	82.5
N. Atlantic 415 m (B)	1750	277	7	0.4	0.2	1223	83	833	68.1	87.3
N. Atlantic 3000 m (A)	1690	285	19	1.1	0.6	1231	88	833	67.7	87.6
N. Atlantic 3000 m (B)	1732	275	11	0.6	0.4	1265	87	833	65.8	86.6
N. Pacific 5 m (A)	1228	149	87	7.1	16.2	869	81	627	72.2	85.1
N. Pacific 5 m (B)	1125	124	84	7.5	15.8	815	81	603	74.0	86.5
N. Pacific 674 m (1)	2607	400	87	3.3	8.3	1797	81	833	46.4	76.6
N. Pacific 674 m (2A)	1993	309	116	5.8	16.0	1332	79	833	62.5	83.1
N. Pacific 674 m (2B)	2040	323	112	5.5	15.9	1387	81	833	60.1	82.2
N. Pacific 674 m (3)	2629	427	50	1.9	4.3	1802	82	833	46.2	78.1
N. Pacific 3500 m (A)	2705	424	78	2.9	5.4	1849	81	833	45.1	76.4
N. Pacific 3500 m (B)	2194	329	59	2.7	5.0	1507	81	833	55.3	81.0

$$\% \#_1 = (\text{Number of salt peaks} / \text{Total number of peaks}) \times 100$$

$$\% w_1 = (\text{Sum of peak magnitudes of salt peaks} / \text{Summed total peak magnitude}) \times 100$$

$$\% \#_2 = (\text{Number of common formula peaks} / \text{Total number of formula assigned peaks}) \times 100$$

$$\% w_2 = (\text{Sum of peak magnitudes of common formula peaks} / \text{Summed peak magnitude of formula assigned peaks}) \times 100$$

3.4. Molecular formulas identified in RO/ED DOM

To better characterize the molecular diversity, further data analysis was conducted with the identified formulas in each sample. First, the various formulas were grouped into three categories: 1) formulas containing only C, H, and O (CHO formulas); 2) formulas containing only C, H, O, and N (CHON formulas); and, 3) formulas containing S or P (labeled as others). In all samples, CHO formulas are the dominant components, representing 55-80% and 75-90% based on number percentages and magnitude-weighted percentages, respectively (Table 9). The magnitude-weighted percentages for CHO formulas are higher than their corresponding number percentages, indicating that CHO formulas occur at higher intensities than other formulas in the spectra. Whether this also indicates CHO molecules exist at higher concentrations in the original DOM remains unclear as fractionation can occur during sample isolation and ESI FTICR-MS analysis. CHON magnitude-weighted percentages (10-25%) are lower than their number based percentages (20-45%; Table 9). The other heteroatomic formulas (i.e., formulas with S or P) together represent < 3% of identified molecular formulas, based on either number percentages or magnitude-weighted percentages. Percentage variation among samples is minor with the exception of the North Pacific surface (5m) sample, which has a higher % of CHO formulas and lower % of CHON formulas compared to the other samples (Table 9).

Table 9

Percentage of three different types of molecular formulas in all samples.

Sample	Assigned	CHO	CHON	others	CHO	CHON	others
	#	%#	%#	%#	%w	%w	%w
N. Atlantic Upwelling Edge 5 m	1451	62.2	36.7	1.2	78.9	20.6	0.5
N. Atlantic Upwelling Core 5 m	2304	54.2	42.3	3.5	74.4	24.2	1.4
N. Atlantic 415 m (A)	1510	58.1	41.1	0.7	77.9	21.9	0.2
N. Atlantic 415 m (B)	1223	60.8	38.3	0.9	78.7	20.7	0.5
N. Atlantic 3000 m (A)	1231	59.0	40.0	1.0	78.3	21.3	0.3
N. Atlantic 3000 m (B)	1265	58.4	40.2	1.3	77.6	21.9	0.5
N. Pacific 5 m (A)	869	78.0	21.2	0.8	88.1	11.5	0.4
N. Pacific 5 m (B)	815	79.5	20.1	0.4	89.1	10.8	0.2
N. Pacific 674 m (1)	1797	55.0	43.1	1.9	75.9	23.5	0.6
N. Pacific 674 m (2A)	1332	59.9	39.0	1.1	79.3	20.3	0.4
N. Pacific 674 m (2B)	1387	59.3	39.8	0.9	78.9	20.8	0.4
N. Pacific 674 m (3)	1802	55.3	42.8	1.9	76.3	23.1	0.6
N. Pacific 3500 m (A)	1849	57.3	40.0	2.7	76.8	22.0	1.2
N. Pacific 3500 m (B)	1507	59.4	39.1	1.5	78.0	21.4	0.6

%# = (Number of specific formula peaks/Total number of formula assigned peaks) × 100

%w = (Sum of peak magnitudes of specific formula peaks/Summed peak magnitude of formula assigned peaks) × 100

The abundant CHO formulas were further examined across the samples. To obtain additional structural information, double bond equivalents (DBE) and aromaticity indices (AI, Koch and Dittmar 2006) were calculated using the following equations:

$$\text{DBE} = 1 + \text{C} - 0.5 \text{H} \quad (1)$$

$$\text{AI} = (1 + \text{C} - \text{O} - 0.5\text{H})/(\text{C}-\text{O}) \quad (2)$$

Then, the CHO formulas were grouped by compound class. $AI > 0.5$ provides an unambiguous value for the presence of aromatic compounds (Koch and Dittmar, 2006). Formulas with $DBE/C < 0.3$ and $H/C 1.0-3.0$ are unambiguously assigned as aliphatics (Perdue, 1984). Besides the aromatic and aliphatic compounds that can be defined unambiguously, there are other compounds that can be grouped tentatively. For example, CHO molecular formulas with $O/C 0.7 - 1$, $H/C 1.6 - 2$ have stoichiometries consistent with carbohydrates (Sleighter and Hatcher, 2007), although they are also likely present as saturated organic acids. Here we extracted the CHO formulas with $O/C 0.7 - 1$, $H/C 1.6 - 2$ from the aliphatics to be an individual group, and we name this group as “carbohydrate-like” compounds. We recognize that the carbohydrate-like compounds could have non-carbohydrate structural isomers, but they still provide a way to potentially compare the carbohydrate compounds among samples. Another group of compounds were tentatively defined according to Hertkorn et al. (2006): carboxylic-rich alicyclic molecules (CRAM) that have $DBE/C = 0.30-0.68$, $DBE/H = 0.20-0.95$ and $DBE/O 0.77-1.75$. Here we refer to this group as “CRAM-like” compounds, because we recognize that they likely contain both aromatic and CRAM (alicyclic) isomer structures based on their elemental formulas (Sleighter and Hatcher, 2008). However, Hertkorn et al. (2013) showed with a combination of FTICR-MS and NMR that the majority of these molecules are likely CRAM in marine DOM. Finally, a group of CHO molecules with $O/C 0.60-0.95$, $H/C 0.55-1.40$ were tentatively defined as “tannin-like” compounds (Sleighter and Hatcher, 2007). Again recognizing that in our marine DOM samples, “tannin-like” molecules need not be tannins (i.e. high O-content aromatics, and normally with terrestrial source), but could equally be high O-content CRAM. There is a small overlap area between “CRAM-

like” and “tannin-like” formulas in the van Krevelen diagram but it is assigned to “CRAM-like” rather than “tannin-like” area. Thus, the five compound classes can be well distinguished in various regions of the van Krevelen diagram (Figure 8).

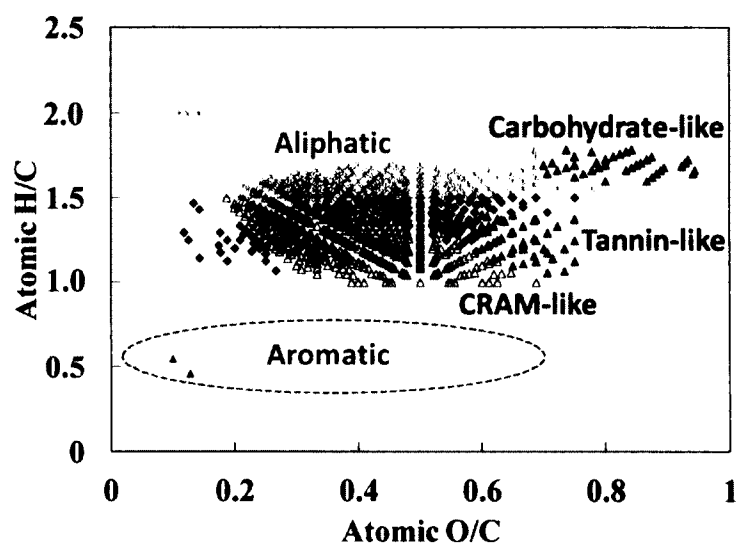


Figure 8. van Krevelen diagram using CHO formulas from the North Atlantic Senegal-Mauritanian upwelling core region surface sample. By labeling peaks as –like we denote that the position on van Krevelen space is merely indicative of molecules having a structural similarity to the molecular group listed.

There are virtually no unambiguously identified aromatic CHO formulas in any of these marine DOM samples (Figure 8), which is consistent with reports from previous studies (Flerus et al., 2012; Hertkorn et al., 2006; Koprivnjak et al., 2009). Percentages of the five compound classes in replicate samples have negligible variance and they are averaged for each site (Figure 9). CRAM-like CHO formulas are the most abundant CHO components in all samples, representing 50-65% and 60-75% of CHO formulas according

to number-based percentages and magnitude-weighted percentages, respectively (Figure 9). CRAM-like CHO formulas account for 40-65% of the total peak intensity of each sample. The second most abundant CHO components are the aliphatics, representing 15-25% and 5-15% of CHO formulas calculated by number percentages and magnitude-weighted percentages, respectively (Figure 9). Aliphatic CHO formulas account for 5-10% of the total peak intensity of each sample. There are lower percentages of CRAM-like CHO formulas and correspondingly higher percentages of aliphatic CHO formulas in the surface water samples, compared with the intermediate and deep water samples (Figure 9). CRAM-like compounds are thought to be major components of refractory DOM, which appear to be more abundant in deeper waters populated by highly degraded, aged DOM (Flerus et al., 2012; Hertkorn et al., 2006).

Another significant difference between the surface waters and the deeper waters is that carbohydrate-like CHO formulas are mainly found in the surface. This supports the view that carbohydrate-like molecules are significant constituents of biolabile and semi-biolabile compounds that are freshly produced in the surface waters (Carlson, 2002). Based on magnitude-weighted measurements, the carbohydrate-derived formulas are only minor contributors even though they are known to dominate structures of surface-water DOM as measured by other techniques such as NMR (Benner et al., 1992; Helms, 2012; Koprivnjak et al., 2009; Repeta et al., 2002). Total dissolved carbohydrate (TCHO) concentrations measured by colorimetry also decrease from surface to deep waters (Table 10). Percentages of TCHO-C in DOC are in the range of 3.7-19.6% in all samples (Table 10), with the North Pacific deep (3500 m) water having the lowest % and the North Atlantic upwelling core surface water having the highest %. While ionization efficiency

for carbohydrate-like components of DOM is suppressed compared to other types of molecules (Shen and Perreault, 1998), there is a positive correlation ($r^2 = 0.69$) between the FTICR-MS data and the colorimetric data for total carbohydrates. The minor contribution of carbohydrate-like formulas to the spectra is not unusual and suggests that FTICR-MS under-represents the contribution of carbohydrates in DOM (Chen et al., 2011; Shen and Perreault, 1998; Stubbins et al., 2010).

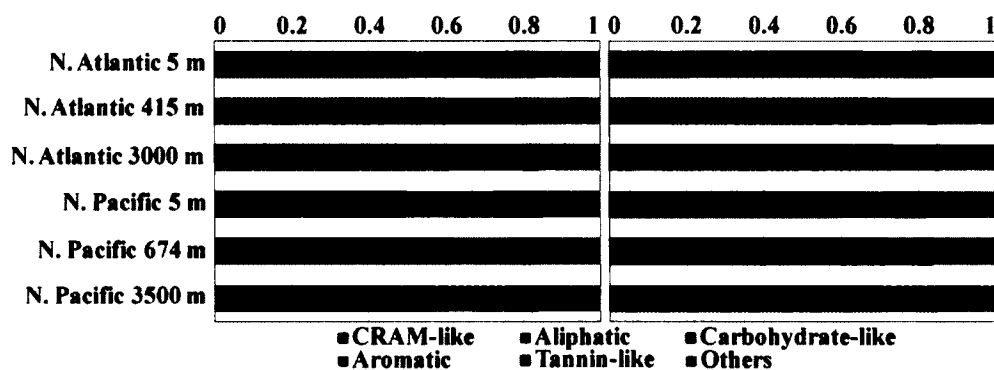


Figure 9. Fraction of different compound classes of CHO molecular formulas in all samples. Left: number fraction (based on numbers of elemental formulas); Right: Magnitude-weighted fraction (based on relative peak magnitudes).

Table 10

Results of total carbohydrate concentrations in RO/ED isolated DOM and the carbohydrate-like peak percentages in FTICR-MS.

Sample	TCHO (mg Glucose L ⁻¹)	TCHO-C* (μMC)	DOC (μMC)	% DOC	peak %# in FTICR-MS
N. Atlantic Upwelling Edge_5 m	18.17 ± 0.09	606	3884	15.6	4.1
N. Atlantic Upwelling Core_5 m	25.28 ± 0.55	843	4298	19.6	4.8
N. Atlantic_415 m	4.73 ± 0.07	158	1523	10.4	0.1
N. Atlantic_3000 m	3.03 ± 0.08	101	1076	9.4	0.1
N. Pacific_5 m	5.80 ± 0.07	193	1325	14.6	4.1
N. Pacific_674 m	1.42 ± 0.04	47	1006	4.7	< 0.1
N. Pacific_3500 m	1.39 ± 0.01	46	1254	3.7	< 0.1

$$* \text{TCHO-C } (\mu\text{MC}) = \text{TCHO (mg Glucose L}^{-1}\text{)} \times 0.4 \times 1000 \div 12$$

3.5 Statistical analysis of the identified molecular formulas

As mentioned in section 3.3, because the percentages of common formula peaks in each spectrum are high (> 67%), we needed to use the relative peak magnitudes to examine the differences among the samples in this study. Firstly, the assigned formulas from each of the 14 mass spectra were compiled together in one data sheet, and condensed to 2880 unique formulas by retaining a single formula for those formulas that were shared in multiple samples. The peak relative magnitudes were calculated from each assigned formula's peak magnitude divided by the total magnitude of the 2880 formula peaks in each spectrum. Hierarchical cluster analysis (HCA) was applied using the peak relative magnitudes. In the resulting dendrogram (Figure 10), each pair of replicates group together, indicating good reproducibility. Overall, all samples have high similarity,

with $r > 0.4$, where r value represents the correlation coefficient between clusters in the dendrogram. The higher the r value is, the more similarity there is between clusters/samples.

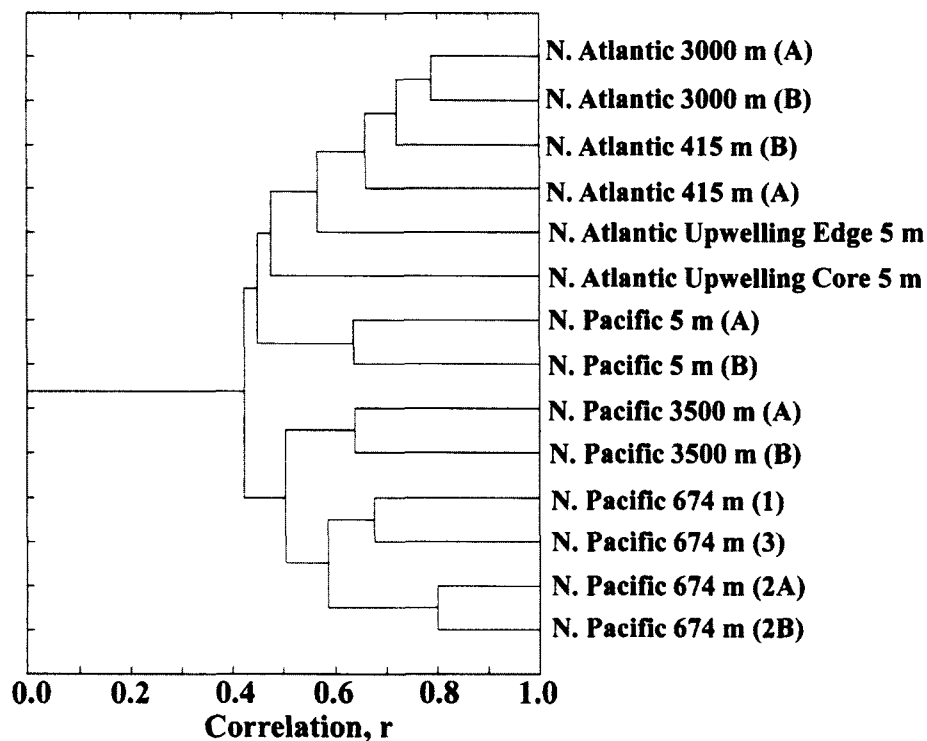


Figure 10. Dendrogram from the cluster analysis using the relative magnitudes of the total 2880 formulas in each sample.

Secondly, principal component analysis (PCA) was applied to our dataset following Sleighter et al. (2010). To minimize the contribution from minor peaks that have magnitudes near the noise level, Sleighter et al. (2010) selected the 500 highest magnitude peaks in each sample. However, such a treatment with our dataset would predominantly select high intensity CHO peaks and discard all the information contained

within the CHON data pool. Thus, two separate PCA analyses were conducted as illustrated below.

CHO formulas: The 500 highest magnitude CHO formulas in each sample represent a range of 40% - 77% (average 57%) of the total number of CHO formulas in each sample. The 500 highest magnitude CHO formulas for each of the 14 spectra were compiled (yielding a total of 7000 formulas) in one data sheet, and then condensed to 750 unique formulas by retaining a single formula for those formulas that were shared in multiple samples. The data matrix was created from the relative magnitudes, which were calculated from each formula's magnitude divided by the total magnitude of the 750 CHO formulas in each of the 14 spectra, respectively. In the cases where the formula is not present in a spectrum, the magnitude is given as the lowest peak magnitude in the whole mass list (near detection limit). Formulas within the 750 CHO formulas are all included as long as they are present in a sample spectrum, no matter if they are in the top 500 CHO highest magnitude formulas in that specific spectrum. In this manner, the percentages of formulas that were included in the statistical analysis were even higher than an average of 57% from each spectrum, as previously calculated by use of the top 500 dominant CHO formulas in each spectrum.

The biplots resulting from PCA of the relative magnitudes of the selected 750 CHO formulas are shown in Figure 11. Scores represent the projections of the original sample onto each principal component (PC). Loadings represent the projections of all the variables onto each PC and indicate the variable's contribution to the data variability along each PC. Here the variables are the specified 750 CHO formulas. The total number of principal components equates to the number of variables thus there are 750 PCs. PC1

and PC2 explain 37% and 30% of the variance respectively. In such a large variable set, this amount of variance is sufficient to indicate that there is a linear relationship between the first two components (Sleighter et al., 2010), which is a promising indication that most samples can be included in the two dimensions space of PC1 and PC2. An additional 16% of the variance can be explained by PC3, but it does not provide additional insight as it is a much smaller component compared to PC1 and PC2, and is not shown.

The samples are grouped in Figure 11a to four score-quadrants, which can be assigned to sampling locations and depth: (1) quadrant 1 represents the North Pacific intermediate and deep samples, (2) quadrant 2 represents the North Pacific subtropical gyre surface sample, (3) quadrant 3 represents the North Atlantic Senegal-Mauritanian upwelling area surface samples, and (4) quadrant 4 represents the North Atlantic oxygen minimum layer and deep samples. The biplots can be used to examine relationships between samples and variables. The co-location of loadings (formulas) and scores (samples) in the same quadrant of the biplot indicates a close correspondence of formulas with higher relative magnitudes in those samples. Figure 11b includes the 750 variables, with those that are distal to the origin as the most important formulas defining the variance of the 14 samples. Thus, densely populated distal areas of the biplot have particular significance within the population and are highlighted by boxes labeled as “areas 1 – 5” (Figure 11b). Area 1 has high positive loadings on PC2 and spans the PC1 axis, corresponding to deeper samples that have high scores on PC2 in Figure 11a. This correspondence indicates that area 1 formulas are enriched in deeper samples in both North Atlantic and North Pacific waters. Area 2 is enriched in the North Pacific

intermediate samples. Area 3 has low negative loadings on PC2 which indicates it is enriched in the North Pacific subtropical gyre surface sample. Area 4 represents the formulas that are enriched in the North Atlantic Senegal-Mauritanian upwelling area surface samples. Area 5 is specifically enriched in the North Atlantic oxygen minimum layer and deep samples, but not samples from the deep Pacific. The relative magnitudes of peaks in each area contributing to the total magnitude of the chosen 750 peaks in each sample are shown in Table 11. The total magnitudes of all 5 areas account for approximately 75% of the total magnitudes of the chosen 750 CHO formulas in each sample.

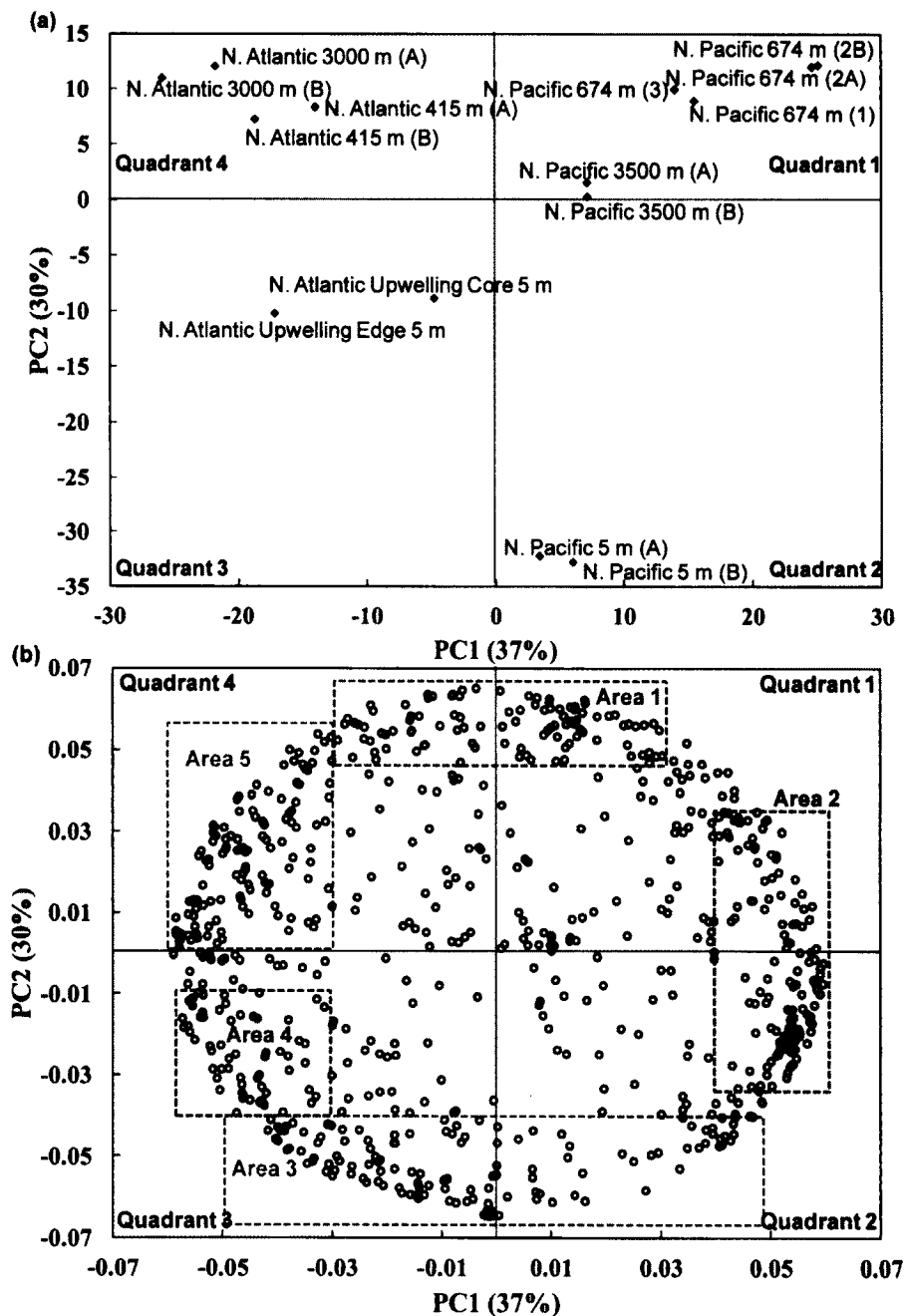


Figure 11. Statistical plots using the relative magnitudes of the selected 750 CHO formulas. (a) Biplot of the scores from the principal component analysis. (b) Biplot of loadings from the principal component analysis. Boxed areas were selected for further analysis and are colored according to the van Krevelen diagram in Figure 12.

Table 11

Sum of relative magnitudes of each area according to Figure 11b and 12 for each sample's CHO formulas. The samples that each area is enriched in are highlighted in *italics*.

Sample	Area 1 (%)	Area 2 (%)	Area 3 (%)	Area 4 (%)	Area 5 (%)	Total (%)
N. Atlantic Upwelling Edge 5 m	12.6	14.9	14.5	10.1	23.1	74.4
N. Atlantic Upwelling Core 5 m	11.9	17.5	13.2	8.3	20.5	70.8
N. Atlantic 415 m (A)	15.4	15.4	10.0	8.6	25.4	74.5
N. Atlantic 415 m (B)	15.1	14.5	10.6	9.3	26.8	75.7
N. Atlantic 3000 m (A)	16.7	12.9	10.1	9.5	27.0	76.0
N. Atlantic 3000 m (B)	16.3	12.1	10.1	9.8	28.0	76.0
N. Pacific 5 m (A)	9.0	21.4	19.1	9.1	17.4	75.5
N. Pacific 5 m (B)	9.1	21.9	19.5	8.8	16.9	75.8
N. Pacific 674 m (1)	15.3	22.6	9.9	5.9	18.4	72.0
N. Pacific 674 m (2A)	17.0	26.6	9.6	5.4	17.1	75.4
N. Pacific 674 m (2B)	17.0	26.5	9.5	5.2	16.9	75.0
N. Pacific 674 m (3)	15.9	22.3	9.9	6.0	18.7	72.6
N. Pacific 3550 m (A)	13.3	21.5	10.4	6.8	20.4	73.0
N. Pacific 3550 m (B)	13.5	21.7	11.3	7.1	20.6	74.2

When plotting the formulas in each area on a van Krevelen diagram (Figure 12), there are remarkably specific regions of the diagram associated with each area of Figure 11b. Formulas in area 1 (those enriched in deeper samples) fall in the middle of the CRAM-like region (Figures 8 and 12), consistent with previous reports that CRAM-like molecules represent a major component of the bio-refractory pool of DOM distributed

throughout the oceans, but dominant in deep waters (Hertkorn et al., 2006). Area 2 formulas (those enriched in the North Pacific intermediate samples) fall in the lower H/C CRAM-like region and some of the tannin-like regions, possibly indicative of more oxidized forms of CRAM. Area 3 formulas (those enriched in the North Pacific subtropical gyre surface sample) are mostly in aliphatic and carbohydrate-like regions, although there are a few formulas that scatter across the plot at higher H/C values. Area 4 formulas (those enriched in the North Atlantic Senegal-Mauritanian upwelling area surface samples) mainly fall in the aliphatic region with lower O/C values than area 3 formulas. Area 5 formulas (those enriched in the North Atlantic deeper samples) fall in the CRAM-like region with lower O/C values than area 1 and area 2 formulas.

Considering all five areas together, peaks enriched in surface samples (area 3 and area 4) tend to have higher H/C values than peaks enriched in deep samples (area 1, area 2 and area 5). Previous studies analyzing photo-degraded river DOM have found that aliphatic compounds can be photo-produced and carbohydrate-like compounds are resistant to photo-irradiation, while aromatic compounds are photo-labile (Helms et al., 2014; Stubbins et al., 2010). DOM is subjected to intense, prolonged solar irradiation in surface water, resulting in extreme DOM photo-bleaching based upon colored DOM optical properties (Kitidis et al., 2006; Nelson and Siegel, 2013). Thus, elevated peak intensities for aliphatics and carbohydrate-like DOM in these waters may be due to the presence of heavily photo-degraded DOM. Trends in carbohydrate-like DOM are undoubtedly also influenced by biological processes. Carbohydrate-like compounds are enriched in surface waters due to biotic production and depleted in deeper waters due to their biolability (Carlson, 2002). North Atlantic oxygen minimum layer and deep water

samples (area 5) have lower O/C values than the North Pacific intermediate and deep water samples (area 2) (Figure 12). This difference may in part be due to oxidation by bacteria as DOM ages along the global ocean conveyor belt.

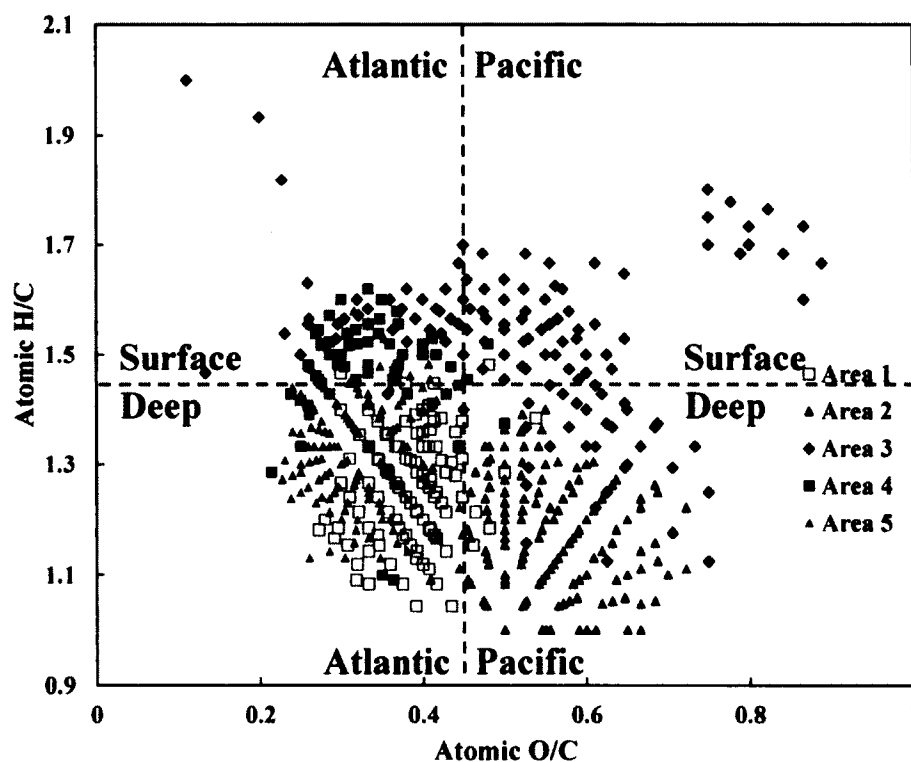


Figure 12. van Krevelen diagram of the selected areas and colored according to the biplot of the loadings shown in Figure 11b for the CHO formulas. Area 1 is enriched in North Atlantic 415 m and 3000 m, and North Pacific 674 m; Area 2 is enriched in North Pacific 674 m; Area 3 is enriched in North Pacific 5 m; Area 4 is enriched in North Atlantic 5 m; and Area 5 is enriched in North Atlantic 415 m and 3000 m. The horizontal dotted line is present to distinguish the formulas enriched in the “surface” waters (above the line) from the formulas enriched in the “deep” waters (below the line). The vertical dotted line is present to distinguish the formulas enriched in the “Atlantic” waters (left side of the line) from the formulas enriched in the “Pacific” waters (right side of the line). Such information is indicated by labeling the location and water depths next to the lines.

CHON formulas: There are much less CHON formulas than CHO formulas in each sample. Consequently, the 300 highest magnitude CHON formulas in each sample were used rather than the 500 highest magnitude CHON formulas. The 300 highest magnitude CHON formulas represent a range of 31% - 75% (average 51%) of the total number of CHON formulas in each sample. Only 184 and 164 identified CHON formulas are present in the two North Pacific 5 m sample replicates respectively, whereas there are at least 400 CHON formulas in each of the other samples. Since the North Pacific 5 m sample is significantly different from the rest of the samples in terms of CHON formulas, including the North Pacific 5 m sample in the CHON PCA analysis resulted in only two extreme components: one being the North Pacific 5 m sample and the other the rest of samples (results not shown). Thus, the two North Pacific 5 m sample spectra were excluded from the CHON PCA to enable differences between the other samples to be discerned. The 300 highest magnitude CHON formulas for each of the other 12 spectra were compiled (yielding a total of 3600 formulas) in one data sheet, and then condensed to 496 distinct formulas by retaining a single formula for those formulas that were shared in multiple samples. As for the CHO PCA, the data matrix for CHON PCA was created using the relative magnitudes of the 496 CHON formulas in each spectrum.

PC1 and PC2 explains 41% and 21%, respectively, of the variance among the 12 spectra based on their differences in the 496 variables, giving a total of 62% of the variance (Figure 13). PC1 groups the samples into two major components: the North Atlantic samples which have negative PC1 values and the North Pacific samples which have positive PC1 values, except that the North Atlantic Senegal-Mauritanian upwelling core region surface sample has a positive PC1 value. On the PC2 axis, the North Pacific

674 m (2A) and (2B) (with high positive PC2 values) and the North Atlantic Senegal-Mauritanian upwelling core region surface (with a low negative PC2 value) samples are mainly responsible for the variance.

Like the CHO formulas, the densely populated distal areas of the CHON biplot are highlighted by boxes labeled as “areas 1 – 4” (Figure 13b). Area 1 co-locates with the North Pacific 674 m (2A) and (2B) samples indicating these CHON formulas tend to be enriched in those two samples. Unlike the close co-location of all four of the North Pacific 674 m spectra in the biplot of the scores from PCA of CHO formulas (Figure 11a), CHON formulas of the North Pacific 674 m (2A) and (2B), which are duplicate FTICR-MS of RO/ED isolated DOM_Day 2, are apart from CHON formulas of the North Pacific 674 m (1) and (3), which are RO/ED isolated DOM_Day 1 and RO/ED isolated DOM_Day 3 (Figure 13a). Thus, there is higher variability in the CHON formulas compared to the CHO formulas. Area 2 represents the formulas that are enriched in North Pacific intermediate and deep water samples. Area 3 contains formulas enriched in the North Atlantic Senegal-Mauritanian upwelling core region sample. Area 4 represents formulas enriched in the North Atlantic oxygen minimum layer and deep water samples. The total magnitudes of all 4 areas account for 61-65% of the total magnitudes of the chosen 496 CHON formulas in each sample (Table 12).

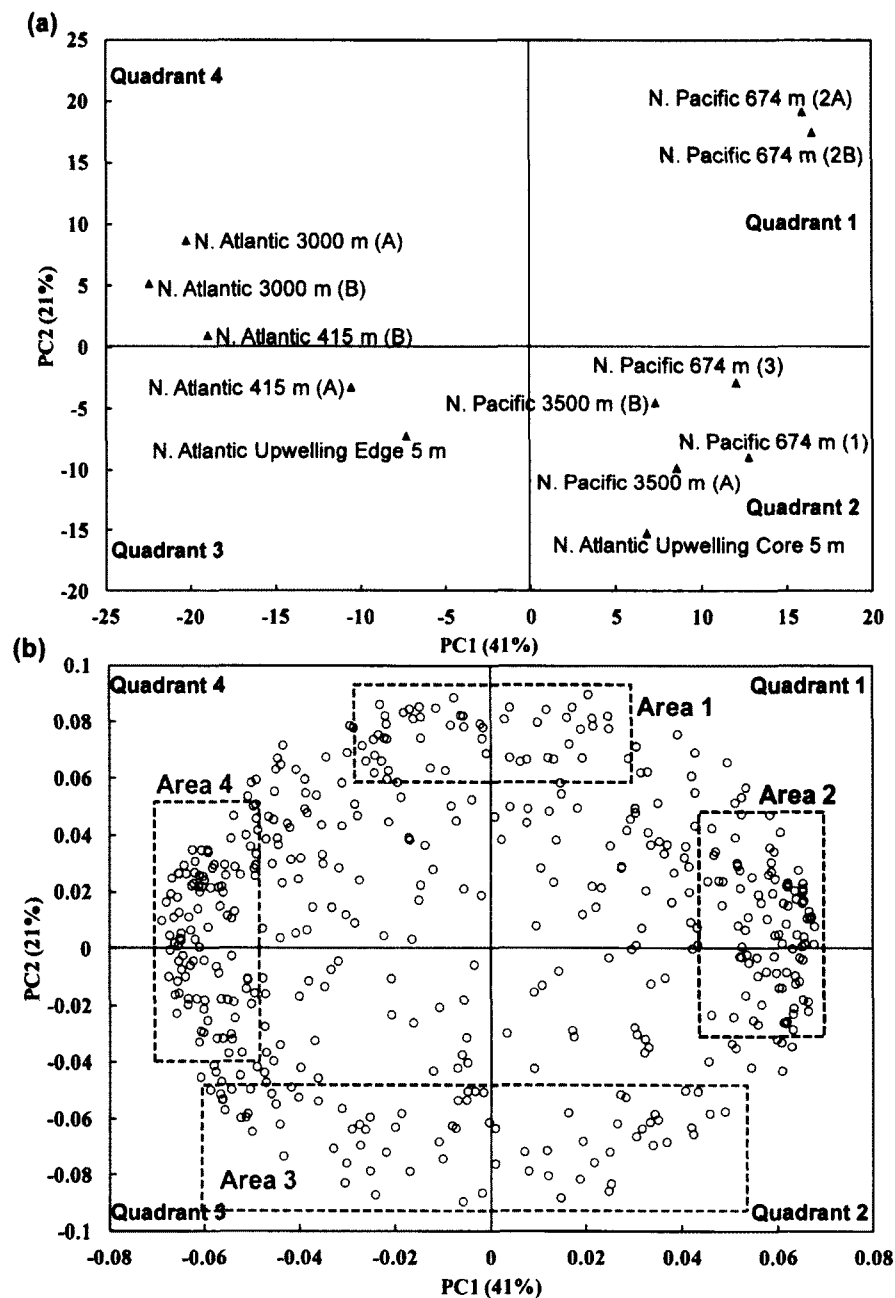


Figure 13. Principal component plots using the relative magnitudes of the selected 496 CHON formulas. (a) Biplot of the scores from the principal component analysis. (b) Biplot of loadings from the principal component analysis. Boxed areas were selected for further analysis and are colored according to the van Krevelen diagram in Figure 14.

Table 12

Sum of relative magnitudes of each area according to Figure 13b and 14 for each sample's CHON formulas. The samples that each area is enriched in are highlighted in *italics*.

Sample	Area 1 (%)	Area 2 (%)	Area 3 (%)	Area 4 (%)	Total (%)
N. Atlantic Upwelling Edge 5 m	11.6	12.9	14.5	25.6	64.5
N. Atlantic Upwelling Core 5 m	10.3	17.4	<i>17.1</i>	20.3	65.1
N. Atlantic 415 m (A)	12.1	11.5	14.2	26.2	64.0
N. Atlantic 415 m (B)	13.1	8.9	12.9	29.6	64.6
N. Atlantic 3000 m (A)	13.8	7.5	10.5	30.0	61.7
N. Atlantic 3000 m (B)	13.3	6.4	11.6	30.4	61.7
N. Pacific 674 m (1)	11.3	19.7	15.6	18.4	64.9
N. Pacific 674 m (2A)	15.1	22.8	6.9	17.6	62.5
N. Pacific 674 m (2B)	14.9	22.9	7.0	18.3	63.0
N. Pacific 674 m (3)	12.3	19.4	13.8	18.6	64.1
N. Pacific 3550 m (A)	10.7	18.9	14.4	20.7	64.7
N. Pacific 3550 m (B)	11.3	19.0	12.0	21.6	64.0

For the CHON formulas, there are not as many specific regions in the van Krevelen diagrams as observed for CHO formulas (Figures 12, 14a and 14b). No significant clustering of H/C values or N/C values among the areas is observed for all samples. However, there is a trend for O/C values in which the North Pacific intermediate and deep samples have higher O/C than the North Atlantic oxygen minimum layer and deep samples. Areas 1 and 2 are enriched in the North Pacific intermediate and deep water samples, and have O/C values of 0.4-0.7. Area 4 is enriched in the North Atlantic

oxygen minimum layer and deep water samples with lower O/C values (<0.45). Area 3 is dispersed in the van Krevelen diagram, because it is mainly enriched in the North Atlantic Senegal-Mauritanian upwelling surface samples which likely have multiple sources and transformation processes for DOM.

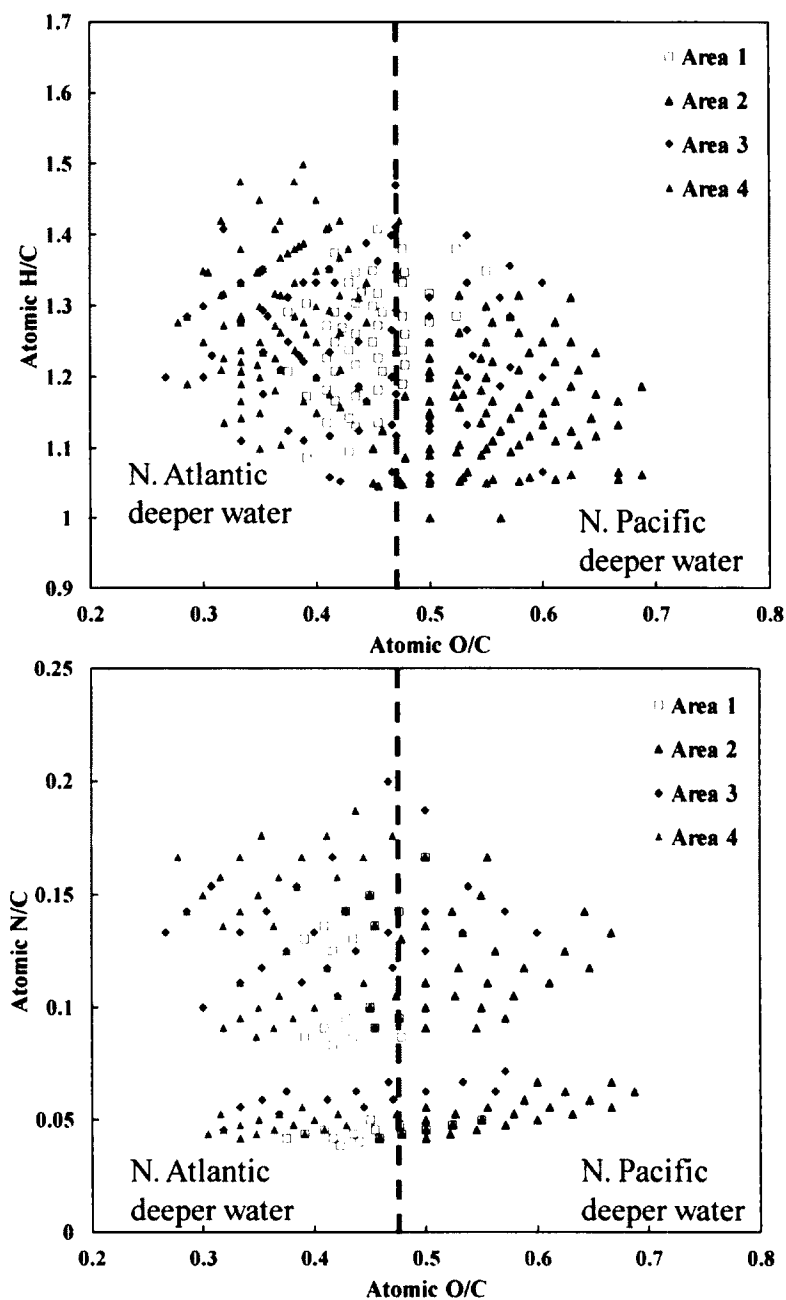


Figure 14. van Krevelen diagrams [(a) H/C vs. O/C, and (b) N/C vs. O/C] of the selected areas and colored according to the biplot of the loadings shown in Figure 13b for the CHON formulas. Area 1 is enriched in North Pacific 674 m; Area 2 is enriched in North Pacific 674 m and 3550 m; Area 3 is enriched in North Atlantic Senegal-Mauritanian upwelling core 5 m; Area 4 is enriched in North Atlantic 415 m and 3000 m.

Figure 14. (continued)

The vertical dotted line is present to distinguish the formulas enriched in the “N. Atlantic deeper water” (left side of the line) from the formulas enriched in the “N. Pacific deeper water” (right side of the line).

Considering CHO and CHON formulas together, relative magnitudes of compounds with higher O/C values increase from the North Atlantic oxygen minimum layer and deep water to the North Pacific intermediate and deep water. This increase suggests an oxygenation process which might be related to microbial activity during the ageing of DOM and/or more intense release of DOM from sinking particles in the deep Pacific Ocean, the latter suggested by trends in colored and fluorescent DOM in the deep Pacific (Jørgensen et al., 2011; Nelson et al., 2010). Whatever the process, it leads to a marked increase in the oxygen content of both CHO and CHON compounds and clearly provides molecular differentiation between the two oceans.

A previous study by Flerus et al. (2012) identified gradients in specific DOM molecules and the radiocarbon age of DOC extracted by PPL SPE along an eastern Atlantic Ocean transect from 50°N to 40°S. However, they did not observe increases in the magnitude-averaged O/C values with increasing DOC radiocarbon age. Our observed difference between the deep waters of the Pacific and Atlantic may be due to the difference in the hydrology and DOM dynamics of the Atlantic and Pacific Ocean basins. Overturn and ventilation is slow in the Pacific Ocean. The relative lack of mixing enables gradients in apparent oxygen utilization and DOM maturation (as indicated by chromophoric and fluorescent DOM) is more developed in the Pacific Ocean, with DOM

becoming increasingly “diagenetically altered and oxidized” in North Pacific Deep Water the further north it travels (Jørgensen et al., 2011; Nelson et al., 2010). In the Atlantic Ocean DOM levels are high in the northern-most Atlantic due to the export of terrestrial DOM from the Arctic Ocean (Amon et al., 2003) and high in the South Atlantic due to the incorporation of high DOM waters from the Atlantic sector of the Southern Ocean (Nelson et al., 2010). Relatively rapid mixing of water masses would probably obscure or weaken any gradients that might be set up by the *in situ* abyssal processing of DOM. As a result only weak correspondences between DOM optical properties and apparent oxygen utilization exist in the North Atlantic (Nelson et al., 2010). It is therefore likely that similarly weak gradients in DOM molecular characteristics as revealed by FTICR-MS are to be found in the Atlantic Ocean versus the slowly overturning Pacific Ocean.

3.6 Photoreactivity related molecular formulas

FTICR-MS data for three pools of DOM classified by their photoreactivity have been reported previously: (1) photo-labile (present only pre-irradiation), (2) photo-produced (present only post-irradiation), and (3) photo-resistant (present both pre- and post-irradiation) (Stubbins et al., 2010). Specific molecular formulas for each pool were identified in the Congo River by comparing whole water DOM before and after photodegradation under simulated sunlight. We identified molecular formulas from each of these photochemically defined pools – as listed in Stubbins et al. (2010) – within the RO/ED isolates (Figure 15). Percentages of the three pools of molecules in replicate samples for all sampling sites have negligible variance and they are averaged for each sampling site (Figure 15).

With the exception of the North Pacific subtropical gyre surface sample, the

RO/ED samples from other sites have similar contributions from photo-labile, -resistant, and -produced molecules (Figure 15). The North Pacific subtropical gyre surface DOM was significantly enriched in photo-produced and photo-resistant DOM but depleted in photo-labile DOM peaks relative to the other RO/ED samples. However, no such pattern was observed in our North Atlantic surface samples, which were collected within an upwelling region, where DOM is mostly sourced from high primary production and the upwelled deeper water DOM. In contrast to the upwelling region sampled in the Atlantic, the subtropical gyre of the Pacific Ocean is a low productivity region where DOM is held in stratified, sunbathed surface waters leading to extensive DOM photo-bleaching (Kitidis et al., 2006; Nelson et al., 2010). The prevalence of photo-resistant and photo-produced DOM in the North Pacific gyre waters suggests that the extensive photo-bleaching that occurs in this open ocean region results in the preservation and accumulation of DOM with molecular signatures similar to those produced and preserved when irradiating river water DOM. Each peak within a FTICR mass spectrum represents many, possibly thousands, of different structural isomers (Hertkorn et al., 2008), meaning the detection of a given peak in two samples does not require that the same molecule is present in both samples. Therefore, the discovery of photo-resistant molecular formulas identified for Congo River DOM within the open ocean could be taken to indicate that the open ocean gyres contain photo-degraded terrigenous DOM. However, a more sound conclusion to draw is that the selection pressure imposed upon DOM by photo-degradation results in the formation of analogous DOM pools whether the irradiated DOM was originally of marine or terrestrial origin. This type of comparison between photo-degraded terrigenous DOM and marine DOM has been made using MS data

(Rossel et al., 2013) elsewhere and in studies noting that, in terms of its optical quality and lignin content, open ocean DOM “resembles” rather than “is” photo-degraded terrigenous DOM (e.g. Helms et al., 2013b, 2014; Spencer et al., 2009).

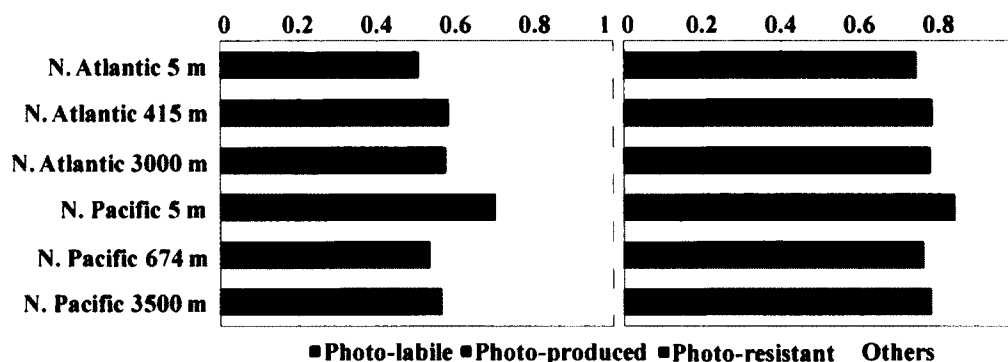


Figure 15. Distribution of the three photochemical pools of molecular formulas defined by Stubbins et al. (2010) at each site. Left: number fraction; Right: Magnitude-weighted fraction.

4. Summary and conclusions

RO/ED extracted oceanic DOM was injected directly into ESI FTICR-MS without organic solvent addition. Analysis of RO/ED samples without the addition of MeOH and NH₄OH suppressed fatty acid ionization efficiency enabling a cleaner spectrum of DOM peaks to be “seen” via ESI FTICR-MS in our instrument. In combination, these techniques can obtain more representative oceanic DOM samples bringing a greater % and diversity of the DOM pool into our analytical window. Compared to the C₁₈ SPE method, the RO/ED technique is able to isolate more N-containing organic compounds and more compounds with high O/C atomic ratio (>0.6).

The mass spectra show general characteristics that are normally observed in ESI FTICR-MS. The North Pacific subtropical gyre surface sample has the lowest number of identified molecular formulas and the sample from the North Atlantic Senegal-Mauritanian upwelling core area surface water has the most. Except for the North Pacific subtropical gyre surface sample, all other samples share a significant number of common formulas, which account for 54-79% of each sample. The peaks corresponding to the common formulas are generally observed at high intensity. The possibility that this high percentage of common formulas is due to preferential ionization of certain compounds is possible, but unlikely as FTICR-MS can discern differences in the quality of DOM when comparing other samples (e.g. Sleighter and Hatcher, 2008; Stubbins et al., 2010). Therefore, the high percentage of common formulas observed in the open ocean RO/ED-DOM mass spectra likely indicates a high degree of similarity in the original DOM within the different water masses studied. This marked compositional similarity of DOM across oceanic regimes suggests that a significant fraction of all of the samples is comprised of a highly refractory “background” DOM that circulates throughout all the oceans (Carlson, 2002). Within our data set, this background DOM is probably best represented by the “old” deep North Pacific sample. Above this background, compositional differences between the samples are likely due to localized processes of production and removal that contribute to semi-labile and labile DOM pools (Carlson, 2002).

FTICR-MS mass peak magnitude is not necessarily correlated to compound concentration because the ionization efficiencies of different compounds are different (e.g. Shen and Perreault, 1998), but it is not certain how significant such differences are.

In addition to this fractionation during FTICR-MS, there is also an unknown degree of compound fractionation during DOM sample isolation. However, the analytical conditions were the same for all samples in the current study enabling novel and informative FTICR-MS data to be obtained. CHO and CHON formulas were the most abundant elemental compositions, with CHO formulas being more abundant than those for CHON. Almost no unambiguously identified aromatic formulas were observed using an AI threshold of 0.5 (Koch and Dittmar, 2006). CRAM-like CHO formulas were the most abundant components, accounting for 40-65% of mass spectral intensity across the samples. However, based upon elemental stoichiometry alone the definition of CRAM is ambiguous and some of these peaks may contain aromatic isomers (Hertkorn et al., 2008). The aliphatic CHO formulas were the second most abundant components, representing 5-10% of total peak intensities. There are lower percentages of CRAM-like CHO formulas and correspondingly higher percentages of aliphatic CHO formulas in the surface water samples compared to the intermediate and deep water samples. Carbohydrate-like CHO formulas are mainly found in the surface samples. Total dissolved carbohydrate (TCHO) concentrations were also measured using a colorimetric method to compare with the results from FTICR-MS. The contribution of carbohydrate-like peaks in FTICR-MS of different samples are well correlated to, but lower than, the measured percentages of TCHO-C in DOC, which are in the range of 3.7% - 19.6% in all samples, with the North Pacific deep (3500 m) water having the lowest % and the North Atlantic upwelling core surface water having the highest %. This finding supports the view that carbohydrate-like molecules are significant constituents of biolabile and semi-labile compounds that are freshly produced in surface waters (Carlson, 2002).

PCA analyses demonstrate molecular differentiation of DOM within the major water masses along the global oceanic conveyor belt. PCA analysis using relative peak magnitudes showed that peaks that are enriched in surface samples have higher H/C values than peaks enriched in deep samples. This was true of samples from both the North Atlantic and the North Pacific. This trend is likely related to photo-degradation of photo-labile compounds and the bio-production of biolabile compounds in surface waters and the biodegradation of biolabile compounds with depth. The North Atlantic oxygen minimum layer and deep DOM had lower O/C values than the North Pacific intermediate and deep DOM, for both CHO and CHON compounds. This result indicates an oxygenation process of DOM that might be due to microbial activity during the ageing of DOM and/or greater remineralization of DOM from sinking particles in the deep Pacific Ocean (Nelson et al., 2010). There is a small chance that the difference between the Atlantic samples and the Pacific samples is partially caused by the different recovery, which is relatively low in the Atlantic deep samples. However, like we have discussed above (section 3.1), looking at the larger body of RO/ED results (Green et al., 2014; Koprivnjak et al., 2009), the RO/ED method has seen greater variability in yields of DOC when samples are isolated from a variety of sources than when isolated from a single source. This fact strongly suggests that compositional differences exist spatially and that they affect yields of DOC.

Photo-resistant and photo-produced molecular formulas that were preserved and produced when irradiating the Congo river water DOM (Stubbins et al., 2010) were also enriched in surface North Pacific subtropical gyre DOM, suggesting that the extensive photo-bleaching in this open ocean region resulted in the preservation and accumulation

of photo-degraded DOM. The similarities in the molecular signatures of photo-degraded Congo DOM and photo-degraded Open Ocean DOM does not mean that the DOM is of the same origin, rather these trends suggest that photochemistry shapes the DOM in both cases to result in similar average molecular properties.

CHAPTER IV

**PRODUCTION OF BLACK CARBON-LIKE AND ALIPHATIC MOLECULES
FROM TERRESTRIAL DISSOLVED ORGANIC MATTER IN THE PRESENCE
OF SUNLIGHT AND IRON**

PREFACE

The content of this Chapter was published in 2014 in Environmental Science and Technology Letters, and below is the full citation. The formatting here has been altered to incorporate the supporting information and additional figures into the body of the manuscript. See Appendix A for the copyright permission.

Chen, H., Abdulla, H. A. N., Sanders, R. L., Myneni, S. C. B., Mopper, K., and Hatcher, P. G., 2014. Production of black carbon-like and aliphatic molecules from terrestrial dissolved organic matter in the presence of sunlight and iron. Environmental Science and Technology Letters, 1: 399-404.

1. Introduction

Rivers worldwide transport approximately 0.4×10^{15} g of C year⁻¹ of terrestrial dissolved organic matter (DOM) to the ocean (Schlesinger and Melack, 1981), with the ratio of dissolved to particulate organic carbon around 1.5 (Meybeck, 1982). These DOM and particulate organic matter (POM) pools transported to oceans could be sufficient to support the annual turnover of marine dissolved organic carbon (DOC) (Williams and Druffel, 1987) and account for all organic matter buried in marine sediments (Berner, 1989; Hedges and Keil, 1995). However, the photochemical transformation of DOM in freshwaters changes the characteristics of both the dissolved and particulate pools

(Mopper et al., 1991; Stubbins et al., 2010), and leads to aggregation of organic matter, commonly referred to as photoflocculation (Helms et al., 2013a; von Wachenfeldt et al., 2008). Here we show that photochemical transformation of DOM produces new molecules that contribute to DOM and POM, some resembling black carbon, an important global contributor to carbon in both dissolved and sedimentary systems. Black carbon, generally thought to be exclusively from combustion, contributes between 50 and 270×10^{12} g of C year⁻¹ to the global pool of carbon and most of this is incorporated in terrestrial sediments but also marine sediments (Kuhlbusch and Crutzen, 1995; Masiello and Druffel, 1998). Dissolved black carbon has recently been estimated to constitute 10% of DOM exported by rivers to the ocean (Jaffé et al., 2013). In addition, sunlight modifies DOM-Fe interactions and Fe speciation (Barbeau, 2006; Faust and Zepp, 1993), which would significantly influence the characteristics of photoflocculated POM and dictating its stability and burial of organic carbon.

To evaluate the dynamics of phototransformation of terrestrial DOM, we examined sterile-filtered (0.1 μm) water from an important headwater to the North Atlantic—the Great Dismal Swamp (in the state of Virginia) (Sleighter and Hatcher, 2008) and subjected it to abiotic photodegradation in a solar simulator for 60 days. These studies offer a means for evaluating phototransformation of DOM in fluvial ecosystems. DOM and POM from the lab experiments were separated by filtration at different intervals during the photoirradiation experiment, and the bulk chemical characteristics of both particulate and dissolved fractions were determined using C, N, and Fe X-ray absorption spectroscopy. The molecular composition of these fractions was obtained using electrospray ionization coupled to Fourier transform ion cyclotron resonance

ultrahigh resolution mass spectrometry (ESI FTICR-MS). The chemical characteristics of newly produced POM in the laboratory photochemical studies were compared with naturally occurring freshwater POM from Dismal Swamp and Pahokee peat (in the state of Florida), as well as DOM from coastal (close to the shore and off-shore Chesapeake Bay, USA) and open ocean (Cape Verde Rise in the North Atlantic Ocean) samples.

2. Materials and methods

Water samples for our experiments were collected from the Portsmouth Ditch in the Great Dismal Swamp (DS), which represents the terrestrial headwaters of the Elizabeth River system on the east coast of the USA. The black swampy water has an ambient pH of 3 – 5 and zero salinity, but contains very high DOC loadings, mainly due to OM input from the degraded vegetation in the swamp. Water samples for our experiments were collected during 2012 and transported to the laboratory in several of 20 L polyethylene containers which were previously cleaned with dilute acid (0.1 M HCl) and base (0.05 M NaOH) solutions. The samples were filtered (within 24 h of collection) through filter capsules (0.1 μm pore size, Whatman PolyCap TC) to remove particles and bacteria. A sample of natural particles (i.e., not lab-irradiated) from the Dismal Swamp was collected by filtering the water through pre-combusted (oven 450 °C for 5h) Whatman GF/F filters (0.7 μm pore size). The sample from the Pahokee peat was humic acid provided as a standard by the International Humic Substances Society.

Initial DOM from the filtrate was used for photoirradiation experiments in a solar simulator system, as described previously (Minor et al., 2007). Initial DOM from the filtrate was mixed homogeneously in a 20 L polyethylene container and separated to aliquots of 450 mL to be transferred to 550 mL quartz round bottom flasks, which were

then placed in a solar simulator equipped with 12 UVA-340 bulbs (Q-PANEL; integrated irradiance estimated as 25 W m^{-2} ; Minor et al., 2007). This solar simulator system has a spectral shape similar to that of natural sunlight from 295 nm to 365 nm (Minor et al., 2007), which are the wavelengths mainly responsible for nearly all environmental photochemical reactions (Mopper and Kieber, 2000). The solar simulator provided 127% of the photobleaching occurring under winter midday sunlight at 36.89°N latitude (Minor et al., 2007), where the DS water is located. Continuous radiation was used in this study to generate sufficient photoflocculation material needed for the chemical and spectroscopic analyses. Even though continuous irradiation was used, photochemical reactions are known to be only dependent upon the integrated light dose (Jankowski et al., 1999), not the light intensity (unless an intense laser is used as the light source as employed in a few past studies; e.g., Wang et al., 2007; Zepp et al., 1987). We estimate that, during the 60 days experiment, the samples were exposed to an equivalent of about 240 days of natural sunlight in winter in our sampling area. Dark controls were wrapped with foil and left in the solar simulator together with photoirradiated samples. All sample flasks were covered with combusted glass lids to avoid bacterial contamination. The flasks were opened and agitated several times each day to assure saturation of dissolved oxygen, which was monitored throughout the experiments. Sample temperature was monitored during the irradiation and was found to be constant at $26.5\text{-}28.5^\circ\text{C}$. At each time point (Day 0, 18, 30, and 60), irradiated water and dark control water samples were harvested and sub-sampled for total Fe, pH, and TOC/TDN determinations. The remainder was filtered through pre-combusted GF/F filters to fractionate the samples into DOM (filtrate) and POM (particles retained on the filter). POC concentrations were

calculated as the difference between TOC concentration and DOC concentration, rather than measured directly from POM samples. The irradiated DOM samples were frozen (-20 °C) immediately for later analysis. The particles were rinsed with organic carbon-free deionized ultra-quality water. Particles were then removed from the GF/F filters by ultra-quality deionized water and freeze-dried for analysis.

DOM samples were frozen (-20 °C) immediately upon sampling. They were thawed prior to the measurements of organic carbon / nitrogen contents, total iron concentration, and FTICR-MS. Part of DOM samples were freeze dried and used for measurements of bulk elemental (C, H and N) contents, and for collecting C, N and Fe K-edge X-ray absorption spectra.

POM samples, both the particles in the initial DS water (natural particles, i.e., not lab-irradiated) and the particles formed by photoflocculation, were freeze dried immediately upon sampling. The dried POM samples were used directly for measurements of bulk elemental contents and collection of X-ray absorption spectra. However, for FTICR-MS analysis, POM samples were extracted by base prior to injection as described in the main text.

Dissolved organic carbon (DOC) and total dissolved nitrogen (TDN) concentrations were measured by high temperature combustion (720 °C) on a Shimadzu TOC-V_{CPH} (Shimadzu Scientific Instruments). Standard calibration curves were made with potassium hydrogen phthalate (KHP) and potassium nitrate (KNO₃) to quantify the DOC and TDN concentrations, respectively.

The bulk proportions of C, H and N in freeze-dried samples were determined using a Flash 1112 series Elemental Analyzer containing a CHN column. Analysis

involved ca. 1.5 mg of sample in a 3.3×5 mm tin cup being combusted at $900\text{ }^{\circ}\text{C}$ in the presence of O_2 . Sample response was calibrated to a standard curve using nicotinamide standard.

Total iron concentration was measured using a Hitachi Z8100 polarized Zeeman flame atomic absorption spectrophotometer equipped with an iron hollow cathode lamp. Iron standards were prepared from a reference standard solution of ferric nitrate in diluted nitric acid (1000ppm, Certified, Fisher Chemical). Standards ranged in concentration from 0.0 to $100\text{ }\mu\text{mol L}^{-1}$. Samples were adjusted to $\text{pH} = 1$ using freshly mixed aqua regia reagent (3 HCl: 1 HNO_3 , trace metal grade acids) and aged overnight before the measurements. Particulate iron concentrations were determined by comparing the iron concentrations of unfiltered (total) and dissolved (filtrate). Acid cleaned and conditioned Teflon vials were used for storage and treatment of iron subsamples. Standards and samples were measured in triplicate.

DOM and POM samples were analyzed on a Bruker Daltonics 12 Tesla Apex Qe FTICR-MS with an Apollo II ESI ion source in the negative ionization mode. The freeze-dried POM samples were weighed (ca. 1 mg each) and suspended in 1 mL ultra-quality water on a shaker (RPM=120) overnight (>10 h). Subsequently, the pH of the solutions was increased to 12 by small additions of concentrated NaOH (50% w/w) for recovery determinations and NH_4OH ($\geq 25\%$ in H_2O) for FTICR-MS analysis, respectively. Dissolution was facilitated on a shaker (RPM=120) 2 hours prior to analysis. The recovery of OM was constantly in the range of 66-74% (organic C) and 53-66% (organic N) for all POM samples. Particles dissolved in NH_4OH ($\text{pH}=12$) were mixed with methanol (50% v/v) and allowed to stand for 0.5 h (to allow settling of insolubles) before

injecting into the ESI source. DOM samples collected at each time point during photoirradiation were frozen (-20 °C) immediately upon sampling for later analysis. DOM samples were thawed and mixed with MeOH (50% v/v) containing NH₄OH (0.5% v/v in final to increase pH to 12) for FTICR-MS analysis conducted as described previously (Chen et al., 2014). All mass spectra were calibrated and assigned molecular formulas to peaks following previous studies (Chen et al., 2014). Assigned formulas included elements C, H, O, N, S, and P. Double bond equivalent (DBE) values were calculated as: $DBE = 1 + C - 0.5 H + 0.5 N + 0.5 P$. Aromaticity indices (AI; Koch and Dittmar, 2006) were calculated as: $AI_{mod} = (1 + C - 0.5 O - S - 0.5 H) / (C - 0.5 O - S - N - P)$. Molecular formulas with $DBE/C < 0.3$ and $H/C 1.0-3.0$ are unambiguously assigned as aliphatics (Perdue, 1984); while formulas with $AI_{mod} \geq 0.5$ and $AI_{mod} \geq 0.67$ are assigned as aromatic compounds and condensed aromatic compounds (Koch and Dittmar, 2006), respectively.

C and N K-edge X-ray absorption near edge structure (XANES) spectra were collected at the Spherical Grating Monochromator beamline 11ID-1 at the Canadian Light Source (Saskatoon, Saskatchewan, Canada). Samples were mounted on Au foil plates. C and N K-edge XANES spectra were collected from 270-320 eV and 380-440 eV, respectively. C spectra were referenced to citric acid at 288.8 eV and N spectra were calibrated with N₂ π^* and Rydberg transitions. Spectral averaging and normalization was conducted using Athena version 0.8.056 (Ravel and Newville, 2005).

Fe K-edge extended X-ray absorption fine structure (EXAFS) spectra were acquired at a bending magnet X-ray source (X18B) at the National Synchrotron Light Source (Brookhaven National Laboratory, Upton, NY). Spectra of the standard were

collected frequently during the XANES data measurements to correct for the systematic error associated with the drift of the monochromator. To ensure little to no contamination, sample preparation was conducted on a clean Kapton table, using polyfilm to prevent Fe contamination. Samples for Fe EXAFS were freeze dried immediately upon sampling to protect Fe speciation from artificial changes during storage. The x-ray beam did not appear to change the Fe speciation. The beamline is equipped with a Si (111) monochromator and a Ge or PIPS detector. A thin layer of sample was mounted on Kapton tape, sealed with polypropylene film, and placed into the sample chamber. Fe K-edge EXAFS spectra were collected from -150 to 550 eV. Samples were referenced to the first inflection point of the pre-edge from Fe foil at 7112 eV (Stöhr, 1992). Spectral averaging of three to twenty spectra based on resolution was done using Athena version 0.8.056 and EXAFS fitting was done in Artemis version 0.8.012 (Ravel and Newville, 2005). Forward Fourier transform of the spectra were conducted with an approximate k -range of 2.5 to 8.7 \AA^{-1} and fit with an R-range of 1 – 3.0. The resulting $\chi(k)$ and their Fourier transforms were fit with calculated phase and amplitude functions for the single and multiple scattering paths of Fe-O, Fe-C/N, and Fe-Fe generated from crystallographic data of goethite (Gualtieri and Venturelli, 1999) and benzene-1,2,4,5-tetracarboxylate (Zhang et al., 2003) using FEFF6. EXAFS data was fit with the adjustable fitting parameters of coordination number (CN), bond distance (R), Debye-Waller factor (σ^2), and the phase shift (ΔE_0). The amplitude reduction factor (S_0^2) was set at 0.9 for all the fits.

3. Results and discussion

Upon photoirradiation, Dismal Swamp DOM was partly remineralized to gases (e.g., CO₂), chemically modified, and flocculated to form particles. The total organic carbon (TOC) concentrations in samples exposed to photoirradiation decreased dramatically with time (Figure 16), and about 76% of the initial organic carbon was lost in 60 days. Particulate organic carbon (POC) concentrations increased during the initial 30 days, but decreased with longer irradiation at Day 60. The pH in samples exposed to light increased gradually from 3.9 initially to 5.5 at Day 18, then 6.1 at Day 30, and finally to 6.9 at Day 60. Buffering by carboxylates controlled the pH initially, but as photoproduct CO₂ accumulated during the irradiation, the pH became buffered at about 5.7 by the bicarbonate system; above pH 5.7 photoproduction of ammonium (as supported by our ammonium measurements) and possibly proton-consuming photoreactions were likely important in controlling the pH. In comparison, flocculation, pH changes, and organic carbon losses were not detectable in dark controls.

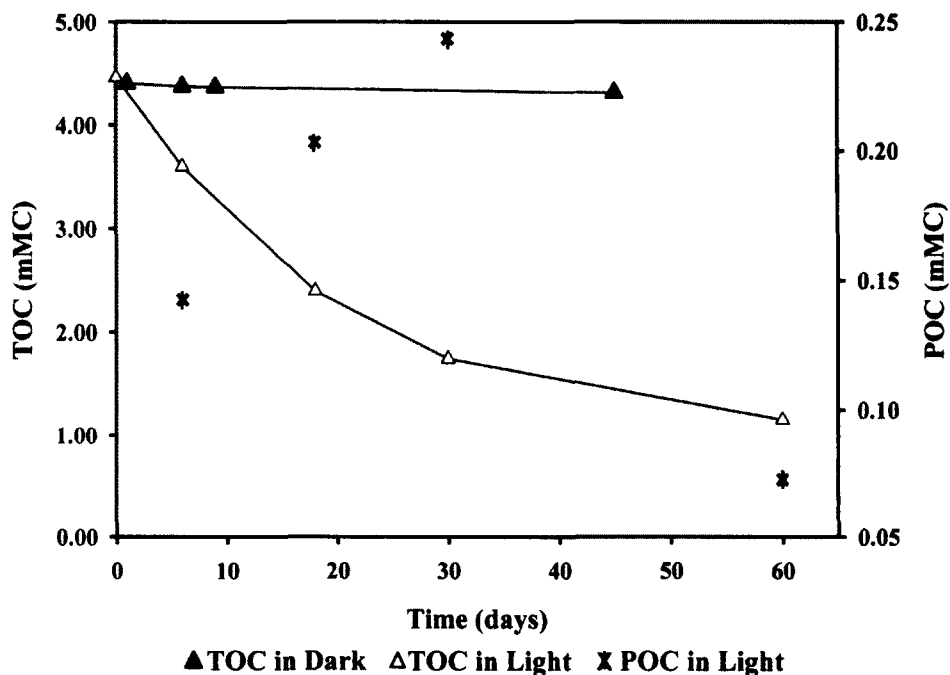


Figure 16. Changes in total organic carbon (TOC) and particulate organic carbon (POC) concentrations during photoirradiation.

The bulk organic carbon and nitrogen of DOM changed significantly with photoirradiation, while the particles, once formed, exhibited similar composition without much variation over time. The bulk C speciation in DOM determined using X-ray absorption spectroscopy showed a dominant proportion of aromatic/unsaturated carbon as well as carboxyl and phenolic carbons suggestive of carboxylated/hydroxylated aromatic structures (Figure 17). With irradiation, the DOM pool showed a loss of aromatic/unsaturated C and a relative increase in the carboxyl C and O-alkyl C (alcohols or carbohydrates). The bulk elemental composition of the photoflocculated POM shows a significantly lower molar H/C ratio than that of the corresponding DOM suggesting that

it contains a greater abundance of aromatic/olefinic structures (Table 13). As photoirradiation continued, the POM maintained its elemental composition but the DOM showed an increase in molar H/C ratio, an indication that the DOM was becoming more aliphatic, consistent with nuclear magnetic resonance (Helms et al., 2013a) and X-ray studies. The N X-ray absorption spectroscopy of DOM also showed significant changes in the amide and oxidized N forms (e.g. nitrosyls) as the photoirradiation of DOM progressed (Figure 18a). The relative abundance of these groups did not vary with time in POM (Figure 18b). However, the newly formed POM is enriched in N compared to the initial DOM (Table 14), in agreement with previous studies (Helms et al., 2013a), and exhibits the same spectral features as DOM without any detectable oxidized N-species.

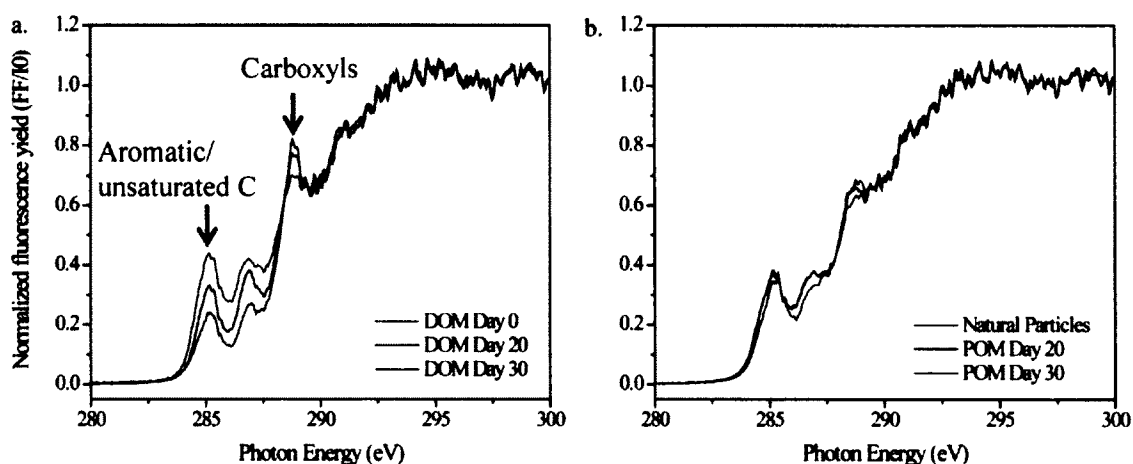


Figure 17. C K-Edge XANES of DOM (a) and POM (b) samples. Over time, the bulk DOM composition lost aromatic/unsaturated C (285 eV) and gained carboxyls (288.8 eV). Bulk POM composition did not change significantly with time. No large differences in Dismal Swamp natural particles compared to lab-generated POM were observed.

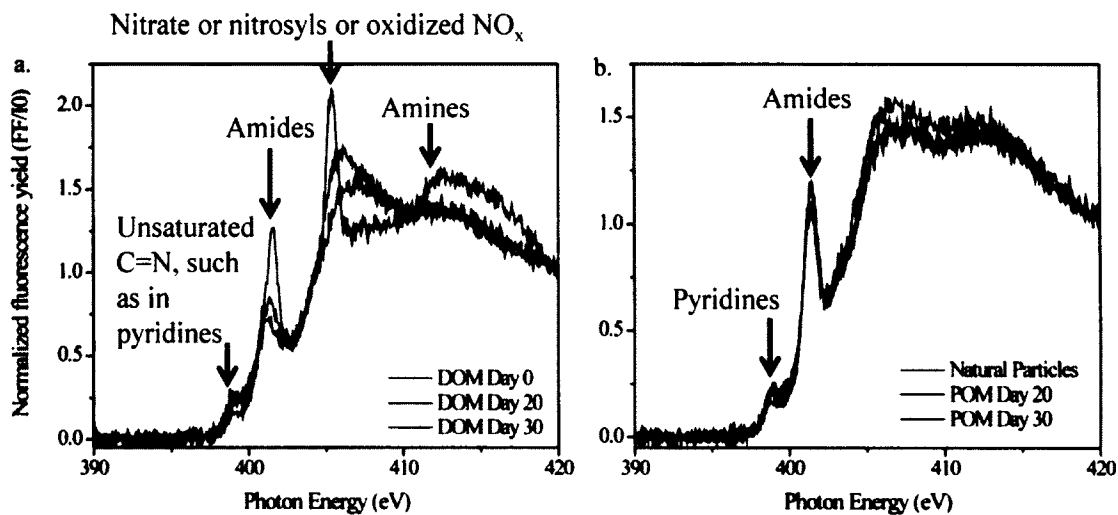


Figure 18. N K-Edge XANES of DOM (a) and POM (b) samples. N features include aromatics (398.7 eV), amides (401.5 eV), nitrosyls (sharp feature at 405.4 eV), and amines (broad feature at 406 eV). Over time, the bulk DOM composition increased in amides and nitrosyls whereas bulk POM composition did not change significantly with time.

Table 13

The elemental H/C ratios from bulk analysis of organic matter in the samples.

	DOM	POM	Control DOM
Day 0	1.16 ± 0.06 (n=12)	--	--
Day 18	1.28 ± 0.04 (n=9)	1.18 ± 0.06 (n=9)	n.d.
Day 21	1.59 ± 0.15 (n=3)	1.16 ± 0.03 (n=3)	1.07 ± 0.04 (n=6)
Day 60	2.45 ± 0.05 (n=2)	n.d.	n.d.
Natural POM	--	1.26 ± 0.07 (n=3)	--

Note: '--' = nonexistent; 'n.d.' = not determined.

Table 14

The elemental C/N ratios from bulk analysis of organic matter in the samples.

	DOM	POM	Control DOM
Day 0	51.8 ± 1.0 (n=11)	--	--
Day 18	32.9 ± 0.5 (n=7)	17.3 ± 0.3 (n=7)	n.d.
Day 21	26.6 ± 0.6 (n=3)	18.9 ± 0.3 (n=3)	51.0 ± 0.9 (n=4)
Day 60	14.0 ± 0.2 (n=2)	n.d.	n.d.
Natural POM	--	26.0 ± 1.3 (n=5)	--

Note: '--' = nonexistent; 'n.d.' = not determined.

The molecular formulas of both DOM and alkali-soluble POM (>60% is soluble at pH 12), obtained from ESI FTICR-MS, suggest 64-94% of all formulas contained only CHO units (Table 15). With increasing photoirradiation time within 30 days, the proportions of CHON formulas increase in DOM but are almost constant in POM, being consistent with the N XANES analysis (Figure 18). The POM samples are enriched in CHON formulas compared to the corresponding DOM at Days 18 and 30. However, the

percentage of CHON formulas and elemental N/C ratios in POM sample decrease at Day 60 (Table 15), which will be examined in a future study. Moreover, the FTICR-MS results show that photoflocculated POM is chemically very different than the respective photoirradiated and original DOM (Figure 19 a&b, Figure 20 a&b). By plotting the H/C ratios as a function of O/C ratios for all molecular formulas associated with POM (on the van Krevelen diagram; Figure 19b), there is a clear segregation of all molecules into two chemically distinct regions: highly aromatic molecules (low H/C), and aliphatic molecules (high H/C and low O/C). There are very few molecules in regions more typically associated with the DOM (Hertkorn et al., 2006; Sleighter and Hatcher, 2008). In addition, the aromatic molecules detected mainly in the POM but also the DOM are primarily condensed aromatic structures with hydroxyl and carboxyl substituents (Figure 21), such as those observed in black carbon produced from combustion (Kramer et al., 2004). These newly formed black carbon-like molecules from photoflocculation are referred to as “photoBC” in this report. The abundances of molecules from these two regions (defined by fields on the van Krevelen diagram in Figure 19b) suggest that the relative proportion of photoBC increases in POM in the first 30 days and then decreases slightly with increasing photoirradiation (Figure 19c). This observation together with the decrease in POM concentration after 30 days (Figure 16) suggests that a portion of photoBC in the POM redissolves, contributes to DOM composition, and becomes photodegradable after 30 days irradiation.

Table 15

Molecular composition for each sample as revealed by ultrahigh resolution mass spectra.

Parameter	DOM				POM			
	Day0	Day18	Day30	Day60	Day18	Day30	Day60	Natural
CHO %	83.1	72.5	72.9	68.9	64.2	64.4	78.9	93.9
CHON %	12.0	23.2	21.6	24.3	32.5	32.4	16.4	3.4
CHOS %	5.2	4.5	5.2	6.4	3.6	4.0	6.0	4.0
CHOP %	0.2	1.0	0.9	2.0	2.1	1.6	2.6	1.5
O/C ratio	0.41	0.44	0.43	0.43	0.42	0.39	0.30	0.28
H/C ratio	1.08	1.12	1.17	1.23	0.97	0.97	1.24	1.20
N/C ratio	0.007	0.017	0.016	0.022	0.021	0.021	0.013	0.003
S/C ratio	0.002	0.003	0.003	0.004	0.002	0.002	0.003	0.002
P/C ratio	<0.001	0.001	<0.001	0.001	0.001	0.001	0.001	0.001
MW	430	409	398	387	422	407	415	517

Note: Elemental ratios and molecular weight (MW) data are number-averaged for all identified formulas in each sample. Considered elements include carbon (C), hydrogen (H), oxygen (O), nitrogen (N), sulfur (S), and phosphorus (P). CHO, compounds containing only C, H, and O; CHON, all compounds containing at least one N, including CHONSP; CHOS, all compounds containing at least one S, including CHONSP; CHOP, all compounds containing at least one P, including CHONSP.

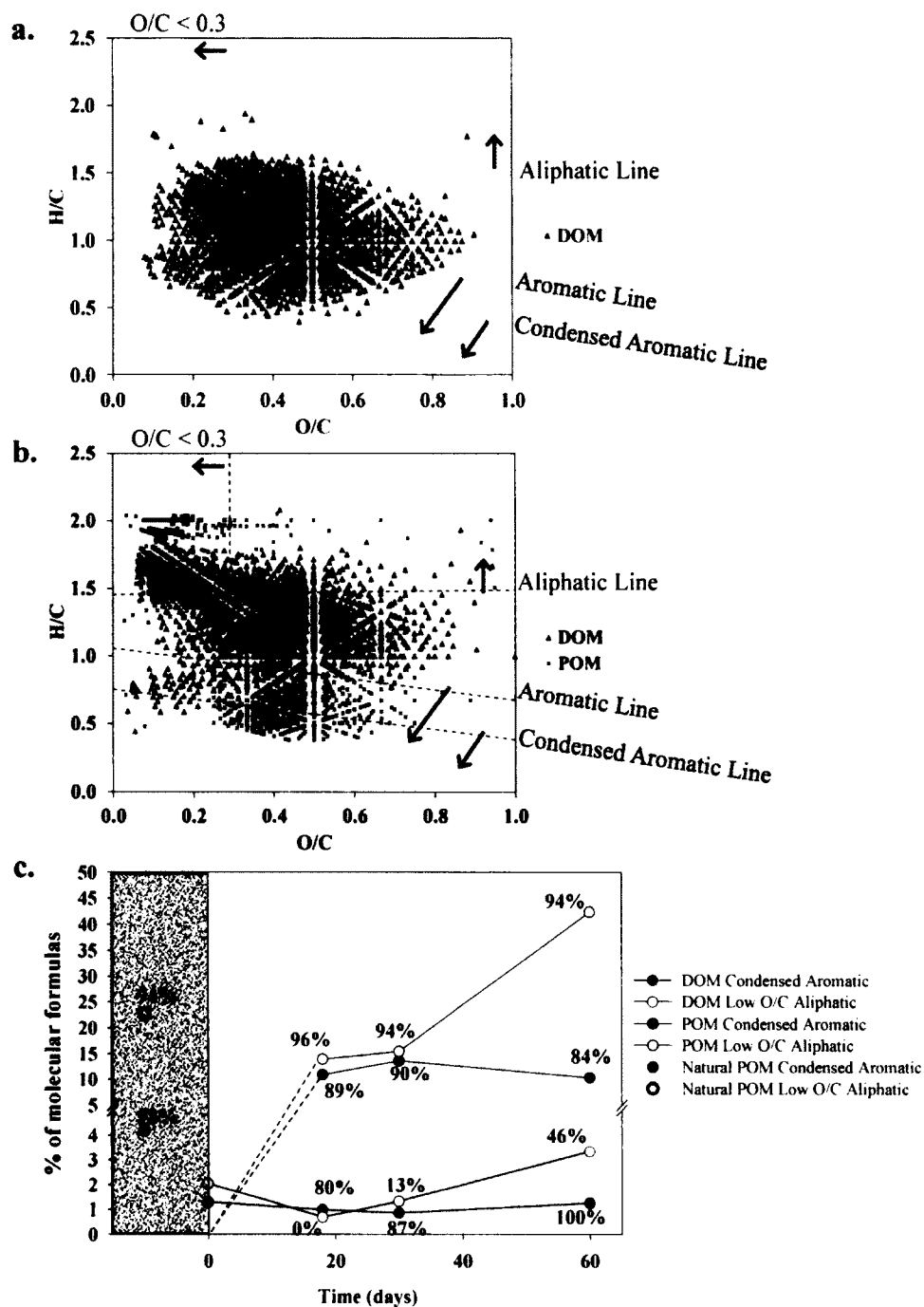


Figure 19. Changes in molecular composition of molecules identified by ultrahigh resolution mass spectrometry. (a) The van Krevelen diagram with elemental H/C and O/C ratios of molecules in Day 0 DOM.

Figure 19. (continued)

(b) The van Krevelen diagram of Day 60 DOM (red) and POM (black). Similar data for other time points are presented in Figure 20a-c. Areas we define as low O/C ($O/C < 0.3$) aliphatic, aromatic and condensed aromatic molecules are marked by dashed lines. (c) Temporal changes in the relative abundance of aromatic (closed circle) or low O/C aliphatic (open circle) formulas (% of total identified formulas) with photoirradiation. With increasing irradiation, the emergence of new molecules (shown next to data points as percentages of condensed aromatic and aliphatic molecules, compared to all identified formulas in DOM at Day 0) increases steadily for DOM and is constant for POM. Also listed in the shaded area are the data for natural POM from the Dismal Swamp.

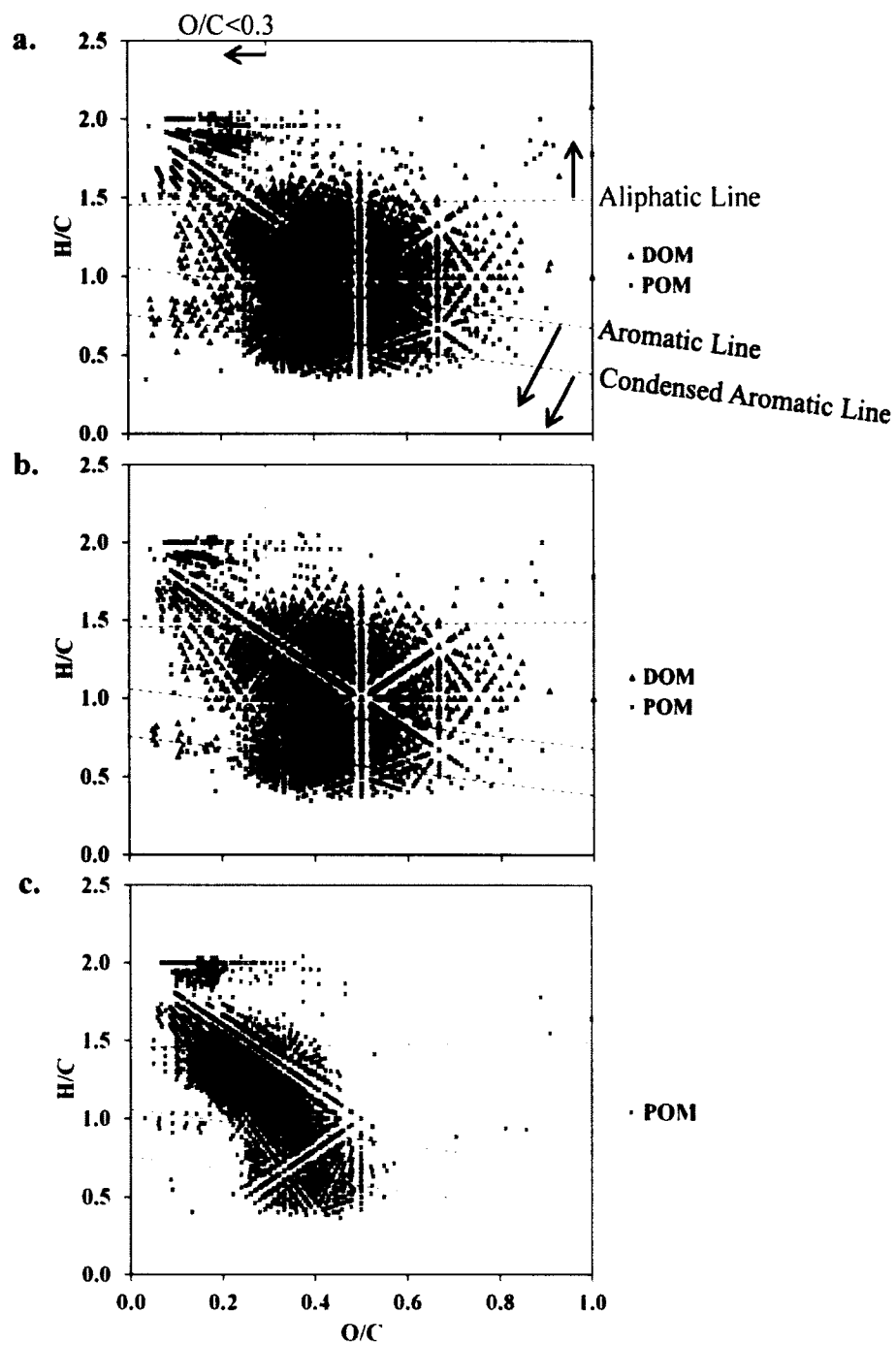


Figure 20. Changes in molecular composition of molecules identified by ESI FTICR-MS. The van Krevelen diagram of molecules of DOM (red) and POM (black) at Day 18 (a) and Day 30 (b), and of POM in the natural particles (c).

Figure 20. (continued)

Aliphatic compounds that are defined as molecules with $\text{DBE/C} < 0.3$ and $\text{H/C} 1.0\text{-}3.0$ (Perdue, 1984) are located above the “Aliphatic Line”. Aromatic compounds that are defined as molecules with $\text{AI}_{\text{mod}} \geq 0.5$ (Koch and Dittmar, 2006) are located below the “Aromatic Line”. Condensed aromatic compounds that are defined as molecules with $\text{AI}_{\text{mod}} \geq 0.67$ (Koch and Dittmar, 2006) are located below the “Condensed Aromatic Line”.

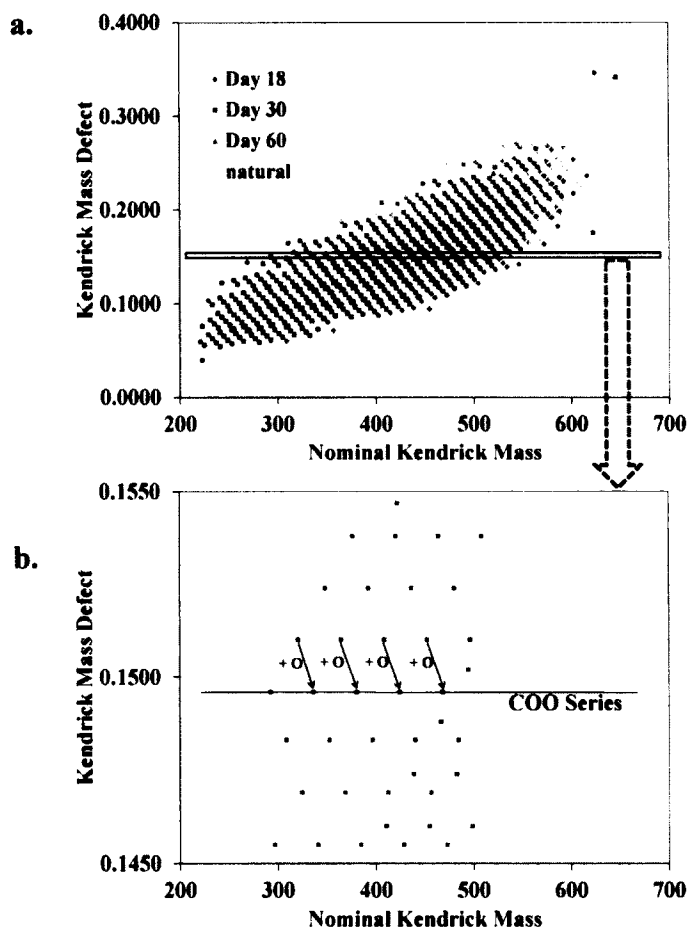


Figure 21. Kendrick mass defect plot of aromatic formulas in photo produced POM and natural POM samples calculated by use of COO KMD analysis. An expanded view of 0.1450-0.1550 KMD at Day 30 is shown in (b), which demonstrates that both hydroxyl and carboxyl function groups are abundant.

The proportion of low O/C aliphatic molecules in the photoflocculated POM (but not the photoBC fraction) appears to increase throughout the course of photoirradiation. The photoproduced aliphatic formulas in POM have H/C ratios from about 1.5 to 2.0 and most have lower O/C ratios compared to the newly formed aliphatic formulas in the

DOM (Figure 22). The majority of the new aliphatic formulas in the photoflocculated POM have H/C ratios around 1.5-1.7, which indicates that the structures are not linear/branched aliphatic but rather either alicyclic or a mixture of aliphatic and olefinic structures, possibly similar to carboxyl-rich alicyclic molecules observed in natural waters (Ball and Aluwihare, 2014; Hertkorn et al., 2006).

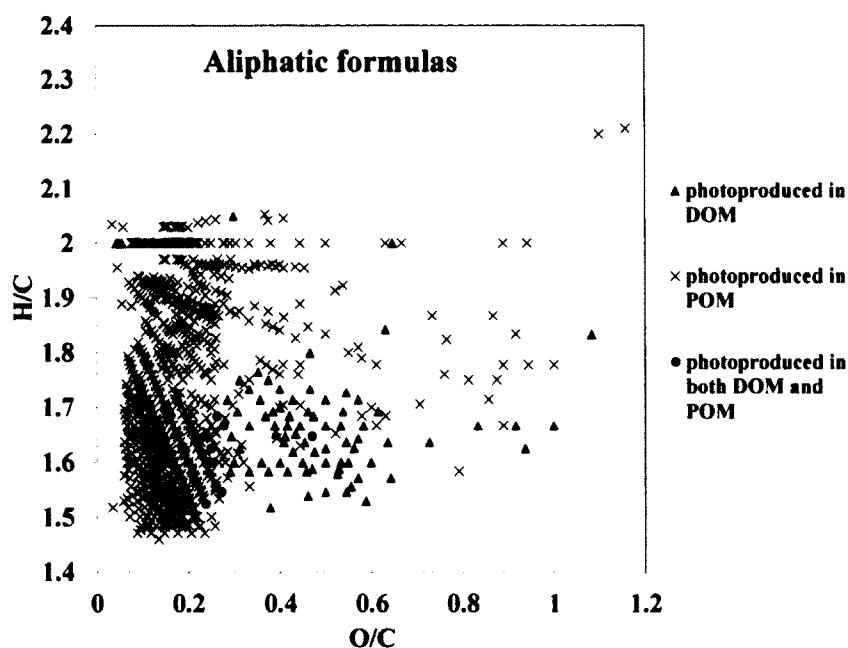


Figure 22. The van Krevelen diagram of molecules identified by ESI FTICR-MS, showing distinct regions for aliphatic formulas photoproduced in POM and DOM, respectively. Photoproduced new aliphatic compounds have higher O/C values in dissolved than particulate phase.

Newly produced aliphatic molecular formulas in DOM increase in relative abundance with greater photoirradiation time and are more oxygenated than their POM

counterparts. The newly formed aliphatics in DOM are more soluble than the newly formed aliphatics in POM due to the oxygenated functional groups (probably carboxyl groups with higher O/C, Figure 22). In the case of photoBC molecules in DOM, a major proportion is absent in the original DOM (80-100%, Figure 19c). It appears that photoirradiation is creating a group of new photoBC molecules, not present initially, that become more prevalent with increasing photodegradation relative to total condensed aromatic DOM molecules. The minor diminution over 30 days is probably because, in solution, these molecules are susceptible to continued photodegradation as shown previously (Stubbins et al., 2012). The increase in photoBC in the DOM pool at 60 days of irradiation is probably from particulate dissolution as this corresponds to the concomitant decline in their abundance in POM (Figure 19c).

In addition to these photochemical changes in organic molecule composition, the concentration and speciation of the associated Fe vary significantly. The Fe/C molar ratios of DOM slightly decreased (from 0.005 to 0.003), while this ratio increased significantly for POM (from 0.040 to 0.244) with photoirradiation time. In addition, the X-ray absorption spectra of Fe (both near-edge and extended X-ray absorption fine structure) associated with both dissolved and particulate pools indicated the presence of both Fe(II) and Fe(III), with more Fe(III) in the POM compared to the DOM (Figure 23a). The interactions of organic molecules with Fe in both DOM and POM also changed with time: initial and Day18 samples at the Fe-absorption edge indicated a significant fraction of Fe coordinated to organic matter with traces of Fe(hydr)oxide polymers (Figure 23 b&c). However, the Fe-organic molecule association decreased and the Fe-Fe polyhedral linkages increased markedly with time (Day 30 and Day 60) suggesting

formation of amorphous ferric hydr(oxide) (Figure 23c). Interestingly, the Fe speciation of natural particles from initial DS water was similar to the Fe speciation of samples from the early stages of photoflocculation with predominant Fe-organic complexation and minimal Fe hydr(oxide) polymerization (Figure 23). These observations are consistent with a previous report that both Fe(II) and Fe(III) form complexes with organic matter in natural waters and soils, often in combination with Fe(III) hydroxides (Sundman et al., 2014). It is noted that the complexation between Fe(III) and organic matter prevents hydrolysis to polymeric Fe(III) hydroxides (Karlsson and Persson, 2012; Sjöstedt et al., 2013). Our study is the first to examine the changes in Fe speciation over time during photoirradiation. The changes in Fe speciation and production of photoBC were correlated with the onset of particle production. However, direct flocculation of DOM by addition of soluble Fe(III) in the absence of light did not result in the production of the same molecules, suggesting the need for photochemical transformation of DOM.

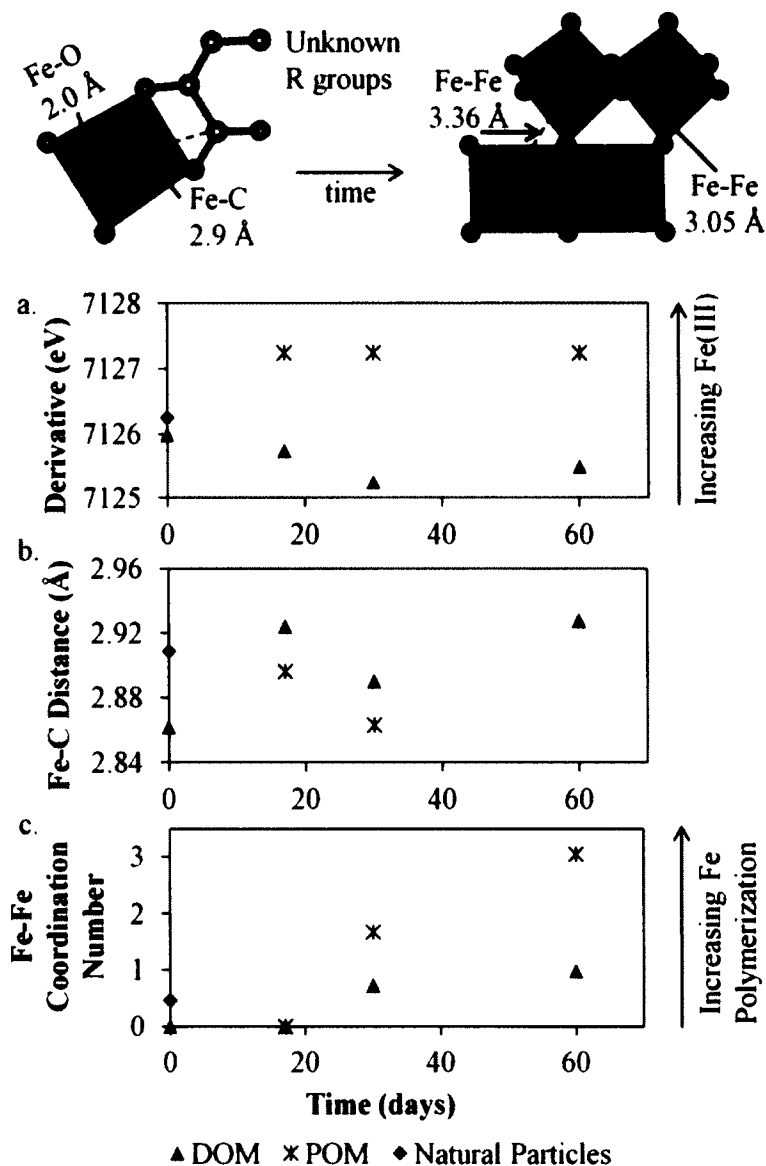


Figure 23. Changes in DOM and POM Fe speciation with time. The derivative energy of the white line from Fe X-ray spectra indicate Fe in the DOM was more reduced (lower energy) than the Fe in the POM (a). Fe-C correlations were observed in all samples except the 60 day POM (b). The coordination number for second neighbor Fe increased with time, indicating increased Fe polymerization in both the DOM and POM with time (c). The top schematic represents the overall trend of Fe speciation- transformation from Fe(II)/(III)-organic complexes to small Fe (III) (hydr)oxide clusters with time.

The X-ray and mass-spectral characteristics of the natural POM (i.e., not lab-irradiated) obtained from Dismal Swamp are similar to the POM generated in the above laboratory studies. Mass spectrometry indicated that approximately 70% of the condensed aromatic formulas observed in natural POM (>60% soluble at pH 12) are also found in the laboratory photoflocculated POM (Figures 19 & 20). As a note of caution, molecular formulas identified among mass spectra from different samples do not necessarily mean the molecules have exactly the same structure, because there could be numerous different structural isomers attributed to a single formula. However, the X-ray spectra of natural POM are almost identical to those of the POM produced during photoflocculation (Figures 17b & 18b), supporting the belief that the chemical structures of these two POM samples are likely similar.

Our new findings document that particulate and dissolved photoBC collectively represent a previously unrecognized source of black carbon in all terrestrial and marine aquatic and sedimentary systems receiving input from freshwater DOM. While a significant portion of the aromatic molecules within dissolved photoBC are considered to be labile in the presence of sunlight (Stubbins et al., 2012), photoBC preservation is tied to its occurrence in the particulate phase (Ward et al., 2014). However, dissolved oxygen and photochemically produced reactive oxygen species oxidize DOM-associated-Fe (II) to Fe (III), leading to the formation of insoluble Fe(III) oxyhydroxides (Faust and Zepp, 1993; Kuma et al., 1996) and subsequent formation of particles which will scavenge photoBC. Thus, there appears to be an important connection between photodegradation of DOM and changes in Fe chemistry.

These results for the first time show that photoflocculation, similar to that observed in the laboratory, is actively producing carboxylated/hydroxylated photoBC compounds, and these are associated with Fe and contributing to the BC POM and DOM in fluvial systems. The photoBC mechanism may partly explain the finding that fluvial BC is isotopically young (compared to fossil fuel combustion derived BC; Ziolkowski and Druffel, 2010), as the ^{14}C age of riverine DOM ranges from modern to only a few thousand years, with most rivers dominated by modern DOM (<500 y; Raymond et al., 2004). Approximately 5% of the initial DOM was removed from the water as photoflocculated POM at Day 60. A conservative estimate, based on the relative percent of condensed aromatic molecules in the POM (Figure 19), indicates that 10% of the POM is photoBC. When one considers that approximately 0.4×10^{15} g of C year⁻¹ of terrestrial DOM is being transported to the ocean (Schlesinger and Melack, 1981), we can estimate a flux of 0.02×10^{15} g of C year⁻¹ of photoBC from rivers to the ocean, mainly to coastal sediments. This flux is almost equal to the estimated global flux of dissolved black carbon from land to the ocean (Jaffé et al., 2013). Moreover, the greatest flux of dissolved BC was from wetlands (Jaffé et al., 2013) where the increased levels of DOM subjected to high solar irradiance will likely magnify the production of photoBC. Although photoBC molecules are mostly present in the particulate phase in our photoirradiation experiment, we observed that they redissolve after extended photoirradiation (e.g., >30 days) and contribute to DOM (noted by an increase in photoBC in the DOM, Figure 19c). It is reasonable to expect that redissolved photoBC will eventually be photodegraded further as shown previously (Stubbins et al., 2012).

Any photoBC remaining as POM will likely be protected from photodegradation (Ward et al., 2014).

These newly discovered photoBC and aliphatic molecules found in our studies were observed in the mass spectral analyses of a peat sample (the Pahokee peat from Florida) as well as the ambient Dismal Swamp POM and peat (Figure 24). DOM from both coastal waters (Chesapeake Bay; in immediately offshore samples) and open ocean (the Cape Verde Rise in North Atlantic Ocean) (Figure 24) also contain compounds similar to the photoproduct molecules but mainly the aliphatic ones, most likely because the aromatic photoBC molecules have been lost through photodegradation. These results suggest that the photoflocculation phenomenon observed in the Dismal Swamp is pervasive, and that this organic matter may be photoproduct globally in all terrestrially influenced coastal waters and adjacent seas. Moreover, the new molecules from natural organic matter are composed of condensed aromatics or alicyclic molecules, similar to those of humified organic matter. As a result, these new molecules are likely to be less biodegradable and contribute to the stabilization/sequestration of carbon and metals such as Fe.

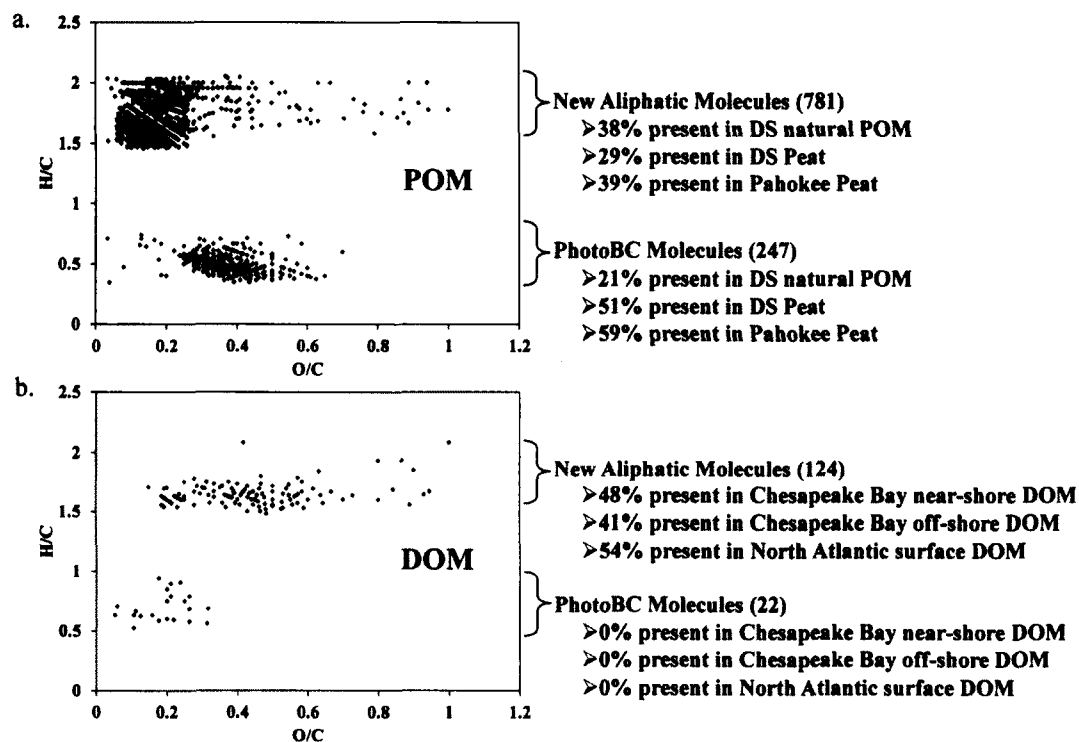


Figure 24. The van Krevelen diagram showing the newly formed POM (a) and DOM (b) molecular formulas from photoflocculation together with the numbers of formulas for both regions observed in ultrahigh resolution mass spectra of various respective samples (base extracts) of peat and DOM from riverine, coastal, and open ocean waters (Chen et al., 2014; Sleighter and Hatcher, 2008). Newly-produced condensed aromatic formulas (photoBC) appear to be only observed in natural POM and peat while new aliphatic formulas persist in both POM and DOM and constitute a large percentage of formulas found in these natural samples.

CHAPTER V

SUMMARY AND CONCLUSIONS

1. Conclusions

Electrospray ionization Fourier transform ion cyclotron resonance mass spectrometry (ESI FTICR-MS) is an analytical technique with ultrahigh resolution and mass accuracy that allows efficient molecular level characterization of dissolved organic matter (DOM) and provides new insight into the nature and reactivity of DOM. When ESI FTICR-MS is applied to saline samples from the coastal zone or the open ocean, the prerequisite is to desalt and isolate DOM ideally with no selective fractionation.

One of the goals of the current study is to develop a method for desalting small volumes of seawater samples for subsequent analysis by ESI FTICR-MS. An affordable, commercially available mini-electrodialysis (mini-ED) system has been evaluated for the efficient desalting of small volume samples of seawater prior to analysis by ESI FTICR-MS. The ESI FTICR-MS spectral data were compared with those of samples that were treated by C₁₈ solid phase extraction, a commonly-used method for rapid sample preparation for this type of preconcentration of the DOM and removal of salts. In this comparison it is clear that the mini-ED provides more representative molecular information, compared to C₁₈ isolation, and recovers the overwhelming majority of peaks from salt-free samples, indicating that it adequately represents the DOM that can be ionized and analyzed by ESI FTICR-MS. The mini-ED system produces a significant carbon blank. However, the substances contributing to this blank are not detectable by ESI FTICR-MS because they are apparently not ionizable. Based on these findings the

mini-ED is recommended as a promising method for the desalting of low-volume aqueous environmental samples prior to analysis by ESI FTICR-MS.

A large volume DOM isolation technique using reverse osmosis coupled with electrodialysis (RO/ED) has achieved the highest recovery of DOM amongst all available methods at present (Green et al., 2014; Koprivnjak et al., 2009). Compared to the traditional C₁₈ SPE method, the RO/ED technique is able to isolate more N-containing organic compounds and more compounds with high O/C atomic ratio (>0.6). The present study has combined the RO/ED technique together with the powerful ESI FTICR-MS with the objective of obtaining more representative marine DOM samples and, therefore, bringing a greater fraction and diversity of the DOM pool into our analytical window. Meanwhile, it was feasible to analyze the RO/ED isolated marine DOM samples by ESI FTICR-MS without any organic solvent addition. Hence, cleaner spectra of DOM peaks were obtained in this study, compared with spectra obtained by additions of methanol where fatty acids appear to be over-represented and dominate the overall response.

The most significant mass spectral characteristics of the RO/ED isolated marine DOM samples is that they all share a significant number of common peaks, accounting for >50% of the total peaks of each MS. Meanwhile, these common peaks are generally observed at high intensity. Whether such high percentages of common peaks are due to preferential ionization of certain compounds has to be further determined. When comparing with other samples (e.g., Sleighter and Hatcher, 2008; Stubbins et al., 2010), ESI FTICR-MS has demonstrated a capability to reveal differences among DOM samples. For example, the abundant aromatic molecules present in river or estuarine DOM (Sleighter and Hatcher, 2008) are absent in all RO/ED isolated marine DOM

samples. When compositional differences are expected, spectral differences are observed. Thus, it is very likely that the high commonality observed in the RO/ED isolated marine DOM mass spectra is indicative of a high degree of similarity of DOM within the different water masses studied. This is consistent with the fact that there is a highly refractory “background” DOM that circulates throughout all the oceans (Carlson, 2002).

It is well recognized that ESI FTICR-MS is not quantitative due to the fact that different compounds have different ionization efficiencies (e.g. Shen and Perreault, 1998). However, the significance of this difference is yet to be measured. The present study has quantified the total dissolved carbohydrate (TCHO) concentrations using a colorimetric method, and subsequently compare with the results from ESI FTICR-MS. The contribution of carbohydrate-like peaks in ESI FTICR-MS of different samples is significantly lower than the measured percentages of TCHO-C in DOC, indicating that ESI FTICR-MS underestimates carbohydrate-like compounds. However, the results from ESI FTICR-MS are well correlated to those from colorimetric assays, suggesting that ESI FTICR-MS is still able to differentiate the concentration level of carbohydrate-like compounds among samples. Another similarity shared in the RO/ED isolated marine DOM samples is that CHO and CHON formulas are the most abundant elemental compositions, with CHO formulas being more abundant than those for CHON. Whether the concentrations of these two classes of compounds are relatively higher than other compounds is uncertain.

Great care was taken to ensure that identical analytical conditions were applied for all RO/ED isolated DOM samples, including the adjustment of concentrations to be the same for all samples. This prevented biasing of the results towards differences caused

by the concentrations or instrument parameters. In this context, the observed differences among the isolated RO/ED DOM samples are more likely associated with the respective characteristics of the samples. Carboxylic-rich alicyclic molecules (CRAM) – like compounds, one ubiquitous component in DOM (Hertkorn et al., 2006), are observed to be the most abundant components across the RO/ED isolated DOM samples, with relatively lower percentage in the surface water samples compared to the intermediate and deep water samples. It is important to state that these overlap significantly with molecules having a lignin-derived character (Sleighter and Hatcher, 2008). The aliphatic compounds are the second most abundant components, with relatively higher abundances in the surface water samples compared to the intermediate and deep water samples. Carbohydrate-like compounds are mainly found in the surface samples, with the North Pacific deep (3500 m) water having the lowest % and the North Atlantic upwelling core surface water having the highest %. This finding supports the view that carbohydrate-like molecules are significant constituents of biolabile and semi-labile compounds that are freshly produced in surface waters (Carlson, 2002) and is consistent with previous studies of DOM examined by solid-state ^{13}C NMR (Benner et al., 1992).

Due to the high similarity of mass spectra among the RO/ED isolated DOM samples, principal component analysis (PCA) was applied to accentuate subtle differences that might exist. We demonstrate PCA to be an useful approach for molecular differentiation of DOM within the major water masses along the global oceanic conveyor belt. PCA analysis employing relative peak magnitudes shows that peaks that are enriched in surface samples have higher H/C values than peaks enriched in deep samples. This is true of samples from both the North Atlantic and the North Pacific. This trend is

likely related to several processes, 1) photo-degradation of photo-labile compounds, 2) the bio-production of biolabile compounds in surface waters, and 3) the biodegradation of biolabile compounds with depth. The North Atlantic oxygen minimum layer and deep DOM have lower O/C values than the North Pacific intermediate and deep DOM, for both CHO and CHON compounds. This finding is indicative of an oxygenation process that could be due to microbial activity during ageing of DOM and/or greater remineralization of DOM from sinking particles in the deep Pacific Ocean (Nelson et al., 2010). There is a small chance that the difference between the Atlantic samples and the Pacific samples is partially the result of recovery efficiency, which is relatively low in the Atlantic deep samples. However, while examining at the larger body of RO/ED results (Green et al., 2014; Koprivnjak et al., 2009), the RO/ED method is noted to have greater variability in yields of DOM when samples are isolated from a variety of sources than when isolated from a single source. This strongly suggests that compositional differences exist spatially and that they affect yields of DOC.

Photo-resistant and photo-produced molecular formulas that are preserved and produced when irradiating the Congo river water DOM (Stubbins et al., 2010) are also enriched in surface North Pacific subtropical gyre DOM. This suggests that extensive photo-bleaching in this open ocean region has resulted in the preservation and accumulation of photo-degraded DOM having the same molecular signature as that observed for photoreacted terrestrial DOM. The similarities in the molecular signatures of photo-degraded Congo DOM and photo-degraded Pacific Open Ocean DOM does not necessarily mean that the DOM is of the same origin; rather this relationship suggests that

photochemistry shapes the DOM in both cases to result in similar average elemental properties.

It is well known that photochemical processing of dissolved organic matter (DOM) in natural waters can alter its composition and structure, supply particulate organic matter (POM) to sediments, and deliver modified terrestrial DOM to the ocean. Our studies show that terrestrial DOM from the Dismal Swamp exposed to simulated sunlight is altered to produce POM with a markedly different molecular composition than original DOM, enriched in newly-formed aliphatic and condensed aromatic molecules. This process is closely tied to the chemistry of iron, which primarily exists as dissolved Fe(II) and Fe(III)-organic complexes in initial DOM and photochemically matures to Fe(III) oxyhydroxides before co-precipitating out with POM. The newly formed condensed aromatic compounds resemble black carbon, which until now was thought to be produced only by combustion. These new molecules contribute a pool of Fe-rich, aliphatic and black carbon-like organic matter to sediments as the terrestrial DOM is transported through rivers. We estimate that the annual global flux of this photoproduct black carbon, most of which may be preserved in sediments, is nearly equivalent to the estimated flux of dissolved black carbon to the ocean from all other sources. Moreover, the production of aliphatic CRAM-like molecules could represent an important new mechanism for export of such molecules to the oceans.

2. Future directions

In the course of this research it has become quite apparent that shortcomings of the analytical approaches have limited our ability to more clearly define the molecular-level characteristics of coastal and marine DOM. Future work focused on mitigating

these is obvious if one is to effectively isolate and characterize both the nature and origin of marine DOM. Below I make some suggestions as to the course of research that would benefit from improvement.

Contamination from the mini-ED system does not significantly affect ESI FTICR mass spectra. However, if mini-ED is applied to desalt samples prior to other analyses, e.g. HPLC or NMR, analysis-specific blanks and recoveries should be assessed. In this regard, future studies should attempt to find a source of other membrane and bath materials to reduce contamination, thereby enabling coupling of mini-ED to other analytical techniques. Significantly, the desalting approach described here can be done quite easily on small amounts of sample either aboard ship or in the laboratory. The small sample size requirement makes this technique amenable to studies of pore waters and other environmental samples and experimental designs where large water volumes are not feasible. There are still a lot of tests to be completed to optimize this method, such as looking for bigger chambers to minimize the processing time. An important consideration when coupling to other analytical techniques will be the DOC mass balance. It is also unknown how the DOC recovery will change under different initial DOC concentrations and qualities. Testing the system with real oceanic DOM samples, which are both much lower in DOC concentration and chemically distinct from those samples studied herein, is a major priority. Finally, as part of this oceanic sample isolation, the mini-ED performance should be systematically compared with currently available DOM isolation techniques such as PPL extraction, ultrafiltration, and the larger volume RO/ED.

Regarding the issue that different compounds have different ionization efficiencies in ESI FTICR-MS, such studies need more effort to evaluate the ionization

efficiencies of specific types of compounds. For example, in the present study, carbohydrate-like compounds were found to be underestimated in ESI FTICR-MS. We are aware of only few studies tentatively quantifying a specific class of compounds using ESI FTICR-MS (quantifying fatty acids; Kamga et al., 2014). Similar studies have to be conducted to potentially direct the ESI FTICR-MS to be a quantitative technique.

Mass spectrometric compound identifications are limited to masses only, which result in proposed molecular formulas with a given set of elements. The major topic in DOM research is the structural identification of DOM compounds. Therefore, mass spectrometry fragmentation experiments and NMR study of DOM compounds need to be coupled with ESI FTICR-MS to discern structure of DOM compounds. The advent of such studies will eventually help to answer several key questions in DOM research. For example, there are a significant amount of common peaks even between river DOM and marine DOM samples. Whether exact peak match represents the same structural isomer is uncertain at present. It is likely that it does not, so this exercise might be in vain or prove to be unattainable.

The most logical extension of this work focuses on questions emanating from the study of phototransformation of terrestrial DOM. For example, whether a similar process occurs for oceanic DOM is uncertain. The oceanic water has high content of salts but extremely low content of DOC, providing a challenge for photoirradiation experiments. If a similar photoflocculation process does occur in the open ocean, those newly produced black carbon-like and aliphatic compounds would be observed in marine particles and in the DOM.

REFERENCES

- Abdulla, H.A.N., Sleighter, R.L., Hatcher, P.G., 2013. Two dimensional correlation analysis of Fourier transform ion cyclotron resonance mass spectra of dissolved organic matter: A new graphical analysis of trends. *Anal. Chem.* 85 (8), 3895-3902. <http://dx.doi.org/10.1021/ac303221j>
- Aiken, G.R., Thurman, E.M., Malcolm, R.L., Walton, H.F., 1979. Comparison of XAD macroporous resins for the concentration of fulvic acid from aqueous solution. *Anal. Chem.* 51 (11): 1799-1803. <http://pubs.acs.org/doi/abs/10.1021/ac50047a044>
- Amon, R.M.W., Budéus, G., Meon, B., 2003. Dissolved organic carbon distribution and origin in the Nordic Seas: Exchanges with the Arctic Ocean and the North Atlantic. *J. Geophys. Res.* 108 (C7), 3221. <http://dx.doi.org/10.1029/2002JC001594>
- Ball, G.I., Aluwihare, L.I., 2014. CuO-oxidized dissolved organic matter (DOM) elucidated by comprehensive two dimensional gas chromatography-time of flight-mass spectrometry (GC×GC-TOF-MS). *Org. Geochem.* 75, 87-98. <http://dx.doi.org/10.1016/j.orggeochem.2014.06.010>
- Bateman, A.P., Walser, M.L., Desyaterik, Y., Laskin, J., Laskin, A., Nizkorodov, S.A., 2008. The effect of solvent on the analysis of secondary organic aerosol using electrospray ionization mass spectrometry. *Environ. Sci. Technol.* 42: 7341-7346. <http://dx.doi.org/10.1021/es801226w>
- Barbeau, K., 2006. Photochemistry of organic iron(III) complexing ligands in oceanic systems. *Photochem. Photobiol.* 82: 1505-1516. <http://dx.doi.org/10.1562/2006-06-16-IR-935>

- Benner, R., Pakulski, J.D., McCarthy, M., Hedges, J.I., Hatcher, P.G., 1992. Bulk chemical characteristics of dissolved organic matter in the ocean. *Science* 255 (5051), 1561-1564. <http://dx.doi.org/10.1126/science.255.5051.1561>
- Benner, R., Opsahl, S., 2001. Molecular indicators of the sources and transformations of dissolved organic matter in the Mississippi river plume. *Org. Geochem.* 32 (4): 597-611. [http://dx.doi.org/10.1016/S0146-6380\(00\)00197-2](http://dx.doi.org/10.1016/S0146-6380(00)00197-2)
- Berner, R.A., 1989. Biogeochemical cycles of carbon and sulfur and their effect on atmospheric oxygen over phanerozoic time. *Palaeogeogr. Palaeoclimatol. Palaeoecol.* 75, 97-122. [http://dx.doi.org/10.1016/0031-0182\(89\)90186-7](http://dx.doi.org/10.1016/0031-0182(89)90186-7)
- Bhatia, M.P., Das, S.B., Longnecker, K., Charette, M.A., Kujawinski, E.B., 2010. Molecular characterization of dissolved organic matter associated with the Greenland ice sheet. *Geochim. Cosmochim. Acta* 74 (13): 3768-3784. <http://dx.doi.org/10.1016/j.gca.2010.03.035>
- Bronk, D.A., 2002. Dynamics of DON. In: Hansell D.A., Carlson C.A. (Eds.), *Biogeochemistry of Marine Dissolved Organic Matter*. Academic Press, San Diego, pp. 153–247. <http://dx.doi.org/10.1016/B978-012323841-2/50007-5>
- Brown, T.L, Rice, J.A., 2000. Effect of experimental parameters on the ESI FT-ICR mass spectrum of fulvic acid. *Anal. Chem.* 72: 384-390. <http://dx.doi.org/10.1021/ac9902087>
- Buesseler, K.O., Bauer, J.E., Chen, R.F., Eglinton, T.I., Gustafsson, O., Landing, W., Mopper, K., Moran, S.B., Santschi, P.H., VernonClark, R., Wells, M.L., 1996. An intercomparison of cross-flow filtration techniques used for sampling marine

colloids: Overview and organic carbon results. *Mar. Chem.* 55 (1–2), 1-31.
[http://dx.doi.org/10.1016/S0304-4203\(96\)00046-1](http://dx.doi.org/10.1016/S0304-4203(96)00046-1)

Burney, C.M., Sieburth, J.McN., 1977. Dissolved carbohydrates in seawater. II, A spectrophotometric procedure for total carbohydrate analysis and polysaccharide estimation. *Mar. Chem.* 5 (1), 15-28. [http://dx.doi.org/10.1016/0304-4203\(77\)90012-3](http://dx.doi.org/10.1016/0304-4203(77)90012-3)

Carlson, C.A., 2002. Production and removal processes. In: Hansell, D.A., Carlson, C.A., (Eds.), *Biogeochemistry of Marine Dissolved Organic Matter*. Academic Press, San Diego, pp. 91-151. <http://dx.doi.org/10.1016/B978-012323841-2/50006-3>

Carlson, C.A., Hansell, D.A., Nelson, N.B., Siegel, D.A., Smethie, W.M., Khatiwala, S., Meyers, M.M., Halewood, E., 2010. Dissolved organic carbon export and subsequent remineralization in the mesopelagic and bathypelagic realms of the North Atlantic basin. *Deep-Sea Res. II* 57 (16), 1433-1445.
<http://dx.doi.org/10.1016/j.dsr2.2010.02.013>

Chen, H., Stubbins, A., Hatcher, P.G., 2011. A mini-electrodialysis system for desalting small volume saline samples for Fourier transform ion cyclotron resonance mass spectrometry. *Limnol. Oceanogr. Methods* 9, 582-592.
<http://dx.doi.org/10.4319/lom.2011.9.582>

Chen, H., Stubbins, A., Perdue, E.M., Green, N.W., Helms, J.R., Mopper, K., Hatcher, P.G., 2014. Ultrahigh resolution mass spectrometric differentiation of dissolved organic matter isolated by coupled reverse osmosis-electrodialysis from various

major oceanic water masses. *Mar. Chem.* 164, 48-59.

<http://dx.doi.org/10.1016/j.marchem.2014.06.002>

D'Andrilli, J., Dittmar, T., Koch, B.P., Purcell, J.M., Marshall, A.G., Cooper, W.T., 2010.

Comprehensive characterization of marine dissolved organic matter by Fourier transform ion cyclotron resonance mass spectrometry with electrospray and atmospheric pressure photoionization. *Rapid Commun. Mass Spectrom.* 24 (5):

643-650. <http://dx.doi.org/10.1002/rcm.4421>

Del Castillo, C.E., Coble, P.G., Morrell, J.M., Lopez, J.M., Corredor, J.E., 1999. Analysis

of the optical properties of the Orinoco River plume by absorption and fluorescence spectroscopy. *Mar. Chem.* 66: 35-51. [http://dx.doi.org/10.1016/S0304-](http://dx.doi.org/10.1016/S0304-4203(99)00023-7)

[4203\(99\)00023-7](http://dx.doi.org/10.1016/S0304-4203(99)00023-7)

Del Vecchio, R., Blough, N.V., 2002. Photobleaching of chromophoric dissolved organic

matter in natural waters: kinetics and modeling. *Mar. Chem.* 78: 231-253.

[http://dx.doi.org/10.1016/S0304-4203\(02\)00036-1](http://dx.doi.org/10.1016/S0304-4203(02)00036-1)

Del Vecchio, R., Subramaniam, A., 2004. Influence of the Amazon River on the surface

optical properties of the western tropical North Atlantic Ocean. *J. Geophys. Res.*

109, C11001. <http://dx.doi.org/10.1029/2004JC002503>

Dittmar, T., Lara, R.J., Kattner, G., 2001. River or mangrove? Tracing major organic

matter sources in tropical Brazilian coastal waters. *Mar. Chem.* 73 (3-4): 253-271.

[http://dx.doi.org/10.1016/S0304-4203\(00\)00110-9](http://dx.doi.org/10.1016/S0304-4203(00)00110-9)

Dittmar, T., Whitehead, K., Minor, E.C., Koch, B.P., 2007. Tracing terrigenous dissolved

organic matter and its photochemical decay in the ocean by using liquid

- chromatography/mass spectrometry. *Mar. Chem.* 107 (3): 378-387.
<http://dx.doi.org/10.1016/j.marchem.2007.04.006>
- Dittmar, T., Koch, B.P., Hertkorn, N., Kattner, G., 2008. A simple and efficient method for the solid-phase extraction of dissolved organic matter (SPE-DOM) from seawater. *Limnol. Oceanogr. Methods* 6: 230-235.
<http://dx.doi.org/10.4319/lom.2008.6.230>
- Doval, M.D., Hansell, D.A., 2000. Organic carbon and apparent oxygen utilization in the western South Pacific and the central Indian Oceans. *Mar. Chem.* 68 (3): 249-264.
[http://dx.doi.org/10.1016/S0304-4203\(99\)00081-X](http://dx.doi.org/10.1016/S0304-4203(99)00081-X)
- Faust, B.C., Zepp, R.G., 1993. Photochemistry of aqueous iron(III)-polycarboxylate complexes: roles in the chemistry of atmospheric and surface waters. *Environ. Sci. Technol.* 27, 2517-2522. <http://dx.doi.org/10.1021/es00048a032>
- Flerus, R., Koch, B.P., Schmitt-Kopplin, P., Witt, M., Kattner, G., 2011. Molecular level investigation of reactions between dissolved organic matter and extraction solvents using FT-ICR MS, *Mar. Chem.* 124 (1): 100-107.
<http://dx.doi.org/10.1016/j.marchem.2010.12.006>
- Flerus, R., Lechtenfeld, O.J., Koch, B.P., McCallister, S.L., Schmitt-Kopplin, P., Benner, R., Kaiser, K., Kattner, G., 2012. A molecular perspective on the ageing of marine dissolved organic matter. *Biogeosciences* 9, 1935-1955.
<http://dx.doi.org/10.5194/bg-9-1935-2012>
- Gao, H.Z., Zepp, R.G., 1998. Factors influencing photoreactions of dissolved organic matter in coastal river of the southern United States. *Environ. Sci. Technol.* 32: 2940-2946. <http://dx.doi.org/10.1021/es9803660>

- Grannas, A.M., Hockaday, W.C., Hatcher, P.G., Thompson, L.G., Mosley-Thompson, E., 2006. New revelations on the nature of organic matter in ice cores. *J. Geophys. Res.* 111, D04304. <http://dx.doi.org/10.1029/2005JD006251>
- Green, N.W., Perdue, E.M., Aiken, G.R., Butler, K.D., Chen, H., Dittmar, T., Niggemann, J., Stubbins, A., 2014. An intercomparison of three methods for the large-scale isolation of oceanic dissolved organic matter. *Mar. Chem.* 161, 14-19. <http://dx.doi.org/10.1016/j.marchem.2014.01.012>
- Gualtieri, A.F., Venturelli, P., 1999. In situ study of the goethite-hematite phase transformation by real time synchrotron powder diffraction. *Am. Mineral.* 84, 895-904.
- Guo, L., Santschi, P.H., 1996. A critical evaluation of the cross-flow ultrafiltration technique for sampling colloidal organic carbon in seawater. *Mar. Chem.* 55 (1-2): 113-127. [http://dx.doi.org/10.1016/S0304-4203\(96\)00051-5](http://dx.doi.org/10.1016/S0304-4203(96)00051-5)
- Hansell, D.A., Carlson, C.A., 1998. Deep-ocean gradients in the concentration of dissolved organic carbon. *Nature* 395 (6699), 263-266. <http://dx.doi.org/10.1038/26200>
- Hansell, D.A., Carlson, C.A., Schlitzer, R., 2012. Net removal of major marine dissolved organic carbon fractions in the subsurface ocean. *Global Biogeochem. Cycles* 26, GB1016. <http://dx.doi.org/10.1029/2011GB004069>
- Hedges, J.I., 1992. Global biogeochemical cycles: progress and problems. *Mar. Chem.* 39 (1-3), 67-93. [http://dx.doi.org/10.1016/0304-4203\(92\)90096-S](http://dx.doi.org/10.1016/0304-4203(92)90096-S)

- Hedges, J.I., 2002. Why dissolved organics matter? In: Hansell, D.A., Carlson, C.A., (Eds.), *Biogeochemistry of Marine Dissolved Organic Matter*. Academic Press, San Diego, pp. 1-33. <http://dx.doi.org/10.1016/B978-012323841-2/50003-8>
- Hedges, J.I., Keil, R.G., 1995. Sedimentary organic matter preservation: an assessment and speculative synthesis. *Mar. Chem.* 49, 81-115. [http://dx.doi.org/10.1016/0304-4203\(95\)00008-F](http://dx.doi.org/10.1016/0304-4203(95)00008-F)
- Hedges, J.I., Keil, R.G., Benner, R., 1997. What happens to terrestrial organic matter in the ocean? *Org. Geochem.* 27: 195-212. [http://dx.doi.org/10.1016/S0146-6380\(97\)00066-1](http://dx.doi.org/10.1016/S0146-6380(97)00066-1)
- Helms, J.R., 2012. Spectroscopic characterization of dissolved organic matter: insights into composition, photochemical transformation and carbon cycling. Doctoral Thesis, Old Dominion University, Norfolk, VA, USA.
- Helms, J.R., Mao, J., Schmidt-Rohr, K., Abdulla, H.A.N., Mopper, K., 2013a. Photochemical flocculation of terrestrial dissolved organic matter and iron. *Geochim. Cosmochim. Acta* 121, 398-413. <http://dx.doi.org/10.1016/j.gca.2013.07.025>
- Helms, J.R., Stubbins, A., Perdue, E.M., Green, N.W., Chen, H., Mopper, K., 2013b. Photochemical bleaching of oceanic dissolved organic matter and its effect on absorption spectral slope and fluorescence. *Mar. Chem.* 155, 81-91. <http://dx.doi.org/10.1016/j.marchem.2013.05.015>
- Helms, J.R., Mao, J., Stubbins, A., Schmidt-Rohr, K., Spencer, R.G.M., Hernes, P.J., Mopper, K., 2014. Loss of optical and molecular indicators of terrigenous

dissolved organic matter during long-term photobleaching. *Aquat. Sci.* 76 (2), 1-21.

<http://dx.doi.org/10.1007/s00027-014-0340-0>

Hernes, P.J., Benner, R., 2006. Terrigenous organic matter sources and reactivity in the North Atlantic Ocean and a comparison to the Arctic and Pacific oceans. *Mar. Chem.* 100 (1-2): 66-79. <http://dx.doi.org/10.1016/j.marchem.2005.11.003>

Hertkorn, N., Benner, R., Frommberger, M., Schmitt-Kopplin, P., Witt, M., Kaiser, K., Kettrup, A., Hedges, J.I., 2006. Characterization of a major refractory component of marine dissolved organic matter. *Geochim. Cosmochim. Acta* 70 (12): 2990-3010. <http://dx.doi.org/10.1016/j.gca.2006.03.021>

Hertkorn, N., Frommberger, M., Witt, M., Koch, B.P., Schmitt-Kopplin, P., Perdue, E.M., 2008. Natural organic matter and the event horizon of mass spectrometry, *Anal. Chem.* 80, 8908-8919. <http://dx.doi.org/10.1021/ac800464g>

Hertkorn, N., Harir, M., Koch, B.P., Michalke, B., Schmitt-Kopplin, P., 2013. High-field NMR spectroscopy and FTICR mass spectrometry: powerful discovery tools for the molecular level characterization of marine dissolved organic matter. *Biogeosciences* 10, 1583-1624. <http://dx.doi.org/10.5194/bg-10-1583-2013>

Huguet, A., Vacher, L., Relexans, S., Saubusse, S., Froidefond, J.M., Parlanti, E., 2009. Properties of fluorescent dissolved organic matter in the Gironde Estuary. *Org. Geochem.* 40: 706-719. <http://dx.doi.org/10.1016/j.orggeochem.2009.03.002>

Jaffé, R., Ding, Y., Niggemann, J., Vähätalo, A.V., Stubbins, A., Spencer, R.G.M., Campbell, J., Dittmar, T., 2013. Global charcoal mobilization from soils via dissolution and riverine transport to the oceans. *Science* 340, 345-347. <http://dx.doi.org/10.1126/science.1231476>

- Jankowski, J.J., Kieber, D.J., Mopper, K., 1999. Nitrate and nitrite ultraviolet actinometers. *Photochem. Photobiol.* 70, 319-328. <http://dx.doi.org/10.1111/j.1751-1097.1999.tb08143.x>
- Johnson, K.M., Burney, C.M., Sieburth, J.McN., 1981. Doubling the production and precision of the MBTH spectrophotometric assay for dissolved carbohydrates in seawater. *Mar. Chem.* 10 (6), 467-473. [http://dx.doi.org/10.1016/0304-4203\(81\)90001-3](http://dx.doi.org/10.1016/0304-4203(81)90001-3)
- Jørgensen, L., Stedmon, C.A., Kragh, T., Markager, S., Middelboe, M., Søndergaard, M., 2011. Global trends in the fluorescence characteristics and distribution of marine dissolved organic matter. *Mar. Chem.* 126 (1–4), 139-148. <http://dx.doi.org/10.1016/j.marchem.2011.05.002>
- Kamga, A.W., Behar, F., Hatcher, P.G., 2014. Quantitative analysis of long chain fatty acids present in a type I kerogen using electrospray ionization Fourier transform ion cyclotron resonance mass spectrometry: compared with BF₃/MeOH Methylation/GC-FID. *J. Am. Soc. Mass Spectrom.* 25: 880-890. <http://dx.doi.org/10.1007/s13361-014-0851-x>
- Karlsson, T., Persson, P., 2012. Complexes with aquatic organic matter suppress hydrolysis and precipitation of Fe(III). *Chem. Geol.* 322-323, 19-27. <http://dx.doi.org/10.1016/j.chemgeo.2012.06.003>
- Kim, S., Simpson, A.J., Kujawinski, E.B., Freitas, M.A., Hatcher, P.G., 2003. High resolution electrospray ionization mass spectrometry and 2D solution NMR for the analysis of DOM extracted by C-18 solid phase disk. *Org. Geochem.* 34 (9), 1325-1335. [http://dx.doi.org/10.1016/S0146-6380\(03\)00101-3](http://dx.doi.org/10.1016/S0146-6380(03)00101-3)

- Kitidis, V., Stubbins, A., Uher, G., Upstill Goddard, R.C., Law, C.S., Woodward, E.M.S., 2006. Variability of chromophoric organic matter in surface waters of the Atlantic Ocean. *Deep-Sea Res. II* 53 (14–16), 1666-1684. <http://dx.doi.org/10.1016/j.dsr2.2006.05.009>
- Koch, B.P., Witt, M.R., Engbrodt, R., Dittmar, T., Kattner, G., 2005. Molecular formulae of marine and terrigenous dissolved organic matter detected by electrospray ionization Fourier transform ion cyclotron resonance mass spectrometry. *Geochim. Cosmochim. Acta* 69 (13): 3299-3308. <http://dx.doi.org/10.1016/j.gca.2005.02.027>
- Koch, B.P., Dittmar, T., 2006. From mass to structure: an aromaticity index for high-resolution mass data of natural organic matter. *Rapid Commun. Mass Spectrom.* 20: 926-932. <http://dx.doi.org/10.1002/rcm.2386>
- Koch, B.P., Ludwichowski, K.U., Kattner, G., Dittmar, T., Witt, M., 2008. Advanced characterization of marine dissolved organic matter by combining reversed-phase liquid chromatography and FT-ICR-MS. *Mar. Chem.* 111 (3-4): 233-241. <http://dx.doi.org/10.1016/j.marchem.2008.05.008>
- Koprivnjak, J.F., Pfromm, P.H., Ingall, E., Vetter, T.A., Schmitt-Kopplin, P., Hertkorn, N., Frommberger, M., Knicker, H., Perdue, E.M., 2009. Chemical and spectroscopic characterization of marine dissolved organic matter isolated using coupled reverse osmosis-electrodialysis. *Geochim. Cosmochim. Acta* 73 (14): 4215-4231. <http://dx.doi.org/10.1016/j.gca.2009.04.010>
- Kramer, R.W., Kujawinski, E.B., Hatcher, P.G., 2004. Identification of black carbon derived structures in a volcanic ash soil humic acid by Fourier transform ion

cyclotron resonance mass spectrometry. *Environ. Sci. Technol.* 38, 3387-3395.
<http://dx.doi.org/10.1021/es030124m>

Kuhlbusch, T.A.J., Crutzen, P.J., 1995. Toward a global estimate of black carbon in residues of vegetation fires representing a sink of atmospheric CO₂ and a source of O₂. *Global Biogeochem. Cycles* 9, 491-501. <http://dx.doi.org/10.1029/95GB02742>

Kujawinski, E.B., Del Vecchio, R., Blough, N.V., Klein, G.C., Marshall, A.G., 2004. Probing molecular-level transformations of dissolved organic matter: insights on photochemical degradation and protozoan modification of DOM from electrospray ionization Fourier transform ion cyclotron resonance mass spectrometry. *Mar. Chem.* 92 (1-4), 23-37. <http://dx.doi.org/10.1016/j.marchem.2004.06.038>

Kujawinski, E.B., Longnecker, K., Blough, N.V., Del Vecchio, R., Finlay, L., Kitner, J.B., Giovannoni, S.J., 2009. Identification of possible source markers in marine dissolved organic matter using ultrahigh resolution mass spectrometry. *Geochim. Cosmochim. Acta* 73 (15), 4384-4399. <http://dx.doi.org/10.1016/j.gca.2009.04.033>

Kuhlbusch, T.A.J., Crutzen, P.J., 1995. Toward a global estimate of black carbon in residues of vegetation fires representing a sink of atmospheric CO₂ and a source of O₂. *Glob. Biogeochem. Cycles* 9, 491-501. <http://dx.doi.org/10.1029/95GB02742>

Kuma, K., Nishioka, J., Matsunaga, K., 1996. Controls on iron(III) hydroxide solubility in seawater: The influence of pH and natural organic chelators. *Limnol. Oceanogr.* 41 (3), 396-407.

Laglara, L.M., Van Den Berg, C.M.G., 2009. Evidence for geochemical control of iron by humic substances in seawater. *Limnol. Oceanogr.* 54: 610-619.
<http://dx.doi.org/10.4319/lo.2009.54.2.0610>

- Lara, R.J., Thomas, D.N., 1994a. XAD-fractionation of "new" dissolved organic matter: is the hydrophobic fraction seriously underestimated? *Mar. Chem.* 47 (1): 93-96. [http://dx.doi.org/10.1016/0304-4203\(94\)90016-7](http://dx.doi.org/10.1016/0304-4203(94)90016-7)
- Lara, R.J., Thomas, D.N., 1994b. Isolation of marine dissolved organic matter: evaluation of sequential combinations of XAD Resins 2, 4, and 7. *Anal. Chem.* 66 (14), 2417-2419. <http://dx.doi.org/10.1021/ac00086a032>
- Louchouart, P., Opsahl, S., Benner, R., 2000. Isolation and quantification of dissolved lignin from natural waters using solid-phase extraction and GC/MS. *Anal. Chem.* 72 (13), 2780-2787. <http://dx.doi.org/10.1021/ac9912552>
- Marshall, A.G., Hendrickson, C.L., Jackson, G.S., 1998. Fourier transform ion cyclotron resonance mass spectrometry: a primer. *Mass Spectrom. Rev.* 17 (1): 1-35.
- Marshall, A.G., Rodgers, R.P., 2008. Petroleomics: Chemistry of the underworld. *Proc. Natl. Acad. Sci. USA* 105 (47), 18090-18095. <http://dx.doi.org/10.1073/pnas.0805069105>
- Masiello, C.A., Druffel, E.R.M., 1998. Black carbon in Deep-Sea sediments. *Science* 280, 1911-1913. <http://dx.doi.org/10.1126/science.280.5371.1911>
- McClafferty, F.W., Tureček, F., 1993. *Interpretation of Mass Spectra*, University Science Books, 4th edition.
- Meybeck, M., 1982. Carbon, nitrogen, and phosphorus transport by world rivers. *Am. J. Sci.* 282, 402-450. <http://dx.doi.org/10.2475/ajs.282.4.401>
- Meyers-Schulte, K.J., Hedges, J.I., 1986. Molecular evidence for a terrestrial component of organic matter dissolved in ocean water. *Nature* 321, 61-63. <http://dx.doi.org/10.1038/321061a0>

- Miller, W.L., 1994. Recent advances in the photochemistry of natural dissolved organic matter. In: Helz, G.R., Zepp, R.G., Crosby, D.G., (Eds.), *Aquatic and Surface Photochemistry*. Lewis Publishers, Roca Raton, pp. 111 –128.
- Minor, E.C., Dalzell, B.L., Stubbins, A., Mopper, K., 2007. Evaluating the photoalteration of estuarine dissolved organic matter using direct temperature-resolved mass spectrometry and UV-visible spectroscopy. *Aquat. Sci.* 69, 440-455. <http://dx.doi.org/10.1007/s00027-007-0897-y>
- Mopper, K., Zhou, X., Kieber, R.J., Kieber, D.J., Sikorski, R.J., Jones, R.D., 1991. Photochemical degradation of dissolved organic carbon and its impact on the oceanic carbon cycle. *Nature* 353, 60-62. <http://dx.doi.org/10.1038/353060a0>
- Mopper, K., Kieber, D.J., 2000. Marine photochemistry and its impact on carbon cycling. In: De Mora, S., Demers, S., Vernet, M., (Eds.), *The effects of UV radiation in the marine environment*. Cambridge University Press, pp. 101-129. <http://dx.doi.org/10.1017/CBO9780511535444.005>
- Mopper, K., Stubbins, A., Ritchie, J.D., Bialk, H.M., Hatcher, P.G., 2007. Advanced instrumental approaches for characterization of marine dissolved organic matter: Extraction techniques, mass spectrometry, and nuclear magnetic resonance spectroscopy. *Chem. Rev.* 107 (2), 419-442. <http://dx.doi.org/10.1021/cr050359b>
- Nelson, N.B., Siegel, D.A., Carlson, C.A., Swan, C.M., 2010. Tracing global biogeochemical cycles and meridional overturning circulation using chromophoric dissolved organic matter. *Geophys. Res. Lett.* 37 (3), L03610. <http://dx.doi.org/10.1029/2009GL042325>

- Nelson, N.B., Siegel, D.A., 2013. The global distribution and dynamics of chromophoric dissolved organic matter. *Annu. Rev. Mar. Sci.*, 5, 447-476. <http://dx.doi.org/10.1146/annurev-marine-120710-100751>
- Perdue, E.M., 1984. Analytical constraints on the structural features of humic substances. *Geochim. Cosmochim. Acta* 48: 1435-1442. [http://dx.doi.org/10.1016/0016-7037\(84\)90400-9](http://dx.doi.org/10.1016/0016-7037(84)90400-9)
- Powell, R., Wilson-Finelli, A., 2003. Photochemical degradation of organic iron complexing ligands in seawater. *Aquat. Sci.* 65: 367-374. <http://dx.doi.org/10.1007/s00027-003-0679-0>
- Ravel, B., Newville, M., 2005. ATHENA, ARTEMIS, HEPHAESTUS: data analysis for X-ray absorption spectroscopy using IFEFFIT. *J. Synchrotron Rad.* 12, 537-541. <http://dx.doi.org/10.1107/S0909049505012719>
- Raymond, P.A., Bauer, J.E., Caracoc, N.F., Cole, J.J., Longworth, B., Petsch, S.T., 2004. Controls on the variability of organic matter and dissolved inorganic carbon ages in northeast US rivers. *Mar. Chem.* 92, 353-366. <http://dx.doi.org/10.1016/j.marchem.2004.06.036>
- Reemtsma, T., These, A., Linscheid, M., Leenheer, J., Spitzzy, A., 2008. Molecular and structural characterization of dissolved organic matter from the deep ocean by FTICR-MS, including hydrophilic nitrogenous organic molecules. *Environ. Sci. Technol.* 42 (5): 1430-1437. <http://dx.doi.org/10.1021/es7021413>
- Repeta, D.J., Quan, T.M., Aluwihare, L.I., Accardi, A.M., 2002. Chemical characterization of high molecular weight dissolved organic matter in fresh and

marine waters. *Geochim. Cosmochim. Acta* 66 (6), 955-962.
[http://dx.doi.org/10.1016/S0016-7037\(01\)00830-4](http://dx.doi.org/10.1016/S0016-7037(01)00830-4)

Rossel, P.E., Vähätalo, A.V., Witt, M., Dittmar, T., 2013. Molecular composition of dissolved organic matter from a wetland plant (*Juncus effuses*) after photochemical and microbial decomposition (1.25 yr): common features with deep sea dissolved organic matter. *Org. Geochem.* 60, 62-71.
<http://dx.doi.org/10.1016/j.orggeochem.2013.04.013>

Santschi, P.H., Guo, L., Baskaran, M., Trumbore, S., Southon, J., Bianchi, T.S., Honeyman, B., Cifuentes, L., 1995. Isotopic evidence for the contemporary origin of high-molecular weight organic matter in oceanic environments. *Geochim. Cosmochim. Acta* 59 (3): 625-631. [http://dx.doi.org/10.1016/0016-7037\(94\)00378-Y](http://dx.doi.org/10.1016/0016-7037(94)00378-Y)

Schlesinger, W.H., Melack, J.M., 1981. Transport of organic carbon in the world's rivers. *Tellus* 33, 172-187. <http://dx.doi.org/10.1111/j.2153-3490.1981.tb01742.x>

Shen, X., Perreault, H., 1998. Characterization of carbohydrates using a combination of derivatization, high-performance liquid chromatography and mass spectrometry. *J Chromatogr. A* 811 (1-2): 47-59. [http://dx.doi.org/10.1016/S0021-9673\(98\)00238-6](http://dx.doi.org/10.1016/S0021-9673(98)00238-6)

Simjouw, J.-P., Minor, E.C., Mopper, K., 2005. Isolation and characterization of estuarine dissolved organic matter: Comparison of ultrafiltration and C₁₈ solid-phase extraction techniques. *Mar. Chem.* 96 (3-4): 219-235.
<http://dx.doi.org/10.1016/j.marchem.2005.01.003>

Sjöstedt, C., Persson, I., Hesterberg, D., Kleja, D.B., Borg, H., Gustafsson, J.P., 2013. Iron speciation in soft-water lakes and soils as determined by EXAFS spectroscopy

and geochemical modelling. *Geochim. Cosmochim. Acta* 105, 172-186.
<http://dx.doi.org/10.1016/j.gca.2012.11.035>

Sleighter, R.L., Hatcher, P.G., 2007. The application of electrospray ionization coupled to ultrahigh resolution mass spectrometry for the molecular characterization of natural organic matter. *J. Mass Spectrom.* 42 (5): 559-574.
<http://dx.doi.org/10.1002/jms.1221>

Sleighter, R.L., Hatcher, P.G., 2008. Molecular characterization of dissolved organic matter (DOM) along a river to ocean transect of the lower Chesapeake Bay by ultrahigh resolution electrospray ionization Fourier transform ion cyclotron resonance mass spectrometry. *Mar. Chem.* 110 (3-4): 140-152.
<http://dx.doi.org/10.1016/j.marchem.2008.04.008>

Sleighter, R.L., Mckee, G.A., Liu, Z., Hatcher, P.G., 2008. Naturally present fatty acids as internal calibrants for Fourier transform mass spectra of dissolved organic matter. *Limnol. Oceanogr. Methods* 6: 246-253.
<http://dx.doi.org/10.4319/lom.2008.6.246>

Sleighter, R.L., Mckee, G.A., Hatcher, P.G., 2009. Direct Fourier transform mass spectral analysis of natural waters with low dissolved organic matter. *Org. Geochem.* 40 (1): 119-125. <http://dx.doi.org/10.1016/j.orggeochem.2008.09.012>

Sleighter, R.L., Liu, Z., Xue, J., Hatcher, P.G., 2010. Multivariate statistical approaches for the characterization of dissolved organic matter analyzed by ultrahigh resolution mass spectrometry. *Environ. Sci. Technol.* 44 (19), 7576-7582.
<http://dx.doi.org/10.1021/es1002204>

- Sleighter, R.L., Chen, H., Wozniak, A.S., Willoughby, A.S., Caricasole, P., Hatcher, P.G., 2012. Establishing a measure of reproducibility of ultrahigh-resolution mass spectra for complex mixtures of natural organic matter. *Anal. Chem.* 84 (21), 9184-9191. <http://dx.doi.org/10.1021/ac3018026>
- Spencer, R.G.M., Stubbins, A., Hernes, P.J., Baker, A., Mopper, K., Aufdenkampe, A.K., Dyda, R.Y., Mwamba, V.L., Mangangu, A.M., Wabakanghanzi, J.N., Six, J., 2009. Photochemical degradation of dissolved organic matter and dissolved lignin phenols from the Congo River. *J. Geophys. Res.* 114, G03010. <http://dx.doi.org/10.1029/2009JG000968>
- Stedmon, C.A., Markager, S., 2005. Resolving the variability in dissolved organic matter fluorescence in a temperate estuary and its catchment using PARAFAC analysis. *Limnol. Oceanogr.* 50: 686-697. <http://dx.doi.org/10.4319/lo.2005.50.2.0686>
- Stenson, A.C., Landing, W.M., Marshall, A.G., Cooper, W.T., 2002. Ionization and fragmentation of humic substances in electrospray ionization Fourier transform-ion cyclotron resonance mass spectrometry. *Anal. Chem.* 74 (17), 4397-4409. <http://dx.doi.org/10.1021/ac020019f>
- Stenson, A.C., Marshall, A.G., Cooper, W.T., 2003. Exact masses and chemical formulas of individual Suwannee River fulvic acids from ultrahigh resolution electrospray ionization Fourier transform ion cyclotron resonance mass spectra. *Anal. Chem.* 75 (6), 1275-1284. <http://dx.doi.org/10.1021/ac026106p>
- Stöhr, J., 1992. *NEXAFS Spectroscopy*. Springer Science & Business Media.
- Stubbins, A., Spencer, R.G.M., Chen, H., Hatcher, P.G., Mopper, K., Hernes, P.J., Mwamba, V.L., Mangangu, A.M., Wabakanghanzi, J.N., Six, J., 2010. Illuminated

- darkness: Molecular signatures of Congo River dissolved organic matter and its photochemical alteration as revealed by ultrahigh precision mass spectrometry. *Limnol. Oceanogr.* 55 (4): 1467-1477. <http://dx.doi.org/10.4319/lo.2010.55.4.1467>
- Stubbins, A., Dittmar, T., 2012. Low volume quantification of dissolved organic carbon and dissolved nitrogen. *Limnol. Oceanogr. Methods* 10, 347-352. <http://dx.doi.org/10.4319/lom.2012.10.347>
- Stubbins, A., Niggemann, J., Dittmar, T., 2012. Photo-lability of deep ocean dissolved black carbon. *Biogeosciences* 9, 1661-1670. <http://dx.doi.org/10.5194/bg-9-1661-2012>
- Stuermer, D.H., Harvey, G.R., 1977. The isolation of humic substances and alcohol-soluble organic matter from seawater. *Deep-Sea Res.* 24 (3), 303-309. [http://dx.doi.org/10.1016/S0146-6291\(77\)80010-6](http://dx.doi.org/10.1016/S0146-6291(77)80010-6)
- Sundman, A., Karlsson, T., Laudon, H., Persson, P., 2014. XAS study of iron speciation in soils and waters from a boreal catchment. *Chem. Geol.* 364, 93-102. <http://dx.doi.org/10.1016/j.chemgeo.2013.11.023>
- Thorn, K.A., Younger, S.J., Cox, L.G., 2010. Order of Functionality Loss during Photodegradation of Aquatic Humic Substances. *J. Environ. Qual.* 39: 1416-1428.
- vanloon, G., Duffy, S., 2010. Organic Matter in Water. In: vanloon, G.W., Duffy, S.J., (Eds.), *Environmental Chemistry: A Global Perspective*. Oxford University Press, Chapter 12.
- Vetter, T.A., Perdue, E.M., Ingall, E., Koprivnjak, J.F., Pfromm, P.H., 2007. Combining reverse osmosis and electro dialysis for more complete recovery of dissolved

- organic matter from seawater. *Separation and Purification Technol.* 56 (3): 383-387. <http://dx.doi.org/10.1016/j.seppur.2007.04.012>
- von Wachenfeldt, E., Sobek, S., Bastviken, D., Tranvik, L.J., 2008. Linking allochthonous dissolved organic matter and boreal lake sediment carbon sequestration: The role of light-mediated flocculation. *Limnol. Oceanogr.* 53, 2416-2426. <http://dx.doi.org/10.4319/lo.2008.53.6.2416>
- Wang, W., Zafiriou, O.C., Chan, I.-Y., Zepp, R.G., Blough, N.V., 2007. Production of hydrated electrons from photoionization of dissolved organic matter in natural waters. *Environ. Sci. Technol.* 41, 1601-1607. <http://dx.doi.org/10.1021/es061069v>
- Ward, C.P., Sleighter, R.L., Hatcher, P.G., Cory, R.M., 2014. Insights into the complete and partial photooxidation of black carbon in surface waters. *ES:P&I.* 16, 721-731. <http://dx.doi.org/10.1039/C3EM00597F>
- Wetzel, R.G., Hatcher, P.G., Bianchi, T.S., 1995. Natural photolysis by ultraviolet irradiance of recalcitrant dissolved organic matter to simple substances for rapid bacterial metabolism. *Limnol. Oceanogr.* 40: 1369-1380.
- White, E.M., Kieber, D.J., Sherrard, J., Miller, W.L., Mopper, K., 2010. Carbon dioxide and carbon monoxide photoproduction quantum yields in the Delaware Estuary. *Mar. Chem.* 118: 11-21. <http://dx.doi.org/10.1016/j.marchem.2009.10.001>
- Williams, P.M., Druffel, E.R.M., 1987. Radiocarbon in dissolved organic matter in the central North Pacific Ocean. *Nature* 330, 246-248. <http://dx.doi.org/10.1038/330246a0>

- Zafiriou, O.C., Jousset-Dubien, J., Zepp, R.G., Zika, R.G., 1984. Photochemistry of natural waters. *Environ. Sci. Technol.* 18: 358A-371A. <http://dx.doi.org/10.1021/es00130a001>
- Zepp, R.G., Schlotzhauer, P.F., 1981. Comparison of photochemical behavior of various humic substances in water: 3. Spectroscopic properties of humic substances. *Chemosphere* 10: 479– 486. [http://dx.doi.org/10.1016/0045-6535\(81\)90148-X](http://dx.doi.org/10.1016/0045-6535(81)90148-X)
- Zepp, R.G., Braun, A.M., Hoigne, J., Leenheer, J.A., 1987. Photoproduction of hydrated electrons from natural organic solutes in aquatic environments. *Environ. Sci. Technol.* 21, 485-490. <http://dx.doi.org/10.1021/es00159a010>
- Zhang, L.J., Xu, J.Q., Shi, Z., Xu, W., Wang, T.G, 2003. Hydrothermal synthesis and characterization of the first oxalate-bta mixed-ligand three-dimensional frameworks: $\{[M_2(\mu_8\text{-bta})(\mu_2\text{-C}_2\text{O}_4)]\cdot(\text{H}_3\text{O})_2(\text{H}_2\text{O})_2\}_n$ ($M = \text{Co}^{\text{II}}, \text{Fe}^{\text{II}}$; bta = benzene-1,2,4,5-tetracarboxylate). *Dalton Trans.* 6, 1148-1152. <http://dx.doi.org/10.1039/B209491F>
- Zhang, Y., Green, N.W., Perdue, E.M., 2013. Acid-base properties of dissolved organic matter from pristine and oil-impacted marshes of Barataria Bay, Louisiana. *Mar. Chem.* 155, 42-49. <http://dx.doi.org/10.1016/j.marchem.2013.05.010>
- Ziolkowski, L.A., Druffel, E.R.M., 2010. Aged black carbon identified in marine dissolved organic carbon. *Geophys. Res. Lett.* 37, L16601. <http://dx.doi.org/10.1029/2010GL043963>

APPENDIX A
COPYRIGHT PERMISSIONS

Permission for Chapter II, which contains the Limnology and Oceanography: Methods article, published by the American Society of Limnology and Oceanography (ASLO)

See the email below from Jo Davis, Database Supervisor, ASLO Business Office.

From: Jo Davis [jdavis@sgmeet.com]

Sent: Monday, April 28, 2014 9:30 AM

To: Chen, Hongmei

Subject: ASLO Copyright Permission - No Fee

To: Ms. Hongmei Chen,

On behalf of the Association for the Sciences of Limnology and Oceanography, we are happy to grant permission to use the figures from Limnology & Oceanography per your application below.

When reproducing the article/figure(s), please cite according to the references that follow:

All copyrighted works, whether displayed electronically or in print, should be properly acknowledged as follows:

"Copyright 2014 by the Association for the Sciences of Limnology and Oceanography, Inc."

Once permission is granted to use an article or any part thereof of a work from L&O, the full citation must include:

1. Name(s) of the author(s);
2. Journal title (Association for the Sciences of Limnology & Oceanography or L&O)
3. Publication date
4. Volume number
5. Issue number
6. Chapter or article name
7. Pages on which the articles, data, and/ or figure(s) appear

For your records, the Association for the Sciences of Limnology and Oceanography is a nonprofit organization. (Taxpayer I.D. Number: 38-1710020)

If you have additional requests or have any questions in regard to this request, you can contact me directly via e-mail at jdavis@sgmeet.com.

Sincerely,

Jo Davis

ASLO Business Office

Database Supervisor

-----Original Message-----

From: webpostings@aslo.org [mailto:webpostings@aslo.org]

Sent: Friday, April 25, 2014 1:11 PM

To: business@aslo.org

Subject: Copyright Permission Request Form

Will the copyrighted material appear in a for-profit publication? no

Will the copyrighted material appear in a not-for-profit publication? yes

Proposed Publication Date: August 2014

REQUESTOR INFORMATION

Requestor: Ms. Hongmei Chen

Contact's Name (if different):

Institution: Old Dominion University

Department: Chemistry and Biochemistry

Mailing Address: 4402 Elkhorn Avenue, PSB room 3100, Norfolk, VA 23529,
USA

Telephone: 757.232.7345

Fax: 757.683.4628

Email: hxchen@odu.edu

INTENDED USE

Publication in which material will appear: Hongmei Chen's Doctoral Dissertation

Publisher: Old Dominion University

MATERIAL TO BE USED

Author(s) Name(s): Hongmei Chen, Aron Stubbins, Patrick G. Hatcher

Journal Title: Limnology and Oceanography: Methods

Publication Date: November 2011

Volume: 9

Issue:

Chapter, article or figure name or title: A mini-electrodialysis system for desalting small volume saline samples for Fourier transform ion cyclotron resonance mass spectrometry

Pages on which articles, data or figures appear: 582-592

Special notes: I want to include the whole paper as one chapter in my doctoral dissertation.

Permission for Chapter III, which contains the Marine Chemistry article, published by Elsevier

See the email below from Hop Wechsler, Permissions Helpdesk Manager, Elsevier.

From: Permissions Helpdesk [permissionshelpdesk@elsevier.com]

Sent: Wednesday, October 22, 2014 3:01 PM

To: Chen, Hongmei

Subject: RE: Copyright Permission Request

Dear Hongmei:

As an Elsevier journal author, you retain various rights to your article as outlined at <http://www.elsevier.com/journal-authors/author-rights-and-responsibilities>,

including Inclusion in a thesis or dissertation, provided that proper acknowledgement is given to the original source of publication. As this is a retained right, no written permission is necessary.

This extends to the posting of the Author Accepted Manuscript version of your article (see <http://www.elsevier.com/about/open-access/open-access-policies/article-posting-policy#accepted-author-manuscript>) **along with or embedded in your dissertation to your university repository.**

If further clarification is necessary or you have any additional questions, please let me know. Best of luck with your dissertation.

Regards,

Hop

Hop Wechsler

Permissions Helpdesk Manager

Elsevier

1600 John F. Kennedy Boulevard

Suite 1800

Philadelphia, PA 19103-2899

Tel: +1-215-239-3520

Mobile: +1-215-900-5674

Fax: +1-215-239-3805

E-mail: h.wechsler@elsevier.com

Contact the Permissions Helpdesk:

+1-800-523-4069 x 3808 permissionshelpdesk@elsevier.com

Permission for Chapter IV, which contains the Environmental Science & Technology Letters article, published by the American Chemical Society (ACS) Publications

Title: Production of Black Carbon-like and Aliphatic Molecules from Terrestrial Dissolved Organic Matter in the Presence of Sunlight and Iron

Author: Hongmei Chen, Hussain A. N. Abdulla, Rebecca L. Sanders, Satish C. B. Myneni, Kenneth Mopper, and Patrick G. Hatcher

Publication: Environmental Science & Technology Letters

Publisher: American Chemical Society

Date: Oct 1, 2014

PERMISSION/LICENSE IS GRANTED FOR YOUR ORDER AT NO CHARGE

This type of permission/license, instead of the standard Terms & Conditions, is sent to you because no fee is being charged for your order. Please note the following:

- **Permission is granted for your request in both print and electronic formats, and translations.**
- **If figures and/or tables were requested, they may be adapted or used in part.**
- **Please print this page for your records and send a copy of it to your publisher/graduate school.**
- **Appropriate credit for the requested material should be given as follows:**

"Reprinted (adapted) with permission from (COMPLETE REFERENCE CITATION). Copyright (YEAR) American Chemical Society." Insert appropriate information in place of the capitalized words.

- One-time permission is granted only for the use specified in your request. No additional uses are granted (such as derivative works or other editions). For any other uses, please submit a new request.

APPENDIX B**ABBREVIATIONS AND ACRONYMS USED**

AI: aromaticity indices

BC: black carbon

C: carbon

CN: coordination number

COSMIC: College of Sciences Major Instrumentation Cluster

CRAM: carboxyl-rich alicyclic molecules

d: day

DBE: double bond equivalents

DIC: dissolved inorganic carbon

DOC: dissolved organic carbon

DOI: digital object identifier

DOM: dissolved organic matter

DS: Dismal Swamp

ED: electro dialysis

ESI: electrospray ionization

ESI FTICR-MS: electrospray ionization Fourier transform ion cyclotron resonance
mass spectrometry

EXAFS: extended X-ray absorption fine structure

FID: free induction decay

FTICR-MS: Fourier transform ion cyclotron resonance mass spectrometry

H: hydrogen

h: hour

HCA: hierarchal cluster analysis

HPLC: high performance liquid chromatography

ICR: ion cyclotron resonance

KHP: potassium hydrogen phthalate

KMD: Kendrick mass defect

L: litter

LC-MS: liquid chromatography – mass spectrometry

MBTH: 3-methyl-2-benzothiazolinone hydrazone hydrochloride

m/z: mass to charge

MS: mass spectrometry

MW: molecular weight

MWCO: molecular weight cut off

N: nitrogen

N. Atlantic: North Atlantic

N. Pacific: North Pacific

NELHA: Natural Energy Laboratory of Hawaii Authority

NHMFL: national high magnetic field laboratory

NMR: nuclear magnetic resonance

NOM: natural organic matter

NPDW: North Pacific Deep Water

NPOC: non-purgeable organic carbon

O: oxygen

P: phosphorus

PC: principal component

PCA: principal component analysis

PEG: polyethylene glycol

photoBC: newly formed black carbon-like molecules from photoflocculation

POC: particulate organic carbon

POM: particulate organic matter

ppm: parts per million

PSU: practical salinity units

RO/ED: reverse osmosis coupled with electrodialysis

RPM: revolutions per minute

S: sulfur

S/N: signal to noise

SPE: solid phase extraction

T: tesla

TCHO: total dissolved carbohydrate

TDN: total dissolved nitrogen

TOC: total organic carbon

VK: van Krevelen

XANES: X-ray absorption near edge structure

APPENDIX C

List of exact masses, elemental formulas, and average peak intensities for the 540 CHO formulas and 293 CHON formulas (shown in Figure 7) shared in marine RO/ED isolated DOM samples in this study.

Exact mass (Da)	C	H	H+1	N	O	Average Peak Intensity
219.102668	13	15	16	0	3	1,883,547
223.097583	12	15	16	0	4	2,200,930
227.201654	14	27	28	0	2	3,065,720
237.113233	13	17	18	0	4	2,278,926
255.232954	16	31	32	0	2	14,583,858
321.134362	17	21	22	0	6	3,736,244
323.150012	17	23	24	0	6	3,986,330
325.129277	16	21	22	0	7	4,878,430
327.108541	15	19	20	0	8	3,713,209
333.134362	18	21	22	0	6	4,074,370
335.113627	17	19	20	0	7	4,436,186
335.150012	18	23	24	0	6	6,960,661
337.092891	16	17	18	0	8	2,955,284
337.129277	17	21	22	0	7	8,983,011
337.165662	18	25	26	0	6	6,634,963
339.108541	16	19	20	0	8	6,783,475
339.144927	17	23	24	0	7	8,652,430
341.124191	16	21	22	0	8	7,400,479
341.160577	17	25	26	0	7	3,623,076
343.103456	15	19	20	0	9	3,651,185
343.139841	16	23	24	0	8	3,758,091
347.113627	18	19	20	0	7	2,930,378
347.150012	19	23	24	0	6	6,028,005
349.129277	18	21	22	0	7	8,771,599
349.165662	19	25	26	0	6	7,694,718
351.108541	17	19	20	0	8	7,387,854
351.144927	18	23	24	0	7	14,594,302
351.181312	19	27	28	0	6	5,263,448
353.124191	17	21	22	0	8	13,672,937
353.160577	18	25	26	0	7	11,654,979
355.103456	16	19	20	0	9	8,222,782

Exact mass (Da)	C	H	H+1	N	O	Average Peak Intensity
355.139841	17	23	24	0	8	11,709,187
355.176227	18	27	28	0	7	5,006,622
357.119106	16	21	22	0	9	7,751,364
357.155491	17	25	26	0	8	4,912,051
359.113627	19	19	20	0	7	2,002,022
359.134756	16	23	24	0	9	3,645,236
359.150012	20	23	24	0	6	5,089,184
361.129277	19	21	22	0	7	7,869,814
361.165662	20	25	26	0	6	9,237,669
363.108541	18	19	20	0	8	7,121,802
363.144927	19	23	24	0	7	17,526,970
363.181312	20	27	28	0	6	9,777,215
365.087806	17	17	18	0	9	3,844,319
365.124191	18	21	22	0	8	18,762,446
365.160577	19	25	26	0	7	20,780,756
365.196962	20	29	30	0	6	5,712,793
367.103456	17	19	20	0	9	10,613,560
367.139841	18	23	24	0	8	25,184,061
367.176227	19	27	28	0	7	12,310,295
369.082720	16	17	18	0	10	4,465,813
369.119106	17	21	22	0	9	15,721,040
369.155491	18	25	26	0	8	16,965,461
369.191877	19	29	30	0	7	4,240,559
371.098370	16	19	20	0	10	6,554,914
371.134756	17	23	24	0	9	10,698,172
371.171141	18	27	28	0	8	5,607,318
373.114020	16	21	22	0	10	4,791,715
373.129277	20	21	22	0	7	3,494,991
373.150406	17	25	26	0	9	3,860,370
373.165662	21	25	26	0	6	4,503,103
375.108541	19	19	20	0	8	3,475,594
375.144927	20	23	24	0	7	10,312,036
375.181312	21	27	28	0	6	5,979,028
377.124191	19	21	22	0	8	12,532,979
377.160577	20	25	26	0	7	17,818,360
377.196962	21	29	30	0	6	4,994,941
379.103456	18	19	20	0	9	8,638,123
379.139841	19	23	24	0	8	25,086,043
379.176227	20	27	28	0	7	17,775,626
381.119106	18	21	22	0	9	19,753,233

Exact mass (Da)	C	H	H+1	N	O	Average Peak Intensity
381.155491	19	25	26	0	8	27,351,915
381.191877	20	29	30	0	7	9,478,939
383.098370	17	19	20	0	10	9,762,352
383.134756	18	23	24	0	9	23,878,261
383.171141	19	27	28	0	8	15,064,783
383.207527	20	31	32	0	7	2,995,274
385.114020	17	21	22	0	10	11,616,680
385.150406	18	25	26	0	9	13,933,272
385.165662	22	25	26	0	6	2,624,922
385.186791	19	29	30	0	8	4,595,207
387.129671	17	23	24	0	10	7,073,716
387.144927	21	23	24	0	7	4,981,473
387.166056	18	27	28	0	9	4,653,497
387.181312	22	27	28	0	6	5,079,654
389.124191	20	21	22	0	8	7,181,627
389.145321	17	25	26	0	10	2,579,720
389.160577	21	25	26	0	7	11,751,829
389.196962	22	29	30	0	6	6,231,023
391.103456	19	19	20	0	9	5,719,805
391.139841	20	23	24	0	8	21,249,858
391.176227	21	27	28	0	7	17,141,745
391.212612	22	31	32	0	6	4,430,027
393.119106	19	21	22	0	9	18,587,202
393.155491	20	25	26	0	8	35,223,793
393.191877	21	29	30	0	7	13,342,540
395.098370	18	19	20	0	10	10,248,854
395.134756	19	23	24	0	9	33,257,967
395.171141	20	27	28	0	8	30,910,623
395.207527	21	31	32	0	7	6,310,649
397.114020	18	21	22	0	10	19,108,417
397.150406	19	25	26	0	9	30,831,686
397.186791	20	29	30	0	8	14,621,599
399.093285	17	19	20	0	11	7,274,981
399.129671	18	23	24	0	10	18,555,881
399.144927	22	23	24	0	7	2,550,443
399.166056	19	27	28	0	9	15,251,779
399.181312	23	27	28	0	6	2,962,821
399.202442	20	31	32	0	8	4,292,296
401.108935	17	21	22	0	11	6,832,565
401.124191	21	21	22	0	8	3,260,407

Exact mass (Da)	C	H	H+1	N	O	Average Peak Intensity
401.145321	18	25	26	0	10	9,507,642
401.160577	22	25	26	0	7	6,671,206
401.181706	19	29	30	0	9	4,635,241
401.196962	23	29	30	0	6	4,430,016
403.124585	17	23	24	0	11	3,632,899
403.139841	21	23	24	0	8	10,440,580
403.160971	18	27	28	0	10	3,183,239
403.176227	22	27	28	0	7	12,668,382
403.212612	23	31	32	0	6	4,710,605
405.119106	20	21	22	0	9	10,695,456
405.155491	21	25	26	0	8	23,460,559
405.191877	22	29	30	0	7	15,022,462
405.228262	23	33	34	0	6	3,199,021
407.098370	19	19	20	0	10	6,715,022
407.134756	20	23	24	0	9	27,126,034
407.171141	21	27	28	0	8	29,561,622
407.207527	22	31	32	0	7	10,509,851
409.114020	19	21	22	0	10	18,228,050
409.150406	20	25	26	0	9	39,053,484
409.186791	21	29	30	0	8	21,460,997
409.223177	22	33	34	0	7	4,379,402
411.093285	18	19	20	0	11	7,893,498
411.129671	19	23	24	0	10	26,036,627
411.166056	20	27	28	0	9	28,900,759
411.202442	21	31	32	0	8	8,607,132
413.108935	18	21	22	0	11	11,143,416
413.145321	19	25	26	0	10	20,814,630
413.160577	23	25	26	0	7	2,887,592
413.181706	20	29	30	0	9	12,354,773
413.196962	24	29	30	0	6	2,695,628
413.218092	21	33	34	0	8	2,365,401
415.124585	18	23	24	0	11	8,762,204
415.139841	22	23	24	0	8	4,322,099
415.160971	19	27	28	0	10	9,189,131
415.176227	23	27	28	0	7	6,179,213
415.197356	20	31	32	0	9	3,550,501
415.212612	24	31	32	0	6	3,413,734
417.119106	21	21	22	0	9	4,393,872
417.140235	18	25	26	0	11	4,263,870
417.155491	22	25	26	0	8	11,726,826

Exact mass (Da)	C	H	H+1	N	O	Average Peak Intensity
417.176621	19	29	30	0	10	2,897,068
417.191877	23	29	30	0	7	9,492,547
417.228262	24	33	34	0	6	3,184,541
419.134756	21	23	24	0	9	13,602,243
419.171141	22	27	28	0	8	20,760,860
419.207527	23	31	32	0	7	9,776,160
421.114020	20	21	22	0	10	10,543,001
421.150406	21	25	26	0	9	27,374,066
421.186791	22	29	30	0	8	22,684,320
421.223177	23	33	34	0	7	6,181,540
423.093285	19	19	20	0	11	5,512,831
423.129671	20	23	24	0	10	23,538,542
423.166056	21	27	28	0	9	31,448,093
423.202442	22	31	32	0	8	14,221,686
423.238827	23	35	36	0	7	2,703,865
425.108935	19	21	22	0	11	11,747,302
425.145321	20	25	26	0	10	28,122,004
425.181706	21	29	30	0	9	19,914,477
425.218092	22	33	34	0	8	5,478,428
427.124585	19	23	24	0	11	14,300,851
427.160971	20	27	28	0	10	18,717,623
427.176227	24	27	28	0	7	2,614,329
427.197356	21	31	32	0	9	7,646,224
429.103850	18	21	22	0	12	5,113,336
429.140235	19	25	26	0	11	9,787,089
429.155491	23	25	26	0	8	4,750,846
429.176621	20	29	30	0	10	7,606,997
429.191877	24	29	30	0	7	5,256,108
431.134756	22	23	24	0	9	5,552,489
431.155885	19	27	28	0	11	4,206,229
431.171141	23	27	28	0	8	10,773,399
431.192271	20	31	32	0	10	2,364,526
431.207527	24	31	32	0	7	7,407,003
431.243912	25	35	36	0	6	2,240,489
433.114020	21	21	22	0	10	4,944,784
433.150406	22	25	26	0	9	15,411,710
433.186791	23	29	30	0	8	16,620,545
433.223177	24	33	34	0	7	6,910,469
435.129671	21	23	24	0	10	14,431,498
435.166056	22	27	28	0	9	26,328,248

Exact mass (Da)	C	H	H+1	N	O	Average Peak Intensity
435.202442	23	31	32	0	8	16,073,233
435.238827	24	35	36	0	7	4,085,738
437.108935	20	21	22	0	11	9,076,456
437.145321	21	25	26	0	10	26,164,928
437.181706	22	29	30	0	9	26,317,167
437.218092	23	33	34	0	8	9,461,703
439.124585	20	23	24	0	11	16,156,100
439.160971	21	27	28	0	10	26,414,279
439.197356	22	31	32	0	9	15,130,826
439.233742	23	35	36	0	8	3,769,165
441.103850	19	21	22	0	12	6,921,047
441.140235	20	25	26	0	11	17,173,701
441.155491	24	25	26	0	8	2,070,235
441.176621	21	29	30	0	10	15,280,157
441.191877	25	29	30	0	7	2,612,830
441.213006	22	33	34	0	9	5,439,179
443.119500	19	23	24	0	12	6,745,598
443.134756	23	23	24	0	9	2,418,879
443.155885	20	27	28	0	11	10,233,622
443.171141	24	27	28	0	8	5,154,754
443.192271	21	31	32	0	10	5,887,001
443.207527	25	31	32	0	7	4,669,808
445.135150	19	25	26	0	12	4,275,232
445.150406	23	25	26	0	9	7,058,273
445.171535	20	29	30	0	11	4,275,256
445.186791	24	29	30	0	8	10,503,353
445.223177	25	33	34	0	7	6,135,910
447.129671	22	23	24	0	10	7,170,042
447.166056	23	27	28	0	9	16,194,215
447.202442	24	31	32	0	8	14,219,434
447.238827	25	35	36	0	7	5,307,181
449.108935	21	21	22	0	11	4,955,939
449.145321	22	25	26	0	10	17,909,392
449.181706	23	29	30	0	9	23,878,291
449.218092	24	33	34	0	8	12,380,992
449.254477	25	37	38	0	7	2,972,675
451.124585	21	23	24	0	11	12,453,491
451.160971	22	27	28	0	10	27,657,334
451.197356	23	31	32	0	9	21,214,670
451.233742	24	35	36	0	8	6,926,203

Exact mass (Da)	C	H	H+1	N	O	Average Peak Intensity
453.103850	20	21	22	0	12	6,435,324
453.140235	21	25	26	0	11	19,983,273
453.176621	22	29	30	0	10	24,858,198
453.213006	23	33	34	0	9	11,355,054
453.249392	24	37	38	0	8	2,678,171
455.119500	20	23	24	0	12	9,568,300
455.155885	21	27	28	0	11	17,733,849
455.171141	25	27	28	0	8	2,403,034
455.192271	22	31	32	0	10	13,394,480
455.207527	26	31	32	0	7	2,443,378
455.228656	23	35	36	0	9	3,897,182
457.135150	20	25	26	0	12	8,656,981
457.150406	24	25	26	0	9	3,209,985
457.171535	21	29	30	0	11	10,105,261
457.186791	25	29	30	0	8	5,343,875
457.207921	22	33	34	0	10	4,791,173
457.223177	26	33	34	0	7	3,939,120
459.129671	23	23	24	0	10	3,072,930
459.150800	20	27	28	0	12	4,681,721
459.166056	24	27	28	0	9	8,275,322
459.187185	21	31	32	0	11	3,907,622
459.202442	25	31	32	0	8	9,592,273
459.238827	26	35	36	0	7	4,300,969
461.145321	23	25	26	0	10	9,373,845
461.166450	20	29	30	0	12	2,251,073
461.181706	24	29	30	0	9	16,386,284
461.218092	25	33	34	0	8	11,844,846
461.254477	26	37	38	0	7	3,495,536
463.124585	22	23	24	0	11	7,151,999
463.160971	23	27	28	0	10	19,310,081
463.197356	24	31	32	0	9	21,077,165
463.233742	25	35	36	0	8	10,162,693
465.103850	21	21	22	0	12	4,150,776
465.140235	22	25	26	0	11	15,654,501
465.176621	23	29	30	0	10	25,343,249
465.213006	24	33	34	0	9	16,846,270
465.249392	25	37	38	0	8	5,381,781
467.119500	21	23	24	0	12	8,942,274
467.155885	22	27	28	0	11	21,214,745
467.192271	23	31	32	0	10	20,313,115

Exact mass (Da)	C	H	H+1	N	O	Average Peak Intensity
467.228656	24	35	36	0	9	8,624,924
469.135150	21	25	26	0	12	11,792,922
469.171535	22	29	30	0	11	17,158,427
469.186791	26	29	30	0	8	2,608,732
469.207921	23	33	34	0	10	10,160,584
469.223177	27	33	34	0	7	2,321,801
469.244306	24	37	38	0	9	3,030,516
471.114414	20	23	24	0	13	4,538,688
471.150800	21	27	28	0	12	9,445,484
471.166056	25	27	28	0	9	3,648,407
471.187185	22	31	32	0	11	8,611,864
471.202442	26	31	32	0	8	5,169,944
471.223571	23	35	36	0	10	3,445,870
471.238827	27	35	36	0	7	3,252,420
473.130064	20	25	26	0	13	3,549,877
473.145321	24	25	26	0	10	4,032,821
473.166450	21	29	30	0	12	5,056,139
473.181706	25	29	30	0	9	8,752,396
473.202835	22	33	34	0	11	3,341,410
473.218092	26	33	34	0	8	7,890,274
473.254477	27	37	38	0	7	3,474,318
475.124585	23	23	24	0	11	3,375,906
475.145715	20	27	28	0	13	2,149,453
475.160971	24	27	28	0	10	10,842,446
475.182100	21	31	32	0	12	2,122,297
475.197356	25	31	32	0	9	15,381,327
475.233742	26	35	36	0	8	8,733,093
475.270127	27	39	40	0	7	2,711,185
477.140235	23	25	26	0	11	9,142,750
477.176621	24	29	30	0	10	19,430,623
477.213006	25	33	34	0	9	17,190,282
477.249392	26	37	38	0	8	6,512,524
479.119500	22	23	24	0	12	5,821,287
479.155885	23	27	28	0	11	16,706,834
479.192271	24	31	32	0	10	22,713,107
479.228656	25	35	36	0	9	13,099,625
479.265042	26	39	40	0	8	3,221,098
481.135150	22	25	26	0	12	10,840,297
481.171535	23	29	30	0	11	20,374,848
481.207921	24	33	34	0	10	16,990,528

Exact mass (Da)	C	H	H+1	N	O	Average Peak Intensity
481.244306	25	37	38	0	9	6,601,793
483.114414	21	23	24	0	13	5,035,897
483.150800	22	27	28	0	12	13,075,471
483.187185	23	31	32	0	11	14,524,602
483.202442	27	31	32	0	8	2,452,155
483.223571	24	35	36	0	10	7,907,856
483.238827	28	35	36	0	7	1,805,126
483.259956	25	39	40	0	9	2,208,742
485.130064	21	25	26	0	13	5,425,303
485.166450	22	29	30	0	12	9,214,168
485.181706	26	29	30	0	9	4,045,528
485.202835	23	33	34	0	11	6,922,883
485.218092	27	33	34	0	8	4,530,733
485.239221	24	37	38	0	10	2,640,771
485.254477	28	37	38	0	7	2,260,654
487.145715	21	27	28	0	13	3,964,269
487.160971	25	27	28	0	10	4,783,256
487.182100	22	31	32	0	12	4,688,792
487.197356	26	31	32	0	9	8,288,921
487.218486	23	35	36	0	11	2,401,955
487.233742	27	35	36	0	8	6,696,430
487.270127	28	39	40	0	7	2,431,513
489.140235	24	25	26	0	11	4,423,803
489.161365	21	29	30	0	13	2,236,667
489.176621	25	29	30	0	10	11,370,235
489.197750	22	33	34	0	12	1,931,772
489.213006	26	33	34	0	9	13,032,187
489.249392	27	37	38	0	8	6,827,516
489.285777	28	41	42	0	7	2,016,871
491.155885	24	27	28	0	11	10,634,156
491.192271	25	31	32	0	10	18,133,932
491.228656	26	35	36	0	9	12,955,394
491.265042	27	39	40	0	8	4,784,343
493.135150	23	25	26	0	12	7,239,766
493.171535	24	29	30	0	11	17,129,387
493.207921	25	33	34	0	10	18,850,048
493.244306	26	37	38	0	9	8,891,648
493.280692	27	41	42	0	8	2,469,653
495.150800	23	27	28	0	12	11,755,939
495.187185	24	31	32	0	11	18,040,909

Exact mass (Da)	C	H	H+1	N	O	Average Peak Intensity
495.223571	25	35	36	0	10	12,532,472
495.259956	26	39	40	0	9	3,944,440
497.130064	22	25	26	0	13	6,079,422
497.166450	23	29	30	0	12	12,617,278
497.181706	27	29	30	0	9	1,662,675
497.202835	24	33	34	0	11	12,119,784
497.218092	28	33	34	0	8	2,051,987
497.239221	25	37	38	0	10	5,821,075
499.145715	22	27	28	0	13	6,199,379
499.182100	23	31	32	0	12	8,551,122
499.197356	27	31	32	0	9	4,140,967
499.218486	24	35	36	0	11	5,826,599
499.233742	28	35	36	0	8	3,596,796
499.254871	25	39	40	0	10	2,044,177
501.161365	22	29	30	0	13	4,259,168
501.176621	26	29	30	0	10	5,370,592
501.197750	23	33	34	0	12	4,092,810
501.213006	27	33	34	0	9	7,464,031
501.234136	24	37	38	0	11	1,935,924
501.249392	28	37	38	0	8	4,584,457
503.155885	25	27	28	0	11	5,152,061
503.177015	22	31	32	0	13	2,182,631
503.192271	26	31	32	0	10	10,728,423
503.228656	27	35	36	0	9	10,072,635
503.265042	28	39	40	0	8	4,614,117
505.135150	24	25	26	0	12	3,833,619
505.171535	25	29	30	0	11	11,072,531
505.207921	26	33	34	0	10	14,971,666
505.244306	27	37	38	0	9	9,659,153
505.280692	28	41	42	0	8	3,240,294
507.150800	24	27	28	0	12	8,097,507
507.187185	25	31	32	0	11	15,795,597
507.223571	26	35	36	0	10	14,116,748
507.259956	27	39	40	0	9	6,453,985
509.130064	23	25	26	0	13	4,492,675
509.166450	24	29	30	0	12	11,970,221
509.202835	25	33	34	0	11	15,056,385
509.239221	26	37	38	0	10	8,688,043
509.275606	27	41	42	0	9	2,938,666
511.145715	23	27	28	0	13	6,367,560

Exact mass (Da)	C	H	H+1	N	O	Average Peak Intensity
511.182100	24	31	32	0	12	11,402,353
511.218486	25	35	36	0	11	9,660,528
511.233742	29	35	36	0	8	1,764,847
511.254871	26	39	40	0	10	3,995,802
513.161365	23	29	30	0	13	6,189,446
513.176621	27	29	30	0	10	2,251,867
513.197750	24	33	34	0	12	7,551,536
513.213006	28	33	34	0	9	3,430,234
513.234136	25	37	38	0	11	4,344,068
513.249392	29	37	38	0	8	2,569,902
515.177015	23	31	32	0	13	3,893,653
515.192271	27	31	32	0	10	4,945,044
515.213400	24	35	36	0	12	3,487,379
515.228656	28	35	36	0	9	5,550,995
515.265042	29	39	40	0	8	3,269,308
517.171535	26	29	30	0	11	5,294,879
517.192665	23	33	34	0	13	1,973,022
517.207921	27	33	34	0	10	9,063,069
517.244306	28	37	38	0	9	7,022,748
517.280692	29	41	42	0	8	2,991,728
519.150800	25	27	28	0	12	4,456,655
519.187185	26	31	32	0	11	10,018,894
519.223571	27	35	36	0	10	11,728,545
519.259956	28	39	40	0	9	6,479,861
519.296342	29	43	44	0	8	2,180,382
521.166450	25	29	30	0	12	8,383,396
521.202835	26	33	34	0	11	13,632,077
521.239221	27	37	38	0	10	10,565,707
521.275606	28	41	42	0	9	4,042,101
523.145715	24	27	28	0	13	4,997,451
523.182100	25	31	32	0	12	11,083,423
523.218486	26	35	36	0	11	11,961,160
523.254871	27	39	40	0	10	6,406,129
523.291257	28	43	44	0	9	1,870,853
525.161365	24	29	30	0	13	6,630,124
525.197750	25	33	34	0	12	9,740,608
525.234136	26	37	38	0	11	6,927,252
525.270521	27	41	42	0	10	2,759,229
527.140629	23	27	28	0	14	3,108,577
527.177015	24	31	32	0	13	5,818,164

Exact mass (Da)	C	H	H+1	N	O	Average Peak Intensity
527.213400	25	35	36	0	12	6,081,160
527.228656	29	35	36	0	9	2,771,079
527.249786	26	39	40	0	11	3,106,310
529.156279	23	29	30	0	14	2,623,269
529.171535	27	29	30	0	11	2,343,716
529.192665	24	33	34	0	13	3,564,067
529.207921	28	33	34	0	10	4,475,341
529.229050	25	37	38	0	12	2,721,270
529.244306	29	37	38	0	9	4,260,896
529.280692	30	41	42	0	8	1,840,201
531.187185	27	31	32	0	11	5,183,844
531.223571	28	35	36	0	10	7,158,882
531.259956	29	39	40	0	9	4,849,248
533.166450	26	29	30	0	12	4,646,221
533.202835	27	33	34	0	11	9,339,552
533.239221	28	37	38	0	10	8,567,027
533.275606	29	41	42	0	9	4,199,452
535.145715	25	27	28	0	13	2,981,384
535.182100	26	31	32	0	12	7,927,515
535.218486	27	35	36	0	11	10,808,025
535.254871	28	39	40	0	10	6,987,137
535.291257	29	43	44	0	9	2,654,186
537.161365	25	29	30	0	13	5,275,112
537.197750	26	33	34	0	12	9,758,736
537.234136	27	37	38	0	11	8,834,830
537.270521	28	41	42	0	10	4,104,631
539.177015	25	31	32	0	13	6,275,227
539.213400	26	35	36	0	12	8,146,499
539.249786	27	39	40	0	11	5,219,820
539.286171	28	43	44	0	10	1,706,772
541.156279	24	29	30	0	14	3,074,210
541.192665	25	33	34	0	13	5,172,256
541.207921	29	33	34	0	10	2,023,391
541.229050	26	37	38	0	12	4,682,696
541.244306	30	37	38	0	9	2,019,869
541.265436	27	41	42	0	11	2,274,801
543.171929	24	31	32	0	14	2,511,204
543.208315	25	35	36	0	13	3,236,685
543.223571	29	35	36	0	10	3,721,676
543.259956	30	39	40	0	9	2,874,740

Exact mass (Da)	C	H	H+1	N	O	Average Peak Intensity
545.202835	28	33	34	0	11	4,860,025
545.223965	25	37	38	0	13	1,486,861
545.239221	29	37	38	0	10	5,555,319
545.275606	30	41	42	0	9	2,771,914
547.182100	27	31	32	0	12	4,516,303
547.218486	28	35	36	0	11	7,184,802
547.254871	29	39	40	0	10	5,945,077
547.291257	30	43	44	0	9	2,561,992
549.161365	26	29	30	0	13	3,404,536
549.197750	27	33	34	0	12	7,227,851
549.234136	28	37	38	0	11	7,724,915
549.270521	29	41	42	0	10	4,717,681
551.177015	26	31	32	0	13	5,333,661
551.213400	27	35	36	0	12	8,158,703
551.249786	28	39	40	0	11	5,996,781
551.286171	29	43	44	0	10	2,642,944
553.156279	25	29	30	0	14	2,806,658
553.192665	26	33	34	0	13	5,727,210
553.229050	27	37	38	0	12	6,179,517
553.265436	28	41	42	0	11	3,218,832
555.171929	25	31	32	0	14	3,146,852
555.208315	26	35	36	0	13	4,473,484
555.244700	27	39	40	0	12	3,482,079
557.187579	25	33	34	0	14	2,445,039
557.202835	29	33	34	0	11	2,097,219
557.223965	26	37	38	0	13	2,790,913
557.239221	30	37	38	0	10	2,757,782
559.182100	28	31	32	0	12	2,240,122
559.218486	29	35	36	0	11	4,190,029
559.254871	30	39	40	0	10	3,651,445
561.197750	28	33	34	0	12	4,096,067
561.234136	29	37	38	0	11	5,633,515
561.270521	30	41	42	0	10	3,465,705
563.177015	27	31	32	0	13	3,370,233
563.213400	28	35	36	0	12	5,897,910
563.249786	29	39	40	0	11	5,734,324
563.286171	30	43	44	0	10	2,591,751
565.192665	27	33	34	0	13	4,595,158
565.229050	28	37	38	0	12	6,077,481
565.265436	29	41	42	0	11	4,153,382

Exact mass (Da)	C	H	H+1	N	O	Average Peak Intensity
567.208315	27	35	36	0	13	4,955,294
567.244700	28	39	40	0	12	4,376,689
567.281086	29	43	44	0	11	2,310,510
569.187579	26	33	34	0	14	2,990,141
569.223965	27	37	38	0	13	3,595,408
569.260350	28	41	42	0	12	2,329,678
571.203229	26	35	36	0	14	2,230,128
571.239615	27	39	40	0	13	2,167,960
571.254871	31	39	40	0	10	1,958,657
573.234136	30	37	38	0	11	3,109,537
573.270521	31	41	42	0	10	2,175,114
575.213400	29	35	36	0	12	3,460,162
575.249786	30	39	40	0	11	3,647,936
577.192665	28	33	34	0	13	2,996,750
577.229050	29	37	38	0	12	4,593,291
577.265436	30	41	42	0	11	3,307,230
579.208315	28	35	36	0	13	3,659,522
579.244700	29	39	40	0	12	4,055,851
581.223965	28	37	38	0	13	3,646,073
581.260350	29	41	42	0	12	3,005,899
583.203229	27	35	36	0	14	2,376,434
583.239615	28	39	40	0	13	2,511,856
587.249786	31	39	40	0	11	2,197,284
589.229050	30	37	38	0	12	2,694,819
591.208315	29	35	36	0	13	2,353,401
591.244700	30	39	40	0	12	2,886,370
593.223965	29	37	38	0	13	2,977,935
593.260350	30	41	42	0	12	2,621,859
595.239615	29	39	40	0	13	2,547,517

Exact mass (Da)	C	H	H+1	N	O	Average Peak Intensity
335.124860	16	19	20	2	6	3,300,903
337.104124	15	17	18	2	7	4,213,472
337.140510	16	21	22	2	6	2,297,509
338.124526	16	20	21	1	7	2,435,468
339.119775	15	19	20	2	7	3,814,517
349.104124	16	17	18	2	7	2,887,947
349.140510	17	21	22	2	6	2,606,747
350.124526	17	20	21	1	7	2,576,410
351.119775	16	19	20	2	7	4,904,677
352.115024	15	18	19	3	7	2,212,848
352.140176	17	22	23	1	7	2,600,756
353.099039	15	17	18	2	8	4,402,235
353.135425	16	21	22	2	7	2,995,775
354.119440	16	20	21	1	8	3,042,260
355.114689	15	19	20	2	8	3,319,530
361.140510	18	21	22	2	6	2,717,879
362.124526	18	20	21	1	7	2,496,491
362.135759	17	20	21	3	6	3,009,272
363.119775	17	19	20	2	7	4,744,204
363.156160	18	23	24	2	6	2,366,737
364.103790	17	18	19	1	8	2,393,419
364.115024	16	18	19	3	7	3,600,258
364.140176	18	22	23	1	7	3,733,595
365.099039	16	17	18	2	8	4,882,721
365.135425	17	21	22	2	7	5,549,051
366.094288	15	16	17	3	8	1,968,992
366.119440	17	20	21	1	8	4,348,953
366.130674	16	20	21	3	7	2,817,318
366.155826	18	24	25	1	7	3,220,148
367.114689	16	19	20	2	8	6,174,607
368.098705	16	18	19	1	9	3,328,002
368.109938	15	18	19	3	8	1,890,926
368.135090	17	22	23	1	8	3,660,338
369.093954	15	17	18	2	9	3,001,431
369.130339	16	21	22	2	8	3,170,641
370.114355	16	20	21	1	9	2,818,351
375.119775	18	19	20	2	7	2,511,766
376.115024	17	18	19	3	7	2,427,049
376.151409	18	22	23	3	6	2,447,246

Exact mass (Da)	C	H	H+1	N	O	Average Peak Intensity
377.099039	17	17	18	2	8	2,645,498
377.135425	18	21	22	2	7	4,329,802
378.119440	18	20	21	1	8	3,275,664
378.130674	17	20	21	3	7	3,906,065
378.155826	19	24	25	1	7	3,213,951
379.114689	17	19	20	2	8	5,744,940
379.151075	18	23	24	2	7	3,462,918
380.109938	16	18	19	3	8	2,858,120
380.135090	18	22	23	1	8	4,421,559
380.146324	17	22	23	3	7	2,365,624
380.171476	19	26	27	1	7	2,433,158
381.093954	16	17	18	2	9	4,039,139
381.130339	17	21	22	2	8	5,467,538
382.114355	17	20	21	1	9	4,158,700
382.125588	16	20	21	3	8	2,154,232
382.150740	18	24	25	1	8	3,376,198
383.109604	16	19	20	2	9	4,139,954
383.145989	17	23	24	2	8	2,094,945
384.130005	17	22	23	1	9	3,241,061
388.140176	20	22	23	1	7	1,796,228
388.151409	19	22	23	3	6	2,279,248
389.135425	19	21	22	2	7	3,292,391
390.119440	19	20	21	1	8	2,416,274
390.130674	18	20	21	3	7	3,794,708
390.155826	20	24	25	1	7	3,141,036
391.114689	18	19	20	2	8	4,339,391
391.151075	19	23	24	2	7	4,645,870
392.109938	17	18	19	3	8	3,620,096
392.135090	19	22	23	1	8	4,745,582
392.146324	18	22	23	3	7	4,277,445
392.171476	20	26	27	1	7	3,377,565
393.093954	17	17	18	2	9	3,280,405
393.130339	18	21	22	2	8	7,108,676
393.166725	19	25	26	2	7	2,830,238
394.114355	18	20	21	1	9	4,596,077
394.125588	17	20	21	3	8	4,265,327
394.150740	19	24	25	1	8	5,351,453
394.161974	18	24	25	3	7	1,946,025
394.187126	20	28	29	1	7	2,284,321
395.109604	17	19	20	2	9	5,982,359

Exact mass (Da)	C	H	H+1	N	O	Average Peak Intensity
395.145989	18	23	24	2	8	4,622,407
396.104853	16	18	19	3	9	2,108,587
396.130005	18	22	23	1	9	5,269,231
396.141238	17	22	23	3	8	2,176,805
396.166390	19	26	27	1	8	3,462,409
397.125254	17	21	22	2	9	4,376,898
398.109269	17	20	21	1	10	3,738,004
398.145655	18	24	25	1	9	3,453,934
399.104518	16	19	20	2	10	2,383,846
399.140904	17	23	24	2	9	1,634,667
400.124920	17	22	23	1	10	2,165,094
401.135425	20	21	22	2	7	1,966,670
402.130674	19	20	21	3	7	2,592,926
402.155826	21	24	25	1	7	2,128,268
402.167059	20	24	25	3	6	2,258,082
403.114689	19	19	20	2	8	2,274,540
403.151075	20	23	24	2	7	3,524,934
404.109938	18	18	19	3	8	2,211,195
404.135090	20	22	23	1	8	3,109,843
404.146324	19	22	23	3	7	4,385,279
404.171476	21	26	27	1	7	2,874,392
405.130339	19	21	22	2	8	5,332,385
405.166725	20	25	26	2	7	3,306,513
406.114355	19	20	21	1	9	3,236,803
406.125588	18	20	21	3	8	4,601,967
406.150740	20	24	25	1	8	4,916,167
406.161974	19	24	25	3	7	3,294,558
406.187126	21	28	29	1	7	2,704,657
407.109604	18	19	20	2	9	4,947,813
407.145989	19	23	24	2	8	6,207,977
408.104853	17	18	19	3	9	2,743,600
408.130005	19	22	23	1	9	5,416,030
408.141238	18	22	23	3	8	4,123,274
408.166390	20	26	27	1	8	4,717,325
409.125254	18	21	22	2	9	6,458,238
409.161639	19	25	26	2	8	3,336,408
410.109269	18	20	21	1	10	3,949,767
410.120503	17	20	21	3	9	2,643,422
410.145655	19	24	25	1	9	5,132,022
410.156888	18	24	25	3	8	1,714,626

Exact mass (Da)	C	H	H+1	N	O	Average Peak Intensity
411.104518	17	19	20	2	10	3,761,595
411.140904	18	23	24	2	9	3,515,178
412.124920	18	22	23	1	10	3,668,422
412.161305	19	26	27	1	9	2,702,859
413.120168	17	21	22	2	10	2,361,636
414.140570	18	24	25	1	10	2,131,330
414.167059	21	24	25	3	6	1,623,035
416.146324	20	22	23	3	7	2,896,868
416.171476	22	26	27	1	7	1,839,879
417.130339	20	21	22	2	8	2,653,116
417.166725	21	25	26	2	7	2,528,939
418.125588	19	20	21	3	8	3,113,855
418.150740	21	24	25	1	8	2,917,677
418.161974	20	24	25	3	7	3,569,795
418.187126	22	28	29	1	7	2,249,947
419.109604	19	19	20	2	9	2,521,942
419.145989	20	23	24	2	8	4,638,063
420.104853	18	18	19	3	9	1,978,796
420.130005	20	22	23	1	9	3,555,503
420.141238	19	22	23	3	8	4,604,635
420.166390	21	26	27	1	8	3,898,760
421.125254	19	21	22	2	9	5,284,207
421.161639	20	25	26	2	8	4,056,222
422.120503	18	20	21	3	9	3,289,647
422.145655	20	24	25	1	9	5,017,137
422.156888	19	24	25	3	8	2,957,426
422.182040	21	28	29	1	8	3,118,197
423.104518	18	19	20	2	10	3,637,526
423.140904	19	23	24	2	9	5,082,693
423.177289	20	27	28	2	8	1,775,112
424.124920	19	22	23	1	10	4,068,011
424.136153	18	22	23	3	9	2,390,786
424.161305	20	26	27	1	9	3,998,852
424.197691	21	30	31	1	8	1,744,467
425.120168	18	21	22	2	10	3,670,418
425.156554	19	25	26	2	9	2,395,521
426.140570	19	24	25	1	10	3,376,165
426.176955	20	28	29	1	9	2,159,017
428.156220	19	26	27	1	10	1,788,634
430.161974	21	24	25	3	7	2,739,403

Exact mass (Da)	C	H	H+1	N	O	Average Peak Intensity
431.145989	21	23	24	2	8	2,634,005
431.182375	22	27	28	2	7	1,721,987
432.141238	20	22	23	3	8	3,531,081
432.166390	22	26	27	1	8	2,654,198
432.177624	21	26	27	3	7	2,391,959
432.202776	23	30	31	1	7	1,481,209
433.125254	20	21	22	2	9	3,109,414
433.161639	21	25	26	2	8	3,431,935
434.120503	19	20	21	3	9	2,750,723
434.145655	21	24	25	1	9	3,421,957
434.156888	20	24	25	3	8	3,775,793
434.182040	22	28	29	1	8	2,951,518
435.140904	20	23	24	2	9	5,032,886
435.177289	21	27	28	2	8	2,466,681
436.124920	20	22	23	1	10	3,358,181
436.136153	19	22	23	3	9	3,568,955
436.161305	21	26	27	1	9	4,185,320
436.197691	22	30	31	1	8	2,253,334
437.120168	19	21	22	2	10	4,220,094
437.156554	20	25	26	2	9	3,838,743
438.140570	20	24	25	1	10	4,047,513
438.151803	19	24	25	3	9	2,102,639
438.176955	21	28	29	1	9	3,026,972
439.135819	19	23	24	2	10	3,503,663
440.156220	20	26	27	1	10	2,944,668
442.161974	22	24	25	3	7	1,778,480
444.141238	21	22	23	3	8	2,284,070
444.177624	22	26	27	3	7	2,139,241
445.161639	22	25	26	2	8	2,413,559
446.120503	20	20	21	3	9	2,002,146
446.145655	22	24	25	1	9	2,028,121
446.156888	21	24	25	3	8	3,719,471
446.182040	23	28	29	1	8	2,370,396
447.140904	21	23	24	2	9	3,371,429
447.177289	22	27	28	2	8	2,475,901
448.136153	20	22	23	3	9	3,630,448
448.161305	22	26	27	1	9	3,468,231
448.172538	21	26	27	3	8	3,124,595
448.197691	23	30	31	1	8	2,357,002
449.120168	20	21	22	2	10	3,093,881

Exact mass (Da)	C	H	H+1	N	O	Average Peak Intensity
449.156554	21	25	26	2	9	4,226,022
450.140570	21	24	25	1	10	3,587,288
450.151803	20	24	25	3	9	3,411,417
450.176955	22	28	29	1	9	3,630,939
451.135819	20	23	24	2	10	4,266,997
451.172204	21	27	28	2	9	2,669,964
452.131068	19	22	23	3	10	2,098,810
452.156220	21	26	27	1	10	3,900,817
452.192605	22	30	31	1	9	2,562,622
453.151469	20	25	26	2	10	3,009,343
454.135484	20	24	25	1	11	2,939,585
454.171870	21	28	29	1	10	2,617,689
456.151134	20	26	27	1	11	2,074,264
458.156888	22	24	25	3	8	2,684,606
459.177289	23	27	28	2	8	1,861,754
460.136153	21	22	23	3	9	2,716,039
460.161305	23	26	27	1	9	2,231,603
460.172538	22	26	27	3	8	3,367,220
460.197691	24	30	31	1	8	1,886,229
461.156554	22	25	26	2	9	3,300,843
462.140570	22	24	25	1	10	2,325,579
462.151803	21	24	25	3	9	4,055,585
462.176955	23	28	29	1	9	2,928,333
462.188188	22	28	29	3	8	1,986,424
463.135819	21	23	24	2	10	3,585,834
463.172204	22	27	28	2	9	2,957,890
464.131068	20	22	23	3	10	2,805,213
464.156220	22	26	27	1	10	3,638,537
464.167453	21	26	27	3	9	3,039,242
464.192605	23	30	31	1	9	3,004,939
465.151469	21	25	26	2	10	3,760,869
466.135484	21	24	25	1	11	3,062,292
466.171870	22	28	29	1	10	3,567,126
466.208255	23	32	33	1	9	1,879,533
467.130733	20	23	24	2	11	2,636,738
467.167119	21	27	28	2	10	2,337,071
468.151134	21	26	27	1	11	2,883,867
468.187520	22	30	31	1	10	2,321,650
470.166784	21	28	29	1	11	1,806,383
472.172538	23	26	27	3	8	2,338,749

Exact mass (Da)	C	H	H+1	N	O	Average Peak Intensity
473.156554	23	25	26	2	9	1,746,400
474.151803	22	24	25	3	9	3,179,629
474.176955	24	28	29	1	9	1,917,912
474.188188	23	28	29	3	8	2,068,163
475.135819	22	23	24	2	10	2,159,991
475.172204	23	27	28	2	9	2,486,883
476.131068	21	22	23	3	10	2,448,065
476.156220	23	26	27	1	10	2,391,895
476.167453	22	26	27	3	9	3,548,183
476.192605	24	30	31	1	9	2,582,637
477.151469	22	25	26	2	10	3,392,777
477.187854	23	29	30	2	9	2,092,362
478.146718	21	24	25	3	10	2,928,569
478.171870	23	28	29	1	10	3,248,847
478.183103	22	28	29	3	9	1,977,146
478.208255	24	32	33	1	9	2,244,880
479.130733	21	23	24	2	11	2,596,455
479.167119	22	27	28	2	10	2,759,272
480.151134	22	26	27	1	11	2,950,954
480.162368	21	26	27	3	10	2,181,866
480.187520	23	30	31	1	10	3,012,736
481.146383	21	25	26	2	11	2,506,687
482.166784	22	28	29	1	11	2,558,803
486.151803	23	24	25	3	9	1,854,371
488.167453	23	26	27	3	9	2,855,115
489.151469	23	25	26	2	10	1,913,873
490.146718	22	24	25	3	10	2,639,999
490.171870	24	28	29	1	10	2,314,517
490.183103	23	28	29	3	9	2,432,298
490.208255	25	32	33	1	9	1,984,149
491.167119	23	27	28	2	10	2,484,183
492.162368	22	26	27	3	10	2,710,317
492.187520	24	30	31	1	10	2,675,266
492.223905	25	34	35	1	9	1,700,567
493.146383	22	25	26	2	11	2,530,475
493.182769	23	29	30	2	10	2,027,350
494.166784	23	28	29	1	11	2,875,048
494.203170	24	32	33	1	10	2,157,373
496.182434	23	30	31	1	11	2,331,825
500.167453	24	26	27	3	9	1,745,914

Exact mass (Da)	C	H	H+1	N	O	Average Peak Intensity
502.146718	23	24	25	3	10	1,741,477
503.167119	24	27	28	2	10	1,747,260
504.162368	23	26	27	3	10	2,641,192
505.182769	24	29	30	2	10	1,897,256
506.166784	24	28	29	1	11	2,152,273
506.178018	23	28	29	3	10	1,949,115
506.203170	25	32	33	1	10	2,154,256
507.162033	23	27	28	2	11	2,009,059
508.182434	24	30	31	1	11	2,283,464
510.198084	24	32	33	1	11	1,743,588
518.178018	24	28	29	3	10	1,940,988
520.218820	26	34	35	1	10	1,674,274
522.198084	25	32	33	1	11	1,994,934
534.198084	26	32	33	1	11	1,544,968

VITA

Hongmei Chen

Department of Chemistry and Biochemistry

hchen015@odu.edu

Old Dominion University

Norfolk, VA 23529

Education

July 2003.....**B.S. Marine Chemistry**, Xiamen University,
Xiamen, Fujian Province, China

July 2007.....**M.S. Environmental Science**, Xiamen University,
Xiamen, Fujian Province, China

December 2014.....**Ph.D. Chemistry**, Old Dominion University,
Norfolk, Virginia, USA

Presentations

Chen, H., Stubbins, A., Hatcher, P.G. "A mini-electrodialysis system for desalting small volume samples for Fourier transform ion cyclotron resonance mass spectrometry." 15th International Humic Substances Society conference, Tenerife, Spain, June, **2010**.

Chen, H., Stubbins, A., Mopper, K., Perdue, E.M., Green, N.W., Hatcher, P.G. "Molecular characterization of dissolved organic matter by ultrahigh resolution mass spectrometry from various oceanic water masses isolated by coupled reverse osmosis-electrodialysis." Gordon Research Conference Program: Chemical Oceanography, Andover, NH, August 14-19, **2011**.

Chen, H., Abdulla, H.A.N., Sun, L., Mopper, K., Hatcher, P.G. "Photochemical transformation of organic matter in iron rich waters studied by ESI FTICR mass spectrometry." ASLO 2013 Aquatic Sciences Meeting, New Orleans, LA, February 17-22, **2013**.

Awards

2011 ODU Graduate Student Travel Award

2010 15th International Humic Substances Society conference Student Travel Award

2009-2011 Old Dominion Scholarship, Old Dominion University

2003 Excellent Graduate (undergraduateship), Xiamen University

2002 National Student Scholarship, China

2002 Sanjiu Scholarship, Xiamen University